10⁶₁

Structural Acoustic Analysis of
Shape Memory Alloy Hybrid Composite Panels

by

William S. Anders

Thesis submitted to the Faculty of the

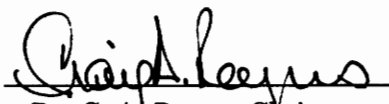Virginia Polytechnic Institute and State University

in partial fulfillment of the requirements for the degree of
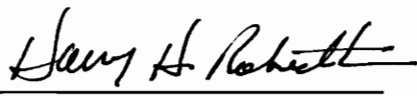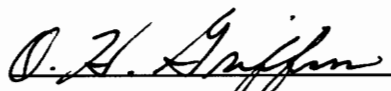
MASTER OF SCIENCE

in

Mechanical Engineering

APPROVED:

Dr. C. A. Rogers, Chairman

Dr. H. H. Robertshaw   Dr. O. H. Griffin

September, 1990

Blacksburg, Virginia

C.2

Structural Acoustic Analysis
of Shape Memory Alloy Hybrid Composite Panels

by

William S. Anders

Committee Chairman: Craig A. Rogers

Mechanical Engineering

Abstract

Shape memory alloy (SMA) hybrid adaptive composites are a class of materials which combine the strain recovery and elastic properties transformation capabilities of SMA fibers with the structural characteristics of advanced composite materials. This study utilizes the Rayleigh-Ritz method and finite panel acoustic radiation theory to investigate the use of SMA hybrid composite materials for adaptive structural acoustic control by active structural tuning. Analytical models are formulated considering classical laminated plate theory (CLPT) and first-order shear deformation theory (FSDT), to predict modal and structural acoustic response to incident low frequency plane wave acoustic excitation. The analysis is further developed to consider simply supported adaptive panels that are tuned by local fiber activation, such that a panel composed of elastically uniform sections can be evaluated in a piece-wise fashion.

Analytical results are presented to demonstrate the utility of the models and their

capabilities, as well as to isolate and identify physical trends which enhance the acoustic transmission control authority of adaptive SMA hybrid composite panels. Studies considering generally activated panels are included with dimensionless analyses to evaluate the effects and influences of panel (length-to-width) aspect ratio, ply layup, panel thickness, and structural damping in the context of active structural acoustic control capability. Case study results are presented to illustrate physical trends concerning active modal modification and structural acoustic response modification for several local activation scenarios. Finally, a concept known as alternate resonance tuning is introduced and analytically demonstrated as an effective means of achieving low frequency adaptive structural acoustic control.

Acknowledgements

I would like to thank Dr. Craig A. Rogers for serving as my course advisor and committe chairman. His guidance regarding course selection and research have enabled me to experience a fulfilling and meaningful experience over the last two years. I also wish to acknowledge Dr. Harry H. Robertshaw and Dr. Odis H. Griffin for serving on my committee and for their advisory role in the completion of this thesis.

Dr. Chen Liang also deserves much credit for his initial work on this project and for his technical advice, encouragement and tutelage throughout the course of my work on this thesis. Liang has been both a friend and valuable source of guidance. Thanks are also in order to Jianhu Jia, Mark Lin, Juzer Mohammedshah, Tracy Dye, Steve Booth, and the rest of Craig's students for their cooperative and friendly nature. Other graduate students who have been most helpful include Robert Wynn and Will Saunders, who have shared thier knowledge and technical advice. My heartfelt thanks

Contents

List of Figures

xi

List of Tables

Nomenclature

a	panel dimension in the global x-direction
A_a	cross sectional area of actuator wire
A_f	austenite finish temperature
A_{ij}	in-plane extensional and transverse shear stiffness coefficients
A_m	cross sectional area of matrix material
$\overline{A}_{mn}$	normalized modal amplitude coefficient
A_s	austenite start temperature
b	panel dimension in the global y-direction
B_{ij}	flexural-extensional stiffness coupling coefficients
c	speed of sound in a viscous medium
C_{Dp}	translational damping coefficient
C_{Dr}	rotational damping coefficient
D	elastic tensor
D_{ij}	laminate flexural stiffness coefficients
E	Young's modulus of elasticity
ELA	unactivated longitudinal Young's modulus
ELU	activated longitudinal Young's modulus
F	SMA fiber recovery force
f	periodic frequency

G	isotropic shear modulus
G_{ij}	orthotropic shear moduli
h	panel thickness
I_i	incident acoustic intensity
I_t	transmitted acoustic intensity
k	transverse shear correction factor
k_{cp}	acoustic wave number
k_p	panel wave number
$\overline{K}_{ij}$	structural stiffness coefficients
M	moment resultants
M_f	martensite finish temperature
M_r	recovery stress-induced moment resultants
M_s	martensite start temperature
m_p	mass density per unit area
m_r	rotary inertia
N	in-plane force resultants
N_r	in-plane recovery stress-induced force resultants
Q	transverse shear force resultants
P_b	blocked acoustic pressure
P_i	incident acoustic pressure
P_{mn}	pressure amplitude coefficients
P_r	reflected acoustic pressure
P_t	transmitted acoustic pressure
Q_{ij}	lamina stiffness coefficients in material coordinate system
$\overline{Q}_{ij}$	rotated lamina stiffness coefficients

r	distance between two points in space
$\overline{S}$	modal radiation efficiency
S_{ij}	lamina compliance coefficients
t	time dimension
T	kinetic energy
TL	acoustic transmission loss
u	displacement in the global x-direction
U	strain energy
$\overline{U}$	spatial time-averaged velocity squared
U_r	far-field particle velocity
U_r^*	complex conjugate of U_r
v	displacement in the global y-direction
V	potential energy
v_a	SMA actuator wire volume fraction
v_m	matrix volume fraction
w	displacement in the global z-direction
W	work energy
X	transverse displacement function of x
Y	transverse displacement function of y

Greek Letters

γ	shear strain
ε	extensional strain

ε_l	recoverable strain limit
ε_r	recovery strain
ε_{res}	martensitic residual strain
θ	polar coordinate angle
Θ	thermoelastic tensor
κ	flexural curvature
λ	acoustic wavelength
ν	poisson's ratio
ξ	mass-proportional damping coefficient
ξ_m	martensitic volume fraction
Π	total energy
Π_i	incident acoustic power
Π_t	transmitted acoustic power
ρ	density
σ	normal stress
σ_r	recovery stress
τ	shear stress
ϕ	azimuthal spherical coordinate angle
Φ	normalized mode shape
ψ	transverse material rotation angle
ω	angular frequency
Ω	material phase transformation tensor

Chapter 1

Introduction

The use of advanced composite materials for structural applications such as aircraft fuselages has become increasingly popular in recent years. Using composite materials for these applications is beneficial in reducing component mass without compromising structural performance, as the orthotropic layers of a laminated composite can be oriented and thereby tailored to optimize the strength, stiffness, and dynamic response of a structural member. By this capability, structural members for advanced technological applications can be better optimized in terms of their mass properties and elastic behavior; however, other critical factors such as structural acoustic behavior must be taken into consideration to obtain satisfactory performance.

The acoustic response of composite structures is often critical to the performance of the systems into which they are incorporated: as excessive engine noise transmitted through the fuselage of an aircraft poses health and safety risks to its passengers and crew; and submarine drive system noise transmitted through hull structures can be readily detected and traced by enemy vessels. For these reasons, much research and development effort has been devoted to understanding, controlling and minimizing the transmission of sound through composite structures.

Passive noise control methods using add-on treatments such as constrained layer damping, porous acoustic materials, limp trim panels and noise barriers (Vaicaitis and Mixson, 1985) have proven effective for attenuating high frequency noise; however for lower frequency sound - particularly where sound pressure levels are high - structural damping does not offer much benefit in terms of noise reduction. Consequently, extensive experimental and theoretical research has been conducted to ensure that the weight advantages gained by using composite materials are not compromised by noise transmission or heavy acoustic treatments (Revell et al., 1982). For applications involving incident sound at specific frequencies - for example the first few harmonic blade passages for propeller-driven aircraft - passive structural tuning techniques have been considered such as intrinsic structural tuning (SenGupta, 1985) and alternate resonance tuning (Bliss and Gottwald, 1990).

To realize the mass benefits of composite materials without compromising structural acoustic performance, research efforts have recently turned to adaptive structural acoustic control using intelligent materials systems. An adaptive structural tuning concept using shape memory alloy (SMA) hybrid composites was introduced by Rogers and Robershaw (1988 a,b). SMA hybrid composite materials consist of SMA fibers embedded in conventional fiber reinforced epoxy laminates. The SMA fibers can be electrically activated to tune the stiffness of a structure by modifying its state of strain energy and transforming its elastic properties. Active structural acoustic control capabilities have been demonstrated analytically by Liang et al. (1989) and experimentally by Barker (1989), and Saunders et al. (1990), considering panel and beam structures with spatially uniform material properties and strain energy distri-

bution.

The primary objective of this thesis is to expand the scope of previous analytical research in structural acoustic control of SMA hybrid composite panels (ie. Rogers, Fuller and Liang, 1990) to study and evaluate physical trends and conditions which influence the effectiveness of this concept. Emphasis is placed on exploring the capabilities of localized activation-induced dynamic tuning for controlling the transmission of sound through panel-like structures fabricated from this novel material. To achieve these stated objectives, analytical models are developed using the Rayleigh-Ritz method, finite panel acoustic radiation theory, classical laminated plate theory (CLPT), and first order shear deformation theory (FSDT). These models, their governing theories, assumptions and formulations are explained in detail in Chapter 3 and Appendix A.

The remainder of this chapter discusses some of the fundamental principals and historical developments in the field of structural acoustics, practical issues in active and passive noise control, and active structural acoustic control. The utility and mechanisms of adaptive tuning of SMA hybrid composites are explained in the latter sections of Chapter 1, and the theoretical elastic models for SMA hybrid composite materials and their constituents are formulated in Chapter 2.

Analytical results for global activation studies - which isolate and evaluate the effects of specific physical parameters including panel dimensions, laminate ply orientation and stacking sequence, panel thickness, material properties and structural damping - are presented in the early sections of Chapter 4 along with a study comparing CLPT

3

and FSDT acoustic transmission analysis results. The work of Liang and Rogers (1989) is expanded to consider locally activated adaptive panels by piece-wise integration of the Rayleigh-Ritz energy expression. The analytical capabilities of this modified analysis are applied for localized activation case studies and to introduce a novel acoustic radiation control technique: active structural acoustic control by adaptive alternate resonance tuning (ART) using SMA hybrid composites. Analytical results for case studies considering localized panel activation and adaptive ART are presented in Chapter 4.

This thesis concludes with Chapter 5, which summarizes observations made during the course of the analysis and makes recommendations for theoretical and experimental follow-up work. Hopefully, these suggestions will be instrumental in guiding future researchers to advance this work by expanding the project from an analytical standpoint and to produce experimental results which demonstrate effective structural acoustic control capabilities. Optimistically, novel ideas and useful concepts will be inspired to advance the capabilities of controlling sound tranmission through shape memory alloy hybrid composites, and perhaps other intelligent material systems as well.

We may in general assume sound to be a blow which passes through the ears, and is transmitted by means of the air, the brains and the blood, to the soul; and that hearing is the vibration of this blow, which begins in the head and ends in the region of the liver...

Plato (429-347 B.C.)

(Hunt, 1976)

Soun is nought but air y-broken,

and every speche that is spoken,

Loud or privee, foul or fair,

In his substaunce is but air;

For as a flaumbe is but lighted smoke,

Right so soun is air y-broke.

Geoffery Chaucer (1340-1400)

(Hunt, 1976)

1.1   The History of Theoretical Acoustics

Acoustics is the name given to the branch of science dealing with the phenomena of sound. The name, which comes from the Greek word *akoustikus*, means "pertaining to hearing" (Morris, 1978). The terminology was introduced by Joseph Sauveur (1653-1716), a French scientist and mathematician as cited in the following context:

> ...I have come then to the opinion that there is a science superior to music, and I call it acoustics; it has for its object sound in general, whereas music has for its object sounds agreeable to the ear.

The science of acoustics has a rich history. The evolution of this field to its current state of maturity has taken nearly 2500 years. The theories of acoustics as we know them today have been pieced together by some of the most brilliant scientists and mathematicians in recorded history. The following paragraphs provide a brief account of some of the historical developments in acoustics which have enabled the advancement of the analytical theories and techniques utilized in compiling this thesis. Tribute and acknowledgement are paid to the scientists and mathematicians who have contributed in this manner. The following account is by no means intended as a comprehensive history of acoustics. Lindsay (1972) and Hunt (1976) present thorough, detailed and comprehensive accounts in this regard, and the reader is referred to these sources for additional information.

1.1.1 Acoustics Before the Renaissance

The study of sound initiated with research in the area of music around 500 B.C. in ancient Greece with the work of Pythagoras (570-497 B.C.), who identified consonances in vibrating strings as ratios of whole numbers, which initiated the branch of musicology known as "canonics" or "harmonics" (Hunt, 1976). This work was followed roughly 200 years later by Aristotle, who conveyed the first understanding of the association between sound and the motion of air, and the nature of echo (Lindsay, p.1972).

Around 25 B.C., a Roman engineer named Marcus Vitruvius Pollio (commonly called Vitruvius) wrote a ten book treatise providing the first ideas on architectural acoustics (Lindsay, 1972). Little more was added to the field of acoustics through the time of the Roman Empire, and the science as a whole all but perished with the fall of Rome in the 5th Century A.D.. The Greek scientific tradition was nourished by the Byzantines, Hindus and Arabs throughout the Dark Ages, as the Western world turned to preoccupation with politics, strife, and conquest for over a thousand years before it was revitalized during the Renaissance period (Hunt, 1976).

1.1.2 Acoustics through the Renaissance

Three key contributers to the science of acoustics during the Renaissance period were Leonardo da Vinci (1452-1519), Gallileo Gallilei (1564-1642), and Marin Mersenne (1588-1648). Leonardo is credited with four key contributions: he was the first to formally identify the wave-like nature of sound; he determined that sound has a finite velocity; he observed and recorded the phenomenon of sympathetic resonance; and

he was the first to suggest the superposition of sound waves. His incredible insight and intuition also enabled him to construe the concept of sonar (Hunt, 1976):

> ... If you cause your ship to stop and place the head of a long tube in the water, and place the other extremity in your ear, you will hear ships at a great distance from you ...

Gallileo, who is said to have "done more than anyone else to bring the field of experimental science to at least the stage of adolescence" observed the periodic nature of oscillating bodies and identified the existance of a relationship between the diameter and tension of a vibrating string and its fundamental frequencies. Marsenne, who was the first to relate tone and frequency, also was the first to estimate the speed of sound to within 10 percent (Hunt, 1976).

1.1.3 Classical Acoustics

The Renaissance age produced several observations about the nature of sound which raised many questions to be addressed by subsequent researchers. The classical age of acoustics answered some of these questions, advancing the science from the stages of observation and experiment, through the formulations of basic theory and mathematics, to the point of application known as the modern age of sound (Lindsay, 1972). The classical developments in acoustics (and science as a whole) began with the work of Sir Issac Newton (1642-1727).

Prior to the time of Newton, the study of sound almost exclusively delt with musicology. As the study of sound began to spill over into other disciplines - such as op-

tics, mathematics, electricity, heat transfer, mechanics and elasticity - and vice-versa, researchers whose names are most often associated with key discoveries and developments in other areas are credited with significant contributions also to acoustics. Such individuals include Sir Issac Newton (1642-1727), Leonhard Euler (1707-1783), Jean Baptiste Joseph Fourier (1760-1830), Simeon Denis Poisson (1751-1840), Jean le Rond D'Alembert (1717-1873), Robert Hooke (1635-1703), Daniel Bernoulli (1700-1782), and G. R. Kircchoff (1824-1887).

Sir Issac Newton, who is most noted for his introduction of calculus, his laws of motion and his theory of universal gravitation, also made significant contributions in the field of acoustics. Newton was the first to attempt to seriously theorize the wave theory of sound in mathematical terms. (Lindsay, 1966) as well as being the first to attempt a theoretical derivation of the speed of sound in light fluids such as air (Lindsay, 1972). Newton's most significant contributions to acoustics were not fully realized until the second half of the 18th Century, when the influence of "The Calculus"(calculus, the laws of motion, and universal gravitation) had matured beyond the stages of refinement and development as "tools", and were advanced to the stage of application by his successors (Hunt, 1976).

Unlike previous developments, the work of Newton was closely followed and critiqued by his colleagues. Quarrels often errupted among the scientists and mathematicians of that era. Sometimes this interraction served to delay progress. For example Newton, who sought to avoid controversy wherever possible, is said to have postponed the publication of his *Opticks* until 1703; a year after the death of Robert Hooke, due to Hooke's adversity to the wave theory (Hunt, 1976). In other instances, research

efforts during the classical period merged in a complimentary manner, producing profound theoretical advances from astute, but incomplete observations. For example, Daniel Bernoulli (1700-1782) demonstrated that a string can vibrate and produce a multitude of single oscillations which occur simultaneously such that each mode contributes to the overall vibration, the displacements at any point on the string being the algebraic sum of the displacement modes. This observation is also known as the coexistence of small oscillations, or more commmonly as the principle of superposition. Leonhard Euler (1707-1783) almost immediately pointed out the true significance of this observation: that the partial differential equation governing the motion of frictionless strings is linear, enabling the principle of superposition to be proven as a theorem. This theory was enhanced even further by the Jean Baptiste Joseph Fourier (1760-1830), whose theorem on the expanded series had "consequences of the greatest value for the advancement of acoustics"(Lindsay, 1966).

The study of vibrating plates and membranes began with the work of Euler, who derived the first appropriate differential equation of motion for a vibrating membrane; however he incorrectly evaluated the boundary conditions and therefore failed to determine the correct normal modes. Simeon Denis Poisson (1751-1840) followed up on Euler's work to rectify this error. The initial work relating to the vibration of elastic plates was done by Ernst Florens Friedrich Chladni (1756-1827), whose experiments showed that sand, when spread over the surface of a vibrating plate, migrates to nodal lines and therefore produces images of mode shapes (Lindsay, 1972). In the early 19th Century, the Emperor Napoleon offered a purse of 3000 francs to whoever could offer a satisfactory mathematical theory to describe the vibration of plates. This award went to Mlle. Sophie Germain in 1815, who produced the correct fourth order dif-

ferential equation; however her boundary conditions proved to be incorrect. It was not until 1850 that G. R. Kirchhoff (1824-1887) provided a more accurate solution (Lindsay, 1966).

Another significant contribution to the field of acoustics during the Classical era of science which shouldn't be over looked was made by Jean le Rond D'Alembert, who published the first differential equation of wave propagation (Lindsay, 1972).

This section is best summed up by the words of the late Dr. Fredrick Vinton Hunt (1976), Gordon McKay Professor of Applied Physics and Rumford Professor of Physics at Harvard Universtiy:

> The two centuries between Newton's time and that of Rayleigh embrace
> a period of development and growth in the parts of physical science now
> designated as 'classical.' The calculus was invented and developed as
> a powerful tool of analysis, and was used to deal exhaustively with the
> problems of analytical mechanics; heat became an understandable mode
> of motion and the laws of thermodynamics a comprehensive account of all
> energy exchange phenomena; and electricity evolved from pith balls and
> amber to a theory and practice of electromagnetism capable of sustaining
> a major industry. Science historians have dealt fondly and extensively
> with these major triumphs of human understanding. With depressing
> uniformity, however, these same historians have found remarkably little
> to say about sound during the same period, their silence tacitly endorsing
> the conclusion Chladni drew in 1802 'that the science of acoustics has
> been more neglected than most other portions of Physics.' But with the

advantage of hindsight, this very science... is enough to arouse rather than supress a lively interest in accounting for the origins of the modern science of physical acoustics in the eighteenth and nineteenth centuries.

1.1.4 Modern Acoustics

The classical era of science produced many key discoveries and observations in physics; however many loose ends remained in the area of acoustics. As many other scientific disciplines were moving to the forefront of technology during the 17th and 18th Centuries, acoustics was not pursued as a separate science until the late 19th Century (Hunt, 1976). The transition from classical to modern acoustics is punctuated by the publication of *The Theory of Sound* by Lord J. W. S. Rayleigh (1842-1919) in the year 1878 (Lindsay(1972).

Rayleigh's work naturally divides into two parts, the first of which relates mechanical vibration phenomena such as the oscillations of strings, bars, membranes and plates to the production of sound. A valuable feature of Rayleigh's treatise on sound is its insistence on the establishment of general principles as well as its application to special cases of practical significance. Rayleigh's background in applied mathematics enabled him to develop useful techniques for solving difficult vibration problems. One of these, the Rayleigh-Ritz method, has had wide application, not only in the area of vibrations of solid structures, but also in quantum mechanics. Rayleigh never lost touch with physical meaning, and his analyses always reflected application to practice.

The second part of Rayleigh's work concentrated on sound propagation through fluid

media. In this work he had to address difficult issues such as acoustic diffraction and sound wave scattering in the presence of discontinuous media. Rayliegh also devoted much attention to the geometric nature of sound radiation from vibrating bodies. Rayleigh, for example was the first to discuss sound transmission through single wall barriers (Holmer, 1969). The work of Rayleigh so clearly and thoroughly summarized the efforts of his predecessors in areas such as the attenuation of sound in fluids by various mechanisms of dissipation; that when the second edition of the *Theory of Sound* appeared between 1894 and 1896, it was widely believed that the whole subject of acoustics as a branch of Physical Science was complete, and there remained nothing more to learn. It was assumed, at that point, to be up to the engineers to carry the field further (Lindsay, 1966).

After Rayleigh, the science of acoustics turned toward practice and application. Several contributions to the field were made in the 20th Century. For example, Wallace Clement Sabine (1868-1919) addressed the issue of architectural acoustics and gained a precise understanding of the subject. He formulated a law relating the reverberation time of a room with its volume and the amount of absorbing material (Lindsay, 1972). Sabine's theory of reverberent sound in rooms also led him to the first quantitative measurement technique for determining the noise reduction of a barrier (Holmer, 1976).

Additional work in the field of acoustics in the earlier years of the 20th Century dealt primarily with sound measurement. For example, Buckingham did the first qualitative work on test methods for determining sound transmission. Buckingham first differentiated noise reduction from transmission loss through a barrier, leading to a

period of consolidation, and enabling other workers in the field of acoustics to pursue other problems (Holmer, 1969).

The science of acoustics has since permeated many areas of modern technology, as the subject of sound has spilled over into the Electrical, Chemical, Architectural, and Mechanical Engineering fields; the life sciences of psychology, physiology, and medicine; studies of the Earth, atmosphere and oceans; as well as the arts, in areas such as speech and music. Specific advanced technologies to which the science of acoustics is now particularly relevant include sonar, seismology, noise and vibration control, and ultrasonics (Lindsay, 1972).

1.2 Practical Issues in Structural Acoustics

The previous section discusses the development of acoustics as a science from the early stages of observation, through experimentation and the formulation of fundamental theory, to its current state of practice and application. This section discusses some practical issues in passive noise control.

1.2.1 General Issues

In technology and industry, noise control is often essential for product quality and customer satisfaction. This is particularly true in the automotive, shipbuilding, architectural, and aircraft industries. In the aircraft and air transportation industries, noise control is essential for passenger comfort (Mixson and Powell, 1985), and underwater sound transmission through ship structures is an issue of considerable importance as well. In other cases, acoustic response is a crucial issue of structural integrity.

During re-entry, for instance, the space shuttle is exposed to high intensity pressure fluctuations resulting from attaching and detaching boundary layers and shock waves. To avoid structural failure, these effects must be taken into account and thoroughly analyzed (Yang and Tsui, 1977).

1.2.2 Passive Noise Control

There exist two main methods for inhibiting the transmission of sound from one region of fluid to another. Sound waves can be absorbed in transit by materials specially chosen to accept energy efficiently from incident sound waves, and dissipated in the form of heat energy; or large changes of acoustic impedance can by introduced in a sound field to reflect or scatter the sound energy (Fahy, 1989).

In architectural acoustics, sound control by absorption is commonly achieved by the use of porous materials, non-porous panels, and by cavity resonance. Porous acoustic materials usually appear in the form of liners, coatings and blankets, which are applied directly to radiating structures. Incident acoustic energy is converted to heat energy in these materials as pressure disperses within their pores and narrow cavities (Kinsler, Frey et.al, 1982)

Noise control using non-porous materials is achieved most effectively in the form of panels offset a finite distance from a solid backing. This distance is usually smaller than the acoustic wavelength, depending on the frequency range to be attenuated. The dissipative mechanism which makes this technique effective is hysteretic damping in the panel material, which converts acoustic energy to heat. This technique is

particularly effective at low frequencies, and improved performance can be obtained by adding porous material between the panel and the solid backing (Kinsler, Frey et. al., 1982).

A modification of this technique is the membrane absorber. Commonly found in recording studios, this device includes a fixed panel (approximately 1 m square) mounted to a wall, with a small air cavity between the two structures. The absorber is tuned to dissipate low-frequency sound energy by resonating in its fundamental bending mode (Fahy, 1989). Not only do these panels absorb acoustic energy, but they also scatter incident sound in many directions. This increases the diffusion in sound fields and reduces sound levels by destructive wave interference (Fahy, 1989).

Cavity resonance is achieved by containing a volume of air within a wall or partition such that the cavity and acoustic control space are connected by a narrow opening. Acoustic energy corresponding to a narrow band of frequencies near the cavity resonance is readily absorbed within the cavity. These cavities most commonly appear in the form of standard concrete block with slotted crevices, perforated paneling, and wood lattices offset from solid backings with absorption blankets interposed (Kinsler, Frey et. al., 1982). Cavity resonance can also be applied in the form of add-on devices such as Helmholtz resonators.

As previously mentioned, noise levels can be reduced by introducing large impedance changes in the propagation path of acoustic flow fields. Examples of this capability include internal combustion engine exhaust systems; and hydraulic line silencers, where sound waves travelling through oil encounter an acoustically "soft" pipe section

16

surrounded by presssurised gas (Fahy, 1989).

Several passive techniques for controlling structurally radiated noise have been introduced and discussed, along with the physical principles and characteristics by which they operate. The remainder of this section is devoted to overviewing passive noise control concepts for aircraft fuselage structures, where low-frequency noise and overall system mass are extremely critical to system performance.

1.2.3 Passive Noise Control in Aircraft

Modern aircraft designs require low mass, high strength structures to meet performance demands in a fuel efficient manner. These requirements have renewed interest in propeller-driven aircraft, owing to their high propulsive efficiency (Revell et al., 1982). Unfortunately, propeller-driven aircraft have also exhibited high levels of interior noise at blade passage frequencies and their harmonics. Much concern has been expressed regarding the acceptability of future propeller-driven aircraft and the weight penalties required to achieve acceptable interior noise conditions (Revell et al., 1982).

Composite fuselage and frame structures offer the benefits of reducing mass and noise. Constructing a fuselage skin and frame structure from composite materials enables mass reduction and provides the opportunity to down-size engines. Although the use of smaller engines reduces noise levels at the key source, this does not resolve the issue of cabin noise entirely (Revell et. al, 1982).

Aircraft cabin noise sources can include propellers, exhaust from reciprocating engines of turbofans, turbomachinery, turbulent air flow, or engine vibrations (Mixson and Powell, 1985). Sound radiating from these souces must be reduced by treatments having minimal weight and limited occupied volume (Heitman and Mixson, 1986).

The mass and stiffness characteristics of most pressurized aircraft fuselages produce structural acoustic response that is stiffness-controlled below about 600 Hz; controlled by damping from 600 to 1500 Hz; and mass controlled above 1500 Hz (Sen-Gupta, 1979). Considerable emphasis has been placed on resolving the aircraft interior noise control issue by applying various arrangements and combinations of add-on treatments, including aluminum honeycomb panels, constrained layer damping tape, porous acoustic materials, noise barriers, and limp trim panels (Vicaitis and Mixson, 1985; Revell et al., 1982; Heitman and Mixson, 1986; Mixson and Powell, 1985). The general conclusion of this work is that these add-on treatments require up to 2.4 percent added aircraft gross take-off weight, however additional improvements are still needed to reduce low frequency noise; especially around 225-250 Hz, which corresponds to the first blade passage frequencies of most propeller-driven aircraft (Bliss and Gottwald, 1990). In fact, according to Vaicaitis and Mixson (1985), "... analytical predictions of noise transmission indicate that adding a large amount of nonload carrying mass to the aircraft skin *increases* the noise transmission at the first propeller blade passage harmonic...". To address this issue, low frequency noise and vibration control devices such as tuned dampers (Vaicaitis and Mixson, 1985), vibration isolators and Helmholtz resonators (Kandepo, 1988) have been proposed.

Other passive low frequency sound control techniques have been put forth which

consider structural tuning. Two such methods include intrinsic structural tuning (SenGupta, 1978) and alternate resonance tuning (Bliss and Gottwald, 1990).

The concept of intrinsic structural tuning was developed considering the response of periodic skin-stringer structures in aircraft to highly correlated, coherent, near-field engine noise enviromnents. For a typical skin-stringer structure, in which the stringer natural frequency is considerably higher than that of the skin; the peak frequency response occurs very close to the natural frequency of the individual skin bays, which are clamped along the stringers and simply supported along the frame. Under these boundary support conditions, strong reflection of flexural waves in the skin are introduced at the stringer and longeron interfaces resulting from the large stiffness discontinuities introduced by these members. Intrinsic structural tuning is achieved by designing the fuselage skin bays and stringers to share a common fundamental frequency, while satisfying the typical static and dynamic strength requirements. In this condition, the skin response at the shared funadamental frequency can be greatly reduced (SenGupta, 1978).

Low frequency response can be further improved by designing the stringers to resonate below the fundamental frequency of the skin bays such that the support structure dominates the response at the first structural resonance and the skin acts like an attached mass (SenGupta, 1979). The concept can then be optimized for noise reduction by applying damping material to the stringers.

Alternate resonance tuning (ART) is a method of reducing sound transmission through flexible, low mass paneled wall structures by controlling the dynamics of

19

the panels. Acoustically compact adjacent panels are designed in ART arrays to have resonant frequencies alternately above and below the frequency to be attenuated.

Low-frequency acoustic energy is particularly difficult to absorb or block, especially given the weight and thickness constraints imposed by most fuselage construction techniques. Fuselage panels are thin, flexible, and lightly damped, with resonances that often coincide with the blade passage frequencies of propeller-driven aircraft. ART takes advantage of the dynamic panel behavior (flexible and lighty damped) although these characteristics are not normally desirable for low-frequency noise control. More conventional approaches (intrinsic structural tuning, for example) emphasize reducing dynamic response amplitudes to control noise. In contrast, ART focuses on controlling the shape of the wall and panel motion to break the acoustic coupling between the structure and the aircraft interior (Bliss and Gottwald, 1990).

At the tuned frequency, ART panel networks oscillate with equal amplitude and near opposite phase, resulting in cancellation of sound radiation from adjacent panels, causing cutoff as the transmitted acoustic modes become evanescent and nonpropagating.

1.3 Active Noise Control

Active noise control (ANC) or antisound is achieved by using secondary control sources to create noise that is 180 degrees out-of-phase with an original sound field such that the overall sound field is reduced by superimposing the two waveforms. ANC has recently received much attention for aircaft applications because of its potential

to reduce low frequency noise levels without introducing much additional weight and cost to the systems in which they are used (Mandic and Jones, 1989).

The earliest experiment in sound wave interference dates back to the 1870's and Lord Rayleigh's study of two carefully tuned organ pipes. In Chapter 23 of his *Theory of Sound*, Rayleigh provided a clear mathematical explanation of the wave interference phenomenon he observed while investigating the source of "grave notes" produced in pipe organs when two different tones were simultaneously played. Unfortunately, the state of technology in the 1800's prevented Rayleigh from delving deeper into sound cancellation due to lack of an adequate experiment (Swanson, 1989).

The invention of radio brought forth the audio technology that enabled Paul Lueg (1937) to patent the first sound cancellation device, which pioneered the concept of using artificially produced sound waves to control noise (Jones, 1987). Unfortunately, at that time the available electronics were insufficient to experimentally verify Lueg's device, and further development had to wait until Olson and May (1953) published their description of an "electronic sound absorber". Conover (1956) followed with the first practical application for ANC in his attempt to reduce electric power transformer noise. Since the structural vibrations producing this noise occurred at the harmonics of the 60 Hz power input, a loudspeaker was directly wired to produce sound that was 180 degrees out-of-phase with the line signal. The speaker was then positioned to effectively reduce sound radiation in a given direction. Global attenuation, however, was found to be unachievable because of the presence of acoustic radiation from many parts of the structure, requiring several control sources - in the ideal situation, one speaker is needed per radiating source (Swanson, 1989).

Further advancement in the field of electronics led to more ANC research the 1960's and 1970's (Jones, 1987). One major refinement was in the area of sensor noise. Previous ANC systems suffered performance-wise because of control noise mixing with the acoustic source noise to produce a standing wave, with cancellation occuring at the speaker and beyond. Pressure nulls at the microphone location then cancelled the signal to the control source (Swanson, 1989).

In the 1970's, ANC efforts were primarily directed toward the attenuation of unidirectional sound waves in ducts, which act like acoustic waveguides, which restrict sound wave propagation to one direction, for frequencies corresponding to acoustic wavelengths at least twice the longest cross-sectional dimension of the duct (Swanson, 1989). This application was originally motivated by the problem of very low frequency pressure fluctuations (on the order of 1 Hz) in a large, very long waste extraction pipeline of a factory ventillation system (Swinbanks, 1972). The problem was addressed considering a plane wave propagating downstream in a long duct and in a uniform flow field. A localized distribution of point sources was sought such that control speakers could be mounted to the interior duct walls to produce a cancelling radiation pattern and attenuate the disturbance noise. It was identified that two rings of point control sources could be located to generate unidirectional plane wave motion such that the control noise would not interrract with the disturbance at the upstream location of the primary sensor (Swinbanks, 1972). The concept has since been enhanced by Chaplin (1979), who proposed inserting an error sensor downstream from the control region to provide error feedback and closed-loop control. Chaplin's system was the first duct noise cancellation system with adaptive signal processing

capability (Swanson, 1989).

Research in the 1980's emphasized attenuation of three-dimensional sound fields. Guicking et al.(1985) proposed coherent active control of sound fields for room acoustics applications. Simpson et al.(1989) have considered using spatially distributed microphone and loudspeaker systems for reducing aircraft cabin noise. Hesselman(1978) revisited the transformer noise control problem using multiple sensors and loudspeakers. Unfortunately, in all of these cases control benefits were only realized near the sensor locations.

Another ANC device that has recently been commercialized is a hearing protection system that was invented in 1953 and eventually patented in 1961 by Hawley and Simshauser (1961). The system, with a configuration quite similar to a that of a stereo headset, includes a microphone and speaker system at each earpiece. This system operates on the principle that incident sound is detected by the microphones, and countertones are produced and broadcast into the ear canals of the wearer to cancel the incident noise (Elmer-Dewitt, 1989). In 1958, RCA issued a report to the U.S. Army that the device was limited by current state of transducer technology and by difficulties in building amplifiers with sufficient phase reponse for stable noise cancellation in the region near the ear (Swanson, 1989). Once again, a useful concept was initiated long (in this case nearly 30 years) before the necessary electronics technology was available to enable its implementation.

Only recently - with the advent of compact, high-speed signal processing - have scientists and engineers had sufficient computing power to make practical antinoise

devices. Bose of Farmington, Mass., now manufactures and sells an antinoise headset for $965, and at least a half dozen other firms in the U.S. and Europe are selling antinoise systems. These companies include: two British firms, Racal Acoustics and Plessey; Digisonix, a division of Nelson Industries located in Stoughton, Wisconsin; Noise Cancellation Technologies of New York City; the DSP Group of Emeryville, California; and Active Noise and Vibration Technologies of Phoenix, Arizona (Elmer-Dewitt, 1989). Active noise control is becoming more than just a technology, but an entire industry in itself.

ANC depends on two basic physical effects for successful implementation: simple superposition and acoustic impedance coupling (Swanson, 1989). A system based on simple superposition alone is effective under two conditions: if the sound cancellation is to occur in a small region in space, or if the the sound waves propagate unidirectionally. For optimum global attenuation, the active control sources must be acoustically coupled with the noise source (Swanson, 1989).

Acoustic impedance coupling is possible when two sources are displaced less than one third of an acoustic wavelength from one another or where the two sources are connected by a waveguide. Coupled sources affect each other's ability to generate sound waves. With two coupled sources radiating in-phase, one source must overcome the pressure produced by the other, therfore producing more acoustic pressure than if it were radiating alone. If the two sources are radiating out-of-phase, their collective ability to produce acoustic pressure is greatly reduced, as one source radiates pressure outward and the other radiates inward. When the sources are less than one third of an acoustic wavelength apart, the air density surrounding them stays almost constant

and sound energy is readily decreased in the near-field. By controlling one source in a coupled system very precisely, active noise attenuation is possible by minimizing the radiation impedance for both sources (Swanson, 1989).

1.4 Active Structural Acoustic Control

The traditional approach to active noise control withinin an enclosed structure involves using a number of secondary sources arranged to generate a control sound field that interferes with the noise sound field, thereby reducing its sound levels. Disadvantages associated with this approach are the need for remote location of the control noise sources from the structure, and the inherent introduction of spillover noise from these sources. Control spillover may be overcome by careful placement of several additional control sources. A sound-radiating structure may require several active sources to achieve effective global noise reduction.

An alternative strategy was put forth for controlling enclosed sound fields by applying secondary vibration forces via shakers to the enclosure sidewall to couple the structure to the interior acoustic field (Mandic and Jones, 1989). This technique has been called "active vibration control", but distinction is needed from the conventional interpretation of the term, as the primary objective of the system in this case is to reduce interior noise levels by controlling structural vibrations, which does not necessarily mean reducing vibrational amplitudes (Fuller and Jones, 1987).

In this context, active vibration control involves modifying the vibrational response of a structure to reduce the important modes which most efficiently radiate acous-

tic energy (Jones, 1987). Rather than controlling the acoustic field, this approach controls the structural response. Essentially this shift of emphasis is a more direct method, which moves the control mechanism to the noise source: to the structure itself. Structural acoustic control is achieved by decoupling the motion of elastic structures from their radiated sound fields (Fuller et al.,1988). A distinction exists therefore between ANC and active structural acoustic control: active noise control involves controlling a sound field by producing counternoise; and active structural acoustic control involves controlling the dynamic response of a structure to reduce or minimize its source strength as an acoustic radiator.

Two radiating sources are acoustically coupled if they are displaced within one third of a wavelength from one another (Swanson, 1989). By applying control sources directly to a radiating structure, acoustic coupling will be automatically and unconditionally achieved between the structure and the control forces. The nature of this coupling enables improved controller design (Fuller et al., 1988). Jones (1987) captures the key mechanism of structural acoustic control in the following context:

> Intensity calculations at the [structural] wall indicated a reduction in intensity under controlled conditions. This implied that the control sources do not act as sinks but, in contrast, modify the acoustic space minimizing noise transmission into the cavity. In other words, the control system created a near zero pressure at the [wall] causing an impedance discontinuity and hence a reflection of a significant fraction of energy incident on the acoustic cavity.

An undesirable consequence of using point actuators is control energy spillover into

the uncontrolled structural modes (Jones and Fuller, 1987). Because of the interface modal filtering (IMF) effect - controlling only those modes which efficiently radiate sound into the control space - spillover energy is primarily confined to the structure, and does not contaminate the control field (Jones and Fuller, 1987). The point sources tend to be "spectrally white", so some control spillover is produced by this method of excitation. Also, mounting problems are forseeable with point force actuators, along with the fact that they add system mass and occupy space (Fuller et al., 1988).

Workers such as Hubbard et al. (1985), and Crawley et al. (1987) have researched the concept of utilizing piezoelectric actuators for vibration control, to overcome the problems of mounting and control spillover (Fuller et al., 1988). Wang et al.(1990) have analytically demonstrated the potential of utilizing multiple piezoelectric actuators to control sound radiation from a harmonically excited elastic panel. The use of induced strain actuators is driven by the ever-increasing number of applications for dynamic and static control of flexible structures. In a rational controlled structure design, the dependence of the control system on structural configuration is recognized in the early stages of the design process. Traditional types of actuators normally used for active structural control are not integral with the structure, but attached separately after construction. This may alter the dynamic behavior of the system. In contrast, induced-strain actuators are attractive because they can be integrated directly into the structure (Anderson, 1989).

The operating principle of piezoelectric sensors and actuators is that when pressure is applied to a piezoelectric material, an electric field is generated in response to modified charge distribution. This is called the direct effect, and it is by this capa-

bility that strain and vibration sensing tasks are possible using these materials. The converse effect can be manipulated by applying an electric field across the material, thereby inducing a strain transformation, in which the material expands or contracts in response to the applied voltage. This strain is induced both uniformly and in the plane normal to the direction of the applied voltage. The resulting expansion or contraction of the material is established by the polarity of the electrical field.

Using piezoelectric materials as induced strain actuators and integral sensors for active structural acoustic control offers numerous advantages. The dynamic response of the material is quick enough that structural vibration can be controlled at frequencies up to several KHz. Another capability of this material is its ability to increase structural damping: for example, Cudney (1989) found that the damping ratio of a tuned mode can be raised from 0.11% to 3.67% of critical damping. Perhaps the most appealing virtue is that the actuation and sensing functions can be built directly into the material, optimizing the control system capabilities by integrating the sensing and actuation functions directly into the structure.

1.5 Adaptive Structural Acoustic Control Using Shape Memory Alloy Hybrid Composites

Recently a novel class of adaptive materials, shape memory alloy (SMA) hybrid composites, was introduced by Rogers and Robertshaw (1988,ab). This material concept (shown in Fig. 1.1) consists of SMA actuator fibers embedded in a host material such as epoxy resin, fiberglass, graphite/epoxy or any other composite, plastic or matrix material (Liang et al., 1989). The embedded SMA fibers can be stiffened in a con-

SMA Fiber Reinforced Epoxy

Conventional Composite Lamina

Conventional Composite Lamina

Conventional Composite Lamina

Conventional Composite Lamina

Conventional Composite Lamina

Conventional Composite Lamina

SMA Fiber Reinforced Epoxy
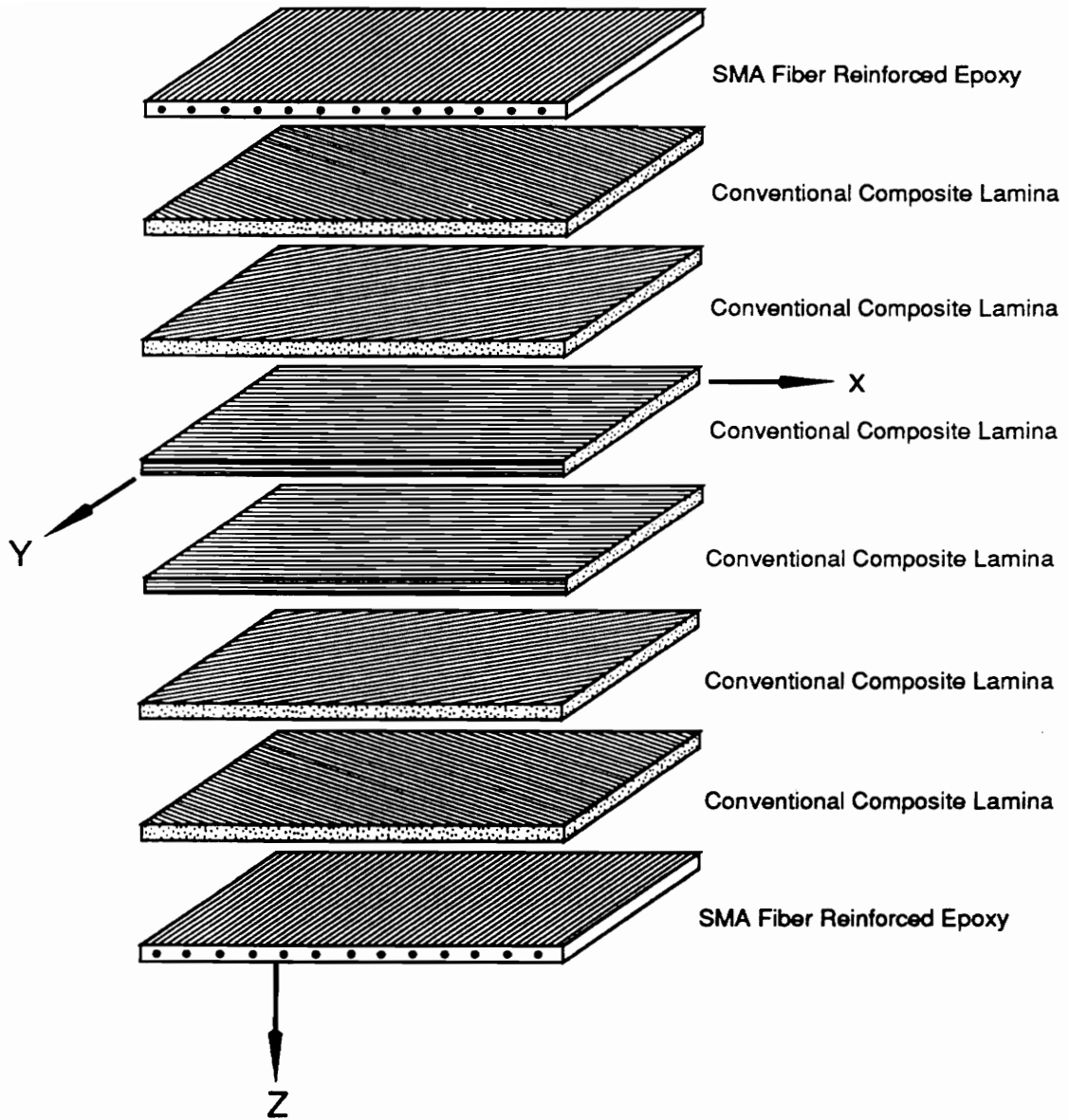
Figure 1.1: Example of an SMA Hybrid Composite Laminate

trolled manner by the addition of heat, which is usually achieved by passing electrical current through them (Rogers and Barker, 1990). When electrically activated, the elastic modulus of the SMA fibers can be increased up to 400 %, and control forces as high as hundreds of pounds, which are caused by thermally-induced martensitic phase transformation, can be generated within the structure.

Adaptive SMA hybrid composite laminates are fabricated by inelastcally elongating SMA fibers, embedding them in a host 'matrix' material, and curing the laminate at high temperatures to consolidate the matrix material. To prevent the SMA fibers from contracting to their 'normal' or 'memory' length, they must be longitudinally constrained prior to and during the cure process. When the cure cycle is complete, the SMA fibers adhere to (and thus are integrated into) the host matrix material. When the SMA hybrid composite is subsequently activated by passing electric current through the embedded SMA fibers, resistive heating causes reverse martensitic phase transformation in the SMA material, and the fibers 'try' to contract to their undeformed length. The SMA fibers are inhibited from contracting, however, because of interfacial shear stresses between them and the host material. It these shear stresses that enable the induced-strain actuation of SMA hybrid composites.

SMA hybrid composite structures can be locally or generally activated to modify their structural acoustic response and modal behavior. These control capabilities are explained by two mechanisms of adaptive structural tuning: active properties tuning (APT), and active strain energy tuning (ASET). The SMA fibers embedded in the material posess many unique properties and characteristics. Two of these characteristics; large increases of Young's modulus which occur when the material is

transformed from martensite to austenite, and the ability to recover large amounts of inelastic strain, are particularly useful for adaptive structural tuning.

Active properties tuning occurs as a result of elastic properties transformation in the SMA fibers due to martensitic phase transformation. For effective APT capability, Liang et al. (1989) recommend including a large volume fraction of SMA fibers in SMA hybrid composite structures. When electrically activated, the resulting phase transformation increases the elastic modulus of these fibers by as much as 400 %. The overall modification of laminate properties is directly proportional to the SMA volume fraction.

Active strain energy tuning is also triggered by thermally activated phase transformation; but another control variable is added: restoring stresses are applied when the embedded SMA fibers are thermally activated (Liang et al., 1989). To provide this capability, the SMA fibers are inelastically elongated and constrained in a fixture to prevent them from contracting while the host material is consolidated or cured at high temperatures. When activated, the SMA fibers 'try' to contract to their 'memory' length. The resulting internal stresses change the state of strain energy in the SMA hybrid composite material, modifying the modal response of the overall structure in a manner quite similar to the tuning of a guitar string, or much like variable stiffness of a human muscle (Liang et al., 1989).

By either APT or ASET, a significant amount of active structural tuning can be achieved using SMA hybrid composite materials (Rogers et al.,1989). The difference between these two structural tuning mechanisms is that by APT, the response of

a structure changes based on its material stiffness alone; by ASET, the distributed recovery forces of the inelastically pre-strained actuators alter the stiffness of the structure. With ASET, the properties transformation effects are also present, but when APT and ASET occur simultaneously, the combined tuning authority is usually due more to strain energy effects than elastic properties transformation (Liang et al., 1989).

Active structural acoustic control using SMA hybrid composites has been recently put forth as an application for this material. Since the natural frequencies and mode shapes of a structure can be actively modified by APT and ASET, it is possible to adaptively alter the acoustic coupling between an SMA hybrid composite panel, shell or beam structure and incident sound waves by activating the embedded SMA fibers. The active input is non-oscillatory in nature for an SMA hybrid composite structure, and the structure is adaptive in the sense that its properties and response can be altered by electrical inputs (Rogers, 1990ab).

The first results of analytical studies considering the active structural tuning of SMA hybrid composite panels were published by Rogers et al.(1988). In these studies, a thin, quasi-isotropic SMA hybrid composite panel was evaluated considering several states of spatially uniform activation. The results of this work show that by activating the fibers embedded in various ply combinations, the higher mode shapes can be altered, and the natural panel frequencies can be changed. These results are presented in Table 1.1 and Fig. 1.2. The demonstrated active modal modification capabilities can be effectively utilized for controlling the transmission of sound through SMA hybrid composite panel-like structures.

32

Simply supported plate structures radiate sound very efficiently when the modes shown in Fig. 1.3 are excited, because of the large volumetric fluid velocities they produce as a result of odd numbers of oscillatory lobes, and the large amplitudes of vibration which occur under structural resonance conditions. When the characteristic 1,1 mode is excited, the entire transverse panel motion occurs in one direction at any given time, and the net fluid displacement velocity on either side of the panel is very large. On the other hand, if the net volumetric fluid velocity is very small, the sound pressure level of the acoustic radiation to the far-field is low. For example, if a characteristic 2,1 mode is excited the vibrating lobes oscillate with equal amplitudes and opposite phase. As fluid on one of the panel surfaces is moved away from the panel by one lobe, the other lobe is drawing the same amount of fluid toward the structure. Rather than radiating high-intensity sound waves to the far-field, wave interaction reduces the radiated sound in the near-field. This phenomenon can also be explained by the concept of acoustic impedance coupling discussed in Section 1.3.

In addition to the structural acoustic control capabilities attainable by active mode shape modification, if a structure is resonating in an efficient sound-radiating mode, it can be adaptively tuned to vibrate off-resonance by changing its fiber activation. By this adaptive capability, vibration control and structural acoustic control benefits can be realized simultaneously. The results published by Rogers et al. (1990) show how sound radiation from a thin, simply supported, quasi-isotropic, SMA hybrid composite panel can be controlled below 1000 Hz by changing its state of activation. The first ten activated and unactivated natural frequencies are summarized in Table 1.2, and the transmission loss versus frequency plots are shown in Fig. 1.4.

33

Table 1.1: Natural Frequency Summary for a square [±45/0/90]$_s$ SMA Hybrid Composite Panel; after Rogers et. al., 1988

| Mode | Natural Frequencies (Hz) | | | | | |
| | Unactivated plate | Activated Plys | | | | |
		45°	−45°	0°	90°	all
1	20	111	119	113	124	225
2	49	179	192	120	132	358
3	50	180	193	143	157	358
4	80	233	249	190	208	456
5	99	263	281	227	250	511
6	99	264	281	234	258	512
7	129	305	326	253	277	587
8	129	312	330	260	285	588
9	167	360	382	287	315	674
10	168	360	382	345	378	676

34
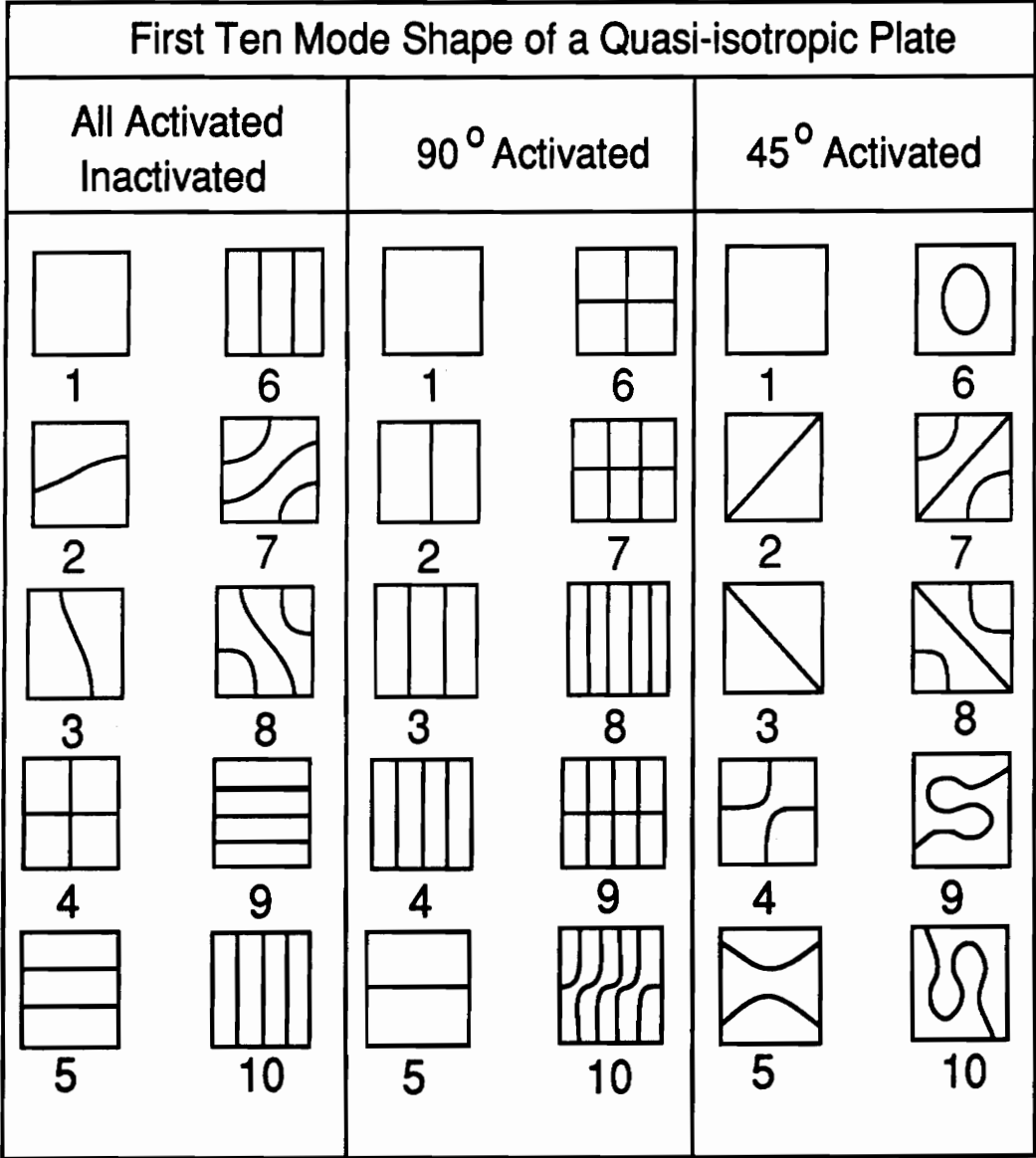
Figure 1.2: First Ten Mode Shapes for a square [±45/0/90]_s SMA Hybrid Composite Panel; after Rogers et. al., 1988
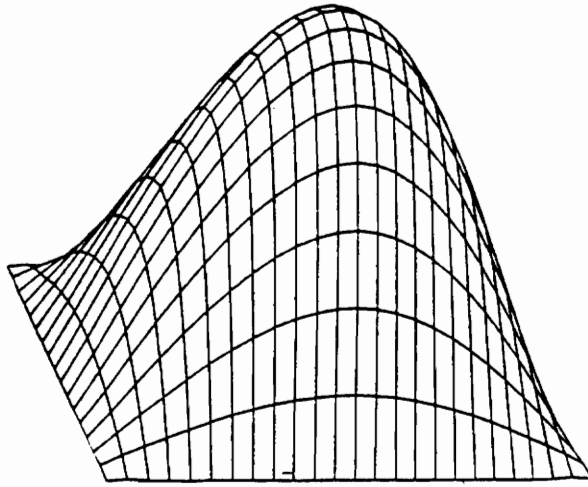
The Characteristic 1,1 Mode Shape
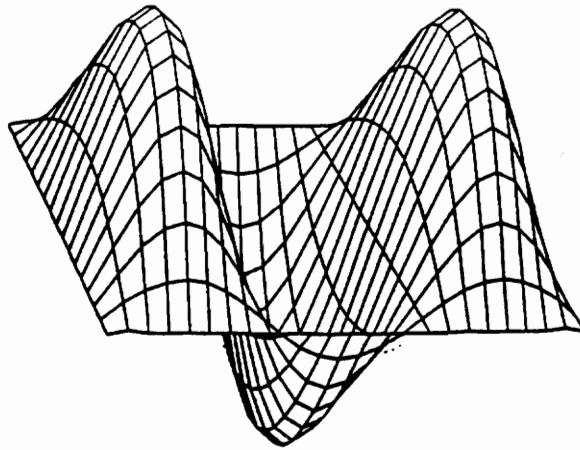
The Characteristic 3,1 Mode Shape

Figure 1.3: Efficient Sound-Radiating Mode Shapes

36

Experimental studies investigating the vibration and structural acoustic control of SMA hybrid composite beams have been done by Barker (1989) and Saunders et al.(1990). The results of Barker demonstrate that the first three natural frequencies of a clamped beam constructed from unidirectional SMA hybrid composite material (Fig. 1.5) can be actively modified. These experimental results are presented in Fig. 1.6. Saunders et al. (1990) used gradient search techniques to minimize sound radiation from a similar beam. The results of this study are presented in Fig. 1.7, and the experimental apparatus utilized for the experimental work of Barker is shown in Fig. 1.8.

The analytical and experimental results discussed in this section demonstrate useful vibration and structural acoustic control capabilities. These favorable results have prompted further investigation into the control capabilities attainable by considering localized activation of SMA hybrid composite panels. Specific objectives for this continued research are to determine a method of effectively modifying the first mode shapes of SMA hybrid composite panels, and identifying new activation strategies for controlling structurally-radiated low-frequency sound. These objectives, as well as the evaluation of physical trends and conditions which influence the adaptive structural tuning capabilities of SMA hybrid composite structures, constitute the central focus of this thesis.

Table 1.2: Natural Frequency Summary for a 0.8m by 1.1m $[0/\mp45/90]_s$ SMA Hybrid Composite Panel; after Rogers et al., 1990

Mode	Natural Frequencies (Hz)	
	Unactivated	Activated
1	41.3	71.5
2	82.8	129.7
3	114.8	146.6
4	144.4	203.4
5	166.9	239.6
6	224.0	246.9
7	233.7	296.5
8	245.5	322.4
9	290.7	355.4
10	317.9	403.5
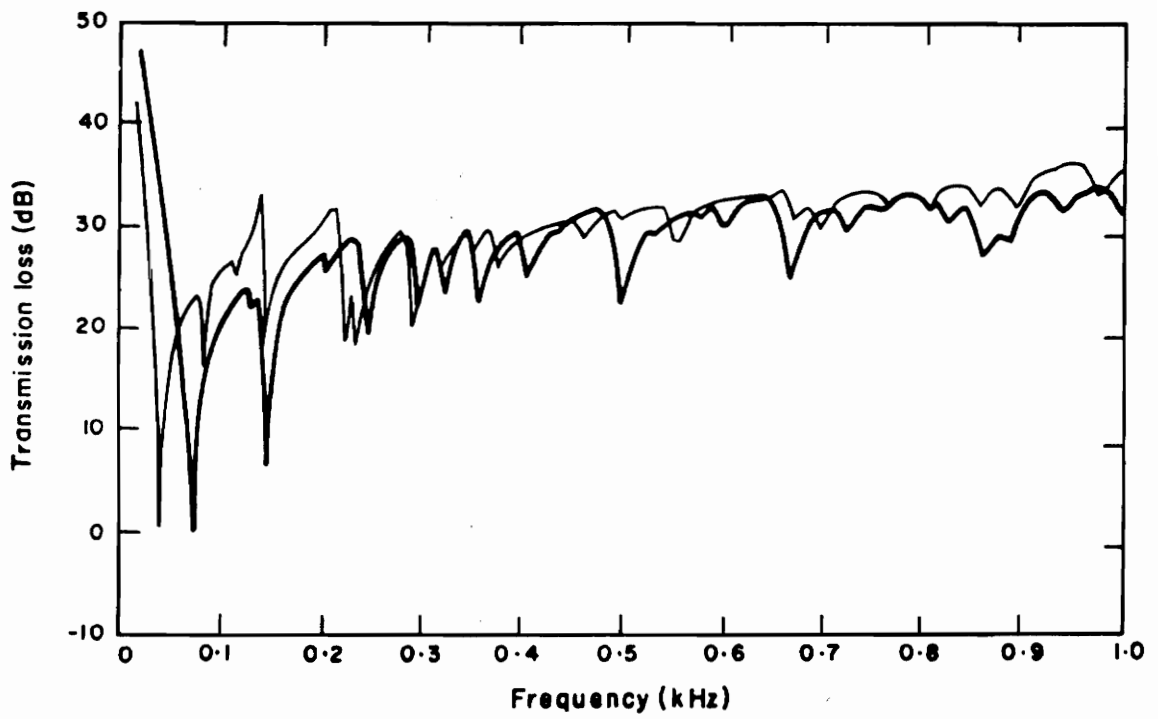
Figure 1.4: Transmission Loss Curves for a 0.8m by 1.1m [0/ ∓ 45/90], SMA Hybrid Composite Panel; after Rogers, Liang and Fuller, 1988

39

Specifications

Graphite epoxy: 5245 prepreg system

Dimensions: Length (L)   = 32.25 in (81.92 cm)
                                 Width (W)   = 0.860 in (2.18 cm)
                                 Spacing (S) = 0.031 in (0.79 mm)
                                 Thickness   = 0.034 in (0.86 mm)

No. of actuators   = 24 x .015 in dia
Nitinol volume fraction = 15%
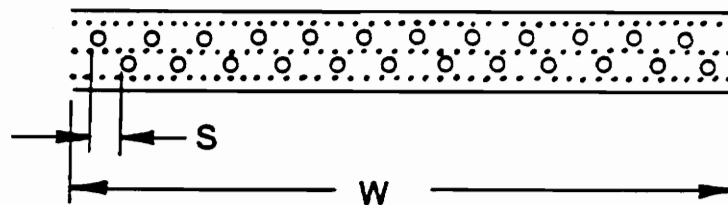
Figure 1.5: Experimental SMA Hybrid Composite Beam (Material Informaion); after Barker, 1989

FFT of Unactivated SMA Beam
vf=15%, free fibers, room temperature

FFT of Activated SMA Beam
vf=15%, free fibers, 300° F
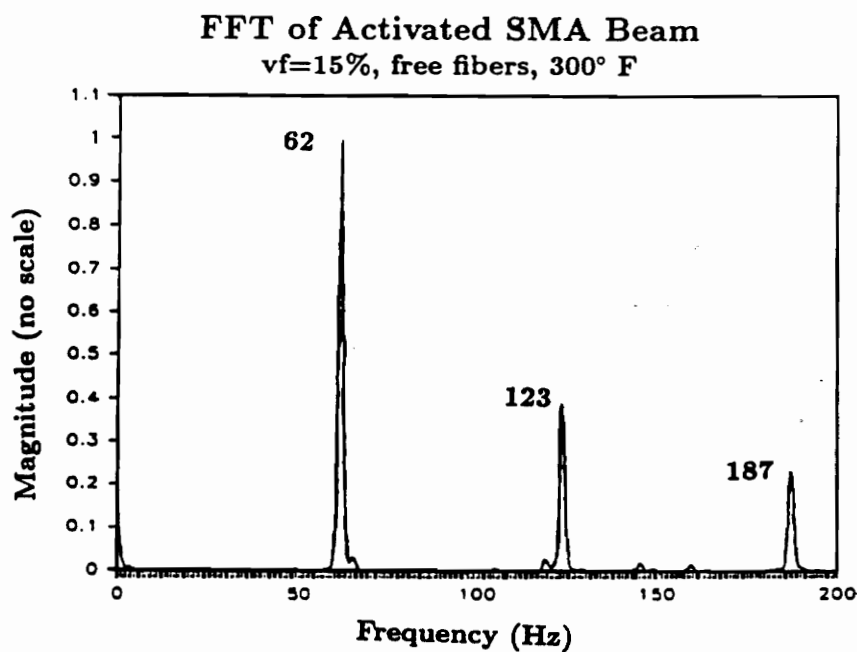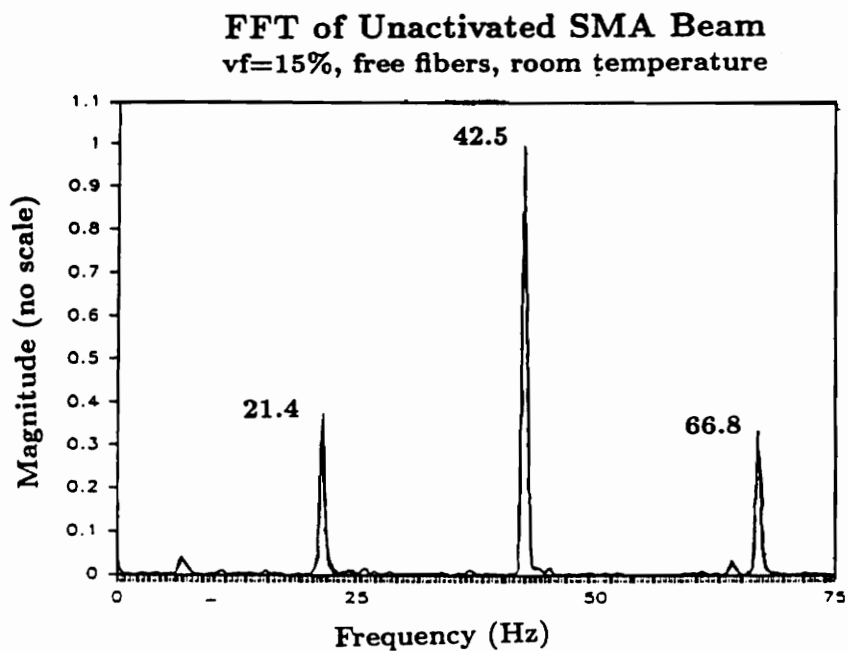
Figure 1.6: Experimental SMA Hybrid Beam Evaluation Results: Active and Unactivated First Three Natural Frequencies; after Barker, 1989

41
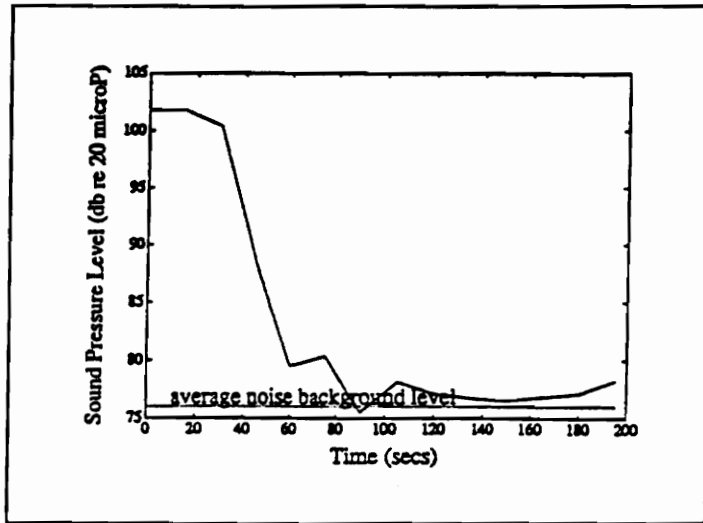
Controlled Sound Pressure (f_o=35 Hz)
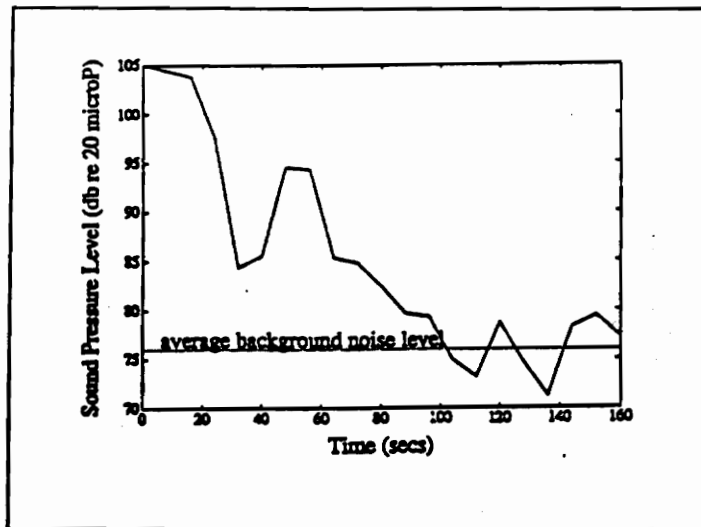
Controlled Sound Pressure (f_o=145 Hz)

Figure 1.7: Time History Plots for Experimental Studies of Beam Noise Minimization Technique; after Saunders et. al., 1990

42
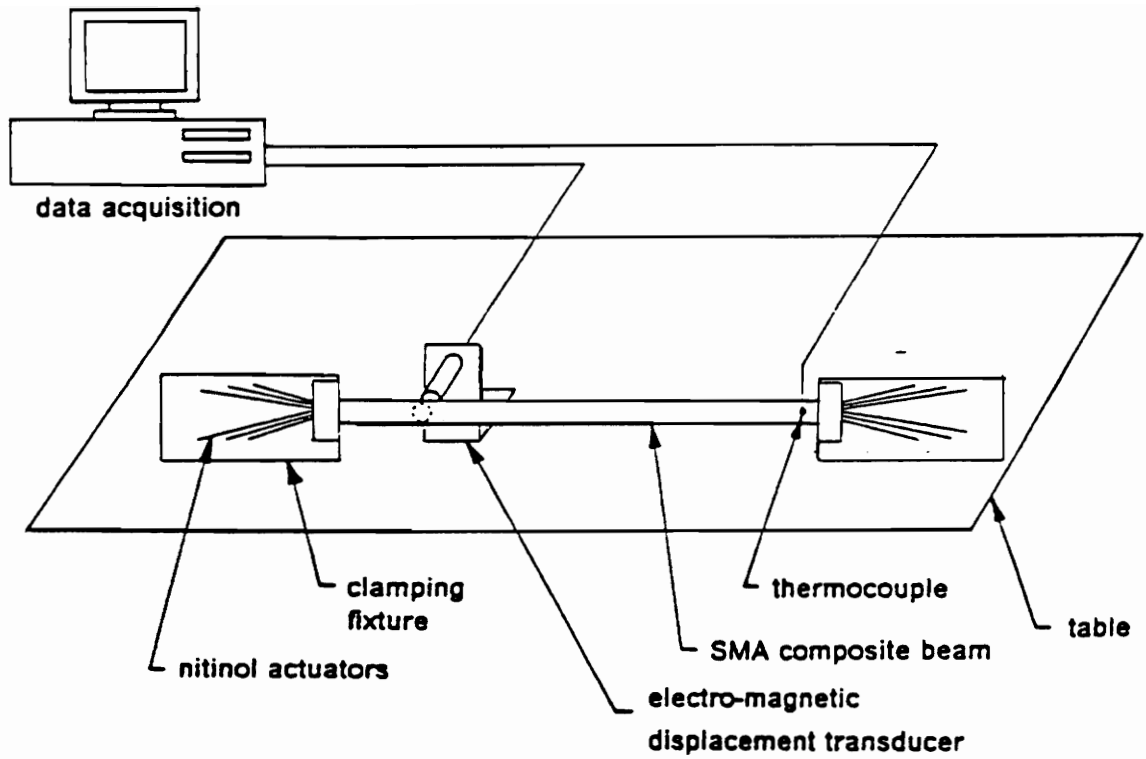
Figure 1.8: Experimental Apparatus for Evaluating SMA Hybrid Composite Beams; after Barker, 1989

43

Chapter 2

The Material Behavior of SMA Hybrid Composites

The structural tuning of an SMA hybrid composite structure is achieved by altering its material properties and state of internal strain energy in a controlled manner. Developing accurate analytical models to predict the dynamic and structural acoustic response of these structures requires a precise understanding of composite materials as well as shape memory alloys. The mechanical properties and the physical nature of martensitic phase transformation in shape memory alloys are subjects which require special attention. Section 1.5 provides a general description of how SMA hybrid composite materials and structures are fabricated and actively tuned. This chapter provides a more definitive explanation of shape memory alloys and discusses the key assumptions and theories utilized to model their elastic behavior. In the later sections of this chapter, the material behavior of SMA fibers is considered in conjunction with classical laminated plate theory to formulate the constitutive relations required for the analysis of SMA hybrid composite structures.

2.1 Shape Memory Alloys

Shape memory alloys have a unique ability to incur large inelastic strains at low temperatures, and return to their original shape when heated above a characteristic phase transformation temperature. This phenomenon is known as the shape memory effect. The shape memory effect was first discovered in 1938, when strain recovery capabilities were noted in Ni-Zn alloys (Hodgson, 1988). Many materials are presently known to exhibit the shape memory effect, including the copper alloy systems of Cu-Zn, Cu-Zn-Al, Cu-Zn-Ga, Cu-Zn-Sn, Cu-Zn-Si, Cu-Al-Ni, Cu-Au-Zn, Cu-Sn, the Au-Cd, Ni-Al, Fe-Pt, alloys and others. The most common - and to date the most useful - of the shape memory alloys or transformation metals is the nickel-titanium alloy known as Nitinol (Rogers et al., 1989).

Nitinol

In 1965, Buehler and Wiley of the U.S. Naval Ordnance Laboratory were granted a United States Patent on a series of engineering alloys that possess a unique mechanical (shape) "memory" capability (Beuhler and Wiley, 1965). The generic name given to this series of alloys is 55-Nitinol. These alloys have chemical compositions ranging from 53 to 57 weight percent nickel. A great deal of effort was spent over the next ten years to characterize the material and develop new applications to exploit its remarkable shape memory effect (SME) and its unique mechanical properties. The Naval Ordnance Laboratory (now known as the Naval Surface Warfare Center) was then (and still is) the leader in characterizing Nitinol. Several other laboratories have significantly contributed to understanding the characteristics of Nitinol, particularly

Battelle Memorial Institute and NASA (Barker, 1989).

Nitinol alloys of proper composition exhibit unique mechanical "memory" or restoration force characteristics. The name is derived from Ni (NIckel) - Ti (TItanium) - NOL (Naval Ordnance Laboratory). The shape recovery capability of Nitinol is phenomenal. The material can be inelastically deformed in its low-temperature martensite phase and then restored to its original configuration by heating it above its martensitic phase transformation temperature. This behavior is unique to NiTi alloys having near-equiatomic composition. Plastic strains of six-to-eight percent may be fully recovered by heating the material to transform it to its austenite phase. Restraining the material to prevent it from returning to its memorized shape during reverse martensitic phase transformation can induce recovery stresses as large as 100,000 psi (Rogers et al., 1989). Due to these noteworthy material characteristics, nitinol has been considered for all SMA hybrid composite applications to date. The analytical studies of this thesis consider only nitinol as the embedded induced-strain actuators; however the same mechanical models apply for all SMA materials.

The Shape Memory Effect

The shape memory effect can be simply described as follows: an SMA specimen in its low-temperature martensite phase, when inelastically deformed with the external stresses removed will regain its original (memory) shape when heated. This shape recovery process (shown schematically in Fig. 2.1) occurs as the result of a thermally triggered reverse martensitic phase transformation.
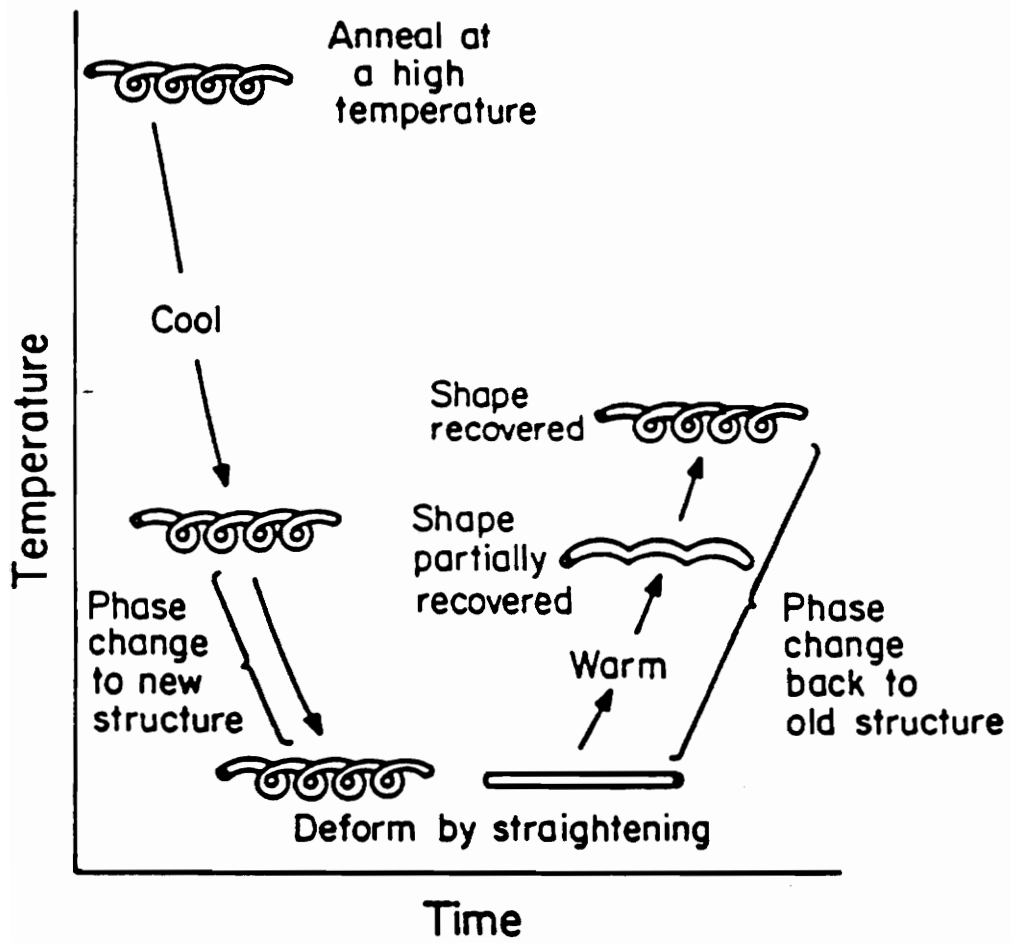
Figure 2.1: The Shape Recovery Process; after Barker, 1989

47

The process of strain recovery is associated with a reverse transformation from the deformed martensite phase to the higher temperature austenite phase (Rogers et al., 1989). As this phase transformation occurs, shape memory alloys undergo changes in their crystalline structure. Below its transformation temperature, nitinol exists primarily in a monoclinic martensite phase. Above this temperature, the material tends to exist in an ordered-cubic austenite phase. The phase transformation of nitinol is shown schematically in Fig. 2.2. The mechanism by which forward and reverse martensitic phase transformation in nitinol occurs is the natural tendency of the material to adjust to temperature changes in order to become thermodynamically stable (Barker, 1989).

Because of the twinned structure of the monoclinic crystalline lattice of martensitic nitinol, phase transformation to and from the ordered cubic austenite structure involves simple shear motion in the form of bond rotations between adjacent atoms. General diffusion, which involves much more atomic rearrangement, is usually required for phase transformation in other alloys. Hence, martensitic phase transformation of nitinol is relatively easy to produce. Referring to Fig. 2.2, the strain recovery of nitinol requires simple shear motion between adjacent atoms to establish thermodynamic equilibrium. In its martensite phase, nitinol has a unique ductility characteristic by which large amounts of inelastic material deformation (up to about 8% strain) can be sustained, whereby adjacent atoms shift without dislocating relative to one another within their monoclinic crystalline lattice structure. Excessive strain in the material can cause diffusion, where the atoms dislocate relative to one-another such that a new state of strain is established to achieve a minimum state of total energy when the material is thermally excited above its phase transformation

48
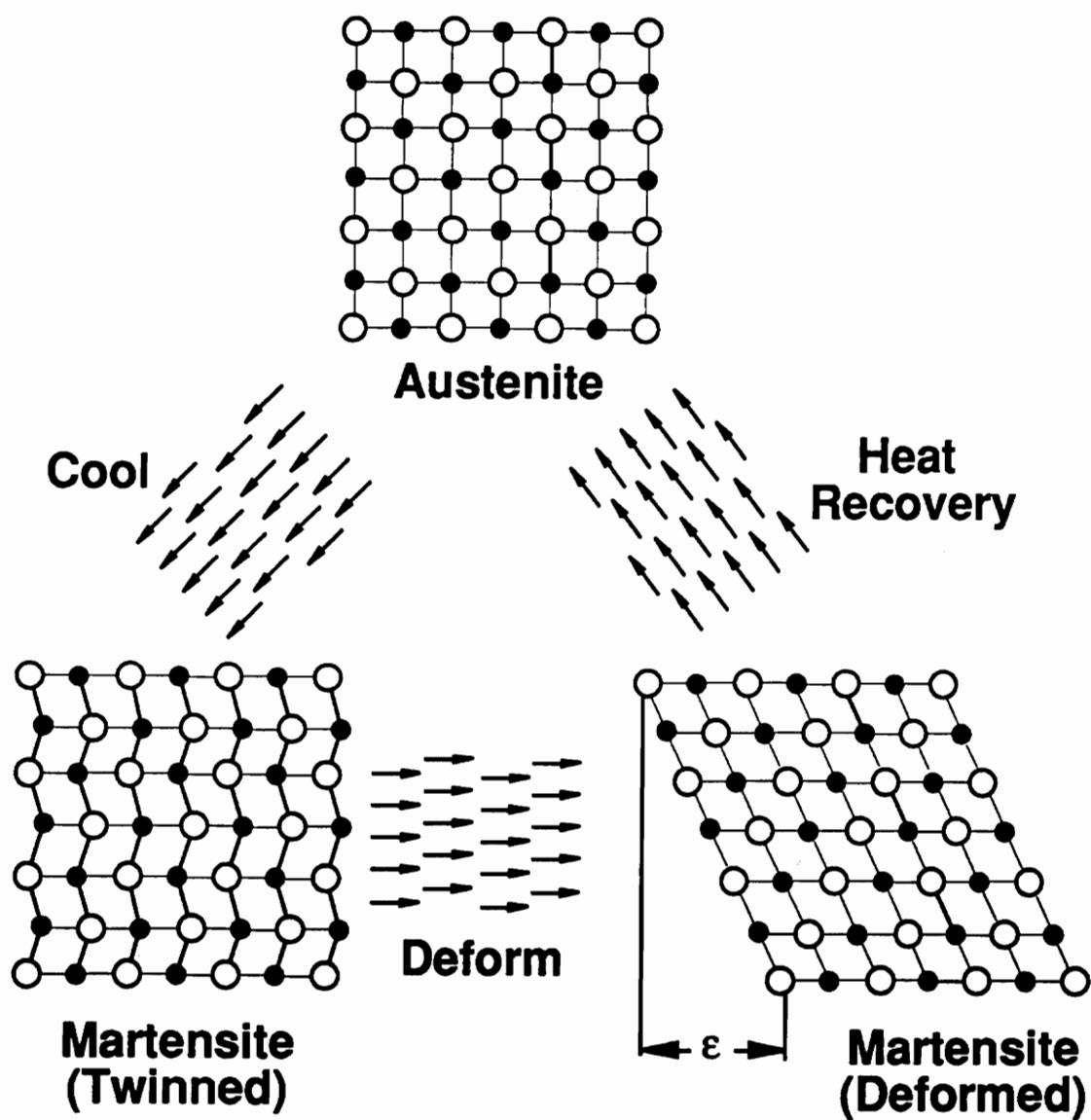
Figure 2.2: Martensitic Phase Transformation of Nitinol; after Hodgson, 1988

temperature.

Straining the material in its high temperature austenite phase can induce martensitic phase transformation with a state of stress present throughout the material, which thermodynamically 'prefers' the austenite phase (Barker, 1989). In this condition, commonly referred to a strain-induced martensite, a restraining force is required to prevent the material from returning to its austenitic state and 'memorized' geometrical configuration.

When a nitinol specimen is inelastically deformed, restrained, and subsequently heated, the crystalline lattice structure attempts to shift from its monoclinic configuration to an ordered cubic arrangement, which is more thermodynamically stable above the phase transformation temperature. If the material is constrained from deforming, a state of induced strain occurs accompanied by mechanical recovery stress. The thermodynamic material response is altered by the presence of strain energy in this situation. The intermolecular forces which drive this attempted phase transformation are of sufficient magnitude that the material does not yield, and the energy balance in the material is established by the resulting state of strain energy rather than phase transformation or yielding.

Summarizing the previous paragraph, when a shape memory alloy component is inelastically deformed from its 'memorized' geometry and heated above its phase transformation temperature, two mechanical reactions may be observed. If the specimen is unconstrained, it will return to its memory shape if the initial deformation has not dislocated the atoms in the material lattice structure. If constrained, a state of

internal recovery stress occurs.

The shape recovery process generally falls into one of the following three categories. *Free recovery* occurs when there is no external load applied to the material and therefor no work is done, and no internal restoring stress is generated. For *fully restrained recovery*, the martensitic residual strain is prevented from being restored as the material is physically constrained from returning to its memory length. This process produces high levels of recovery stress in the material. *Controlled recovery* occurs when some residual martensitic strain is restored, but the material sustains some residual stress that is required to prevent full strain recovery (Liang and Rogers, 1990).

The amount of recovery stress in an SMA material specimen depends on the amount of inelastic strain incurred by the material in its martensite phase, and the temperature of the material in its heated condition. Figure 2.3 shows how this recovery stress varies with temperature for several levels of initial strain. The analyses of this thesis consider initial strain magnitudes of 5% and $250°F$ activation temperatures, which corresponds to activation-induced SMA fiber recovery stress levels of approximately 50 ksi.

Along with the changes of atomic structure and states of mechanical stress and strain, shape memory alloys also undergo significant changes in electrical resistivity, mechanical damping, stiffness, and thermal conductivity (Barker, 1989). Mechanical stiffness increases as reverse martensitic transformation occurs in nitinol. The Young's modulus and yield strength versus temperature for nitinol are shown in Fig. 2.4. The
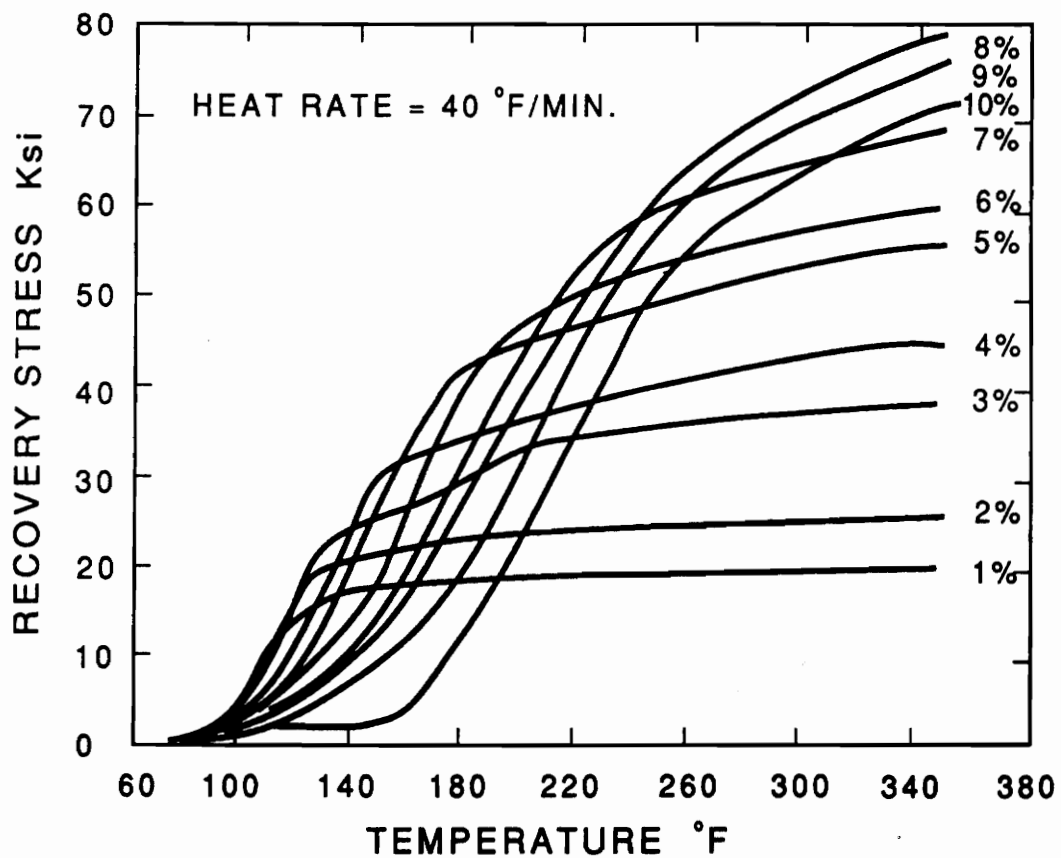
Figure 2.3: Nitinol Tensile Recovery Stress Variation with Initial Strain and Temerature; after Cross et al., 1969

Young's modulus can increase by up to 400 % as the material transforms from its low temperature martensite phase to its higher temperature austenite phase, and the yield strength can be increased by an order of magnitude.

2.2   The Mechanical Behavior of Shape Memory Alloy Fibers

Fabricating SMA hybrid composites requires inelastically elongating SMA fibers, embedding them in a host matrix material and curing or consolidating the composite at high temperatures. The cure cycle establishes interfacial bonding between the host material and the SMA fibers, which restrains the SMA fibers from returning to their 'memory' length when subsequently activated. In their activated condition, the fibers are subjected to a restrained recovery process; where large recovery stresses occur in the SMA fibers as they 'try' to contract to their memorized length, but are physically prevented from doing so. To accurately model the active tuning of SMA hybrid composite structures, the mechanical behavior of the SMA fibers must be understood.

Two approaches exist for determining the material behavior for SMA materials. One method is simply to measure how the material responds under a particular set of conditions. This approach, known as the macroscopic phenomenological method, is utilized for the analyses of this thesis. By considering the experimental data of Figs. 2.3 and 2.4, the material properties of Table 2.1 have been estimated for activated and unactivated SMA fiber conditions. These conditions correspond to 5% initial strain, $25°C$. unactivated reference temperature, and $104°C$ activation temperature.
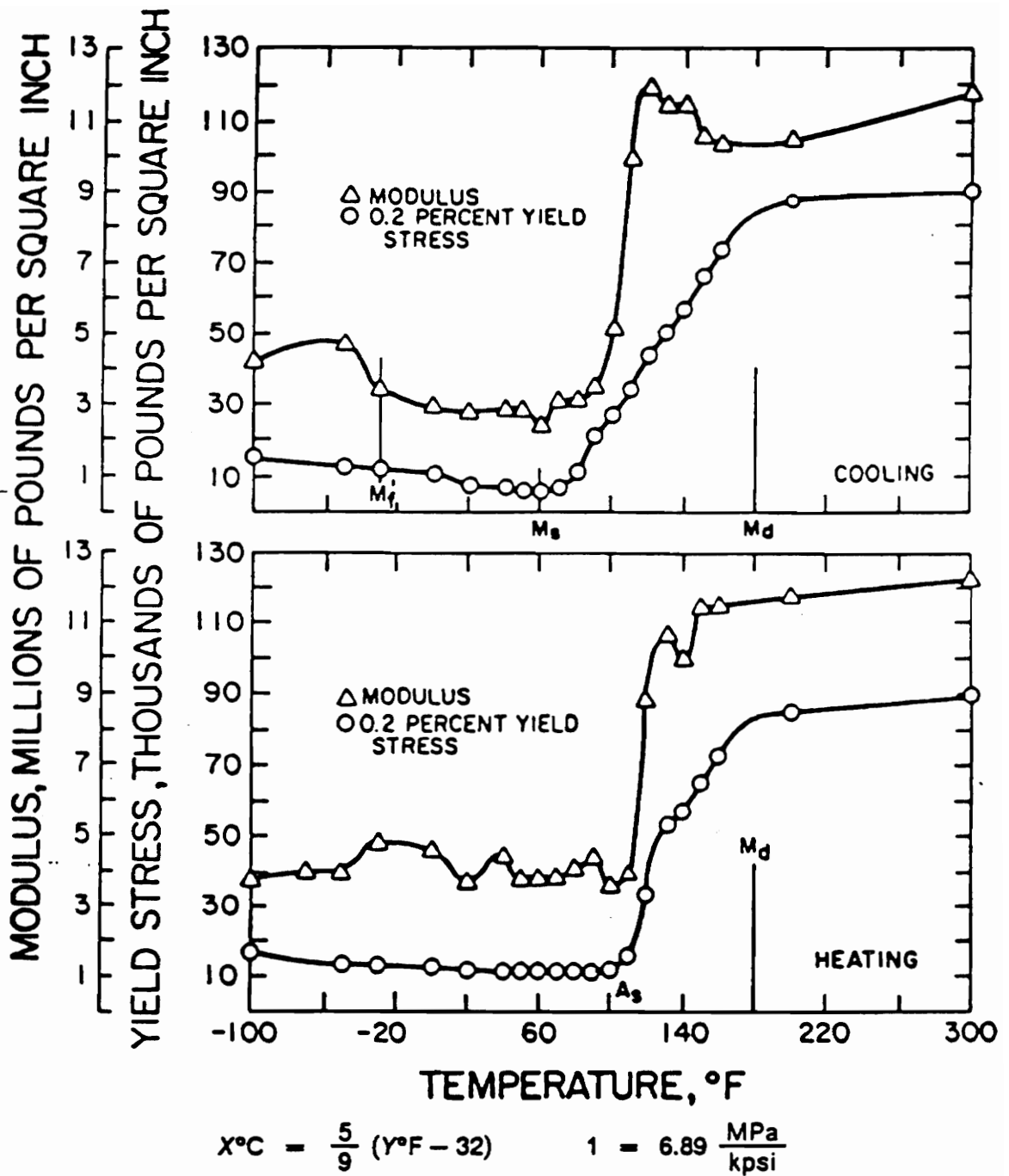
Figure 2.4: Yield Strength and Young's Modulus versus Temperature for Nitinol; after Cross et al., 1969

Table 2.1: Activated and Unactivated Material Properties of Nitinol

Unactivated Embedded Nitinol Fiber	
Temperature	$25°C$.
Phase	martensite
Young's Modulus	4 Msi (28 GPa)
Recovery Stress	0 Ksi
Activated Embedded Nitinol Fiber	
Temperature	$104°C$.
Phase	austenite
Young's Modulus	12 Msi (82 GPa)
Recovery Stress	50 Ksi (344.5 MPa)

Another method for predicting the elastic behavior of the embedded SMA fibers is the microscopic physical approach that derives the constitutive model from fundamental physical concepts. The macroscopic phenomenological approach is used most often in engineering practice; however, it can rarely explain the physics governing the material behavior. The microscopic physical method can successfully provide fundamental explanations to different experimental phenomena; however, its numerical predictions and simulations are often complex and seldom yield useful engineering or design relations (Liang and Rogers, 1990).

One key difference between the macroscopic phenomenological and microscopic physical approaches to estimating the material response of nitinol is that the latter approach considers the simultaneous occurrence of the martensite and austenite phases during the forward and reverse martensitic phase transformation processes; whereas the former only considers specific state-dependent effects. As shown in Fig. 2.5, these phase transformations are characterized by four temperature parameters when strain recovery occurs in a stress-free condition. These characteristic temperatures are defined as M_f, the martensite finish temperature; M_s, the martensite start temperature; A_s, the austenite start temperature; and A_f, the austenite finish temperature (Liang and Rogers, 1990).

When a martensitic nitinol wire is heated through a phase transformation; as the material is heated above A_s, its crystal structure begins to shift to the ordered cubic austenitic phase. The martensite volume fraction reduces as the temperature is increased to A_f, at which point the martensite volume fraction reaches zero, meaning the material has completely transformed to austenite. This process is denoted as:
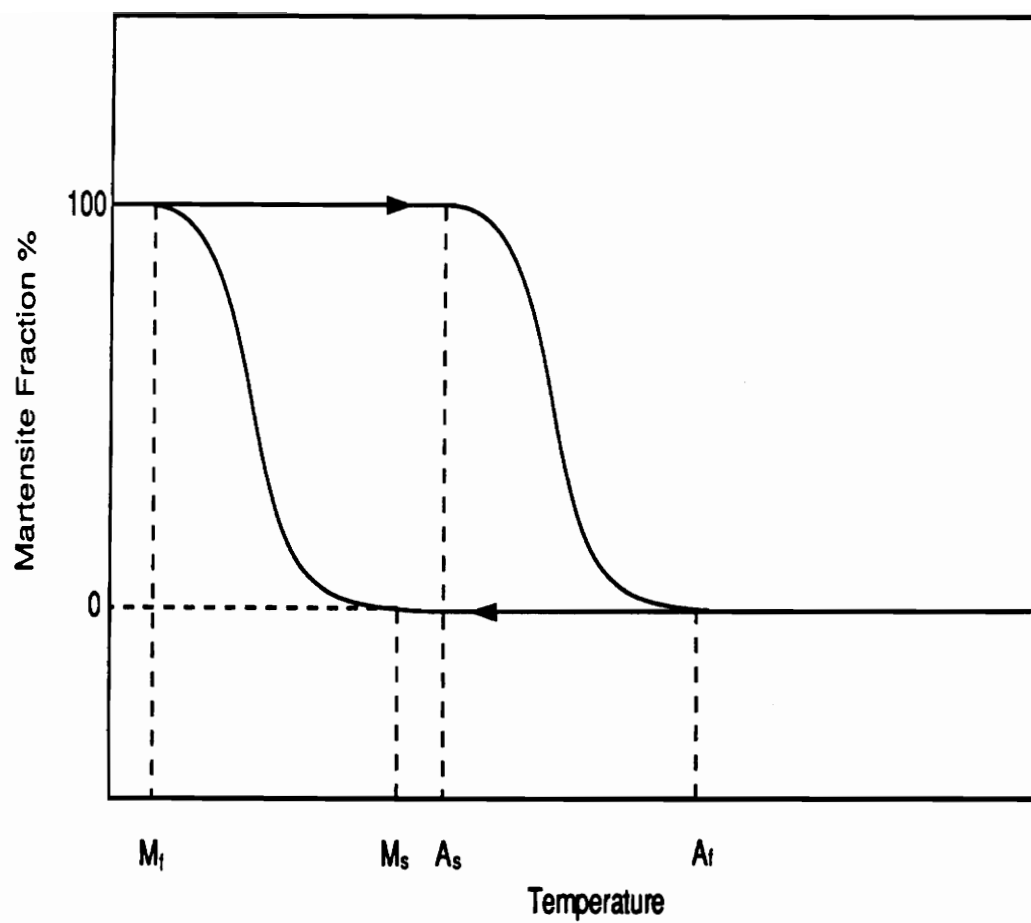
Figure 2.5: Martensite Fraction versus Temperature; after Liang and Rogers,1990

$M \rightarrow A$. When an austenitic nitinol wire cools through reverse phase transformation; as the material temperature decreases to M_s, its crystal structure begins to shift to the monoclinic martensite phase. The austenite volume fraction reduces with temperature until M_f is reached, at which point the austenite volume fraction reaches zero, thus the material has completely transformed to martensite. This process is denoted as: $M \leftarrow A$.

The internal strain energy and elastic properties of nitinol (and SMA materials in general) have been found to vary significantly with stress, strain, temperature, and the amount of phase transformation. Only three of these state variables vary independently; therefore the thermodynamic state of an SMA material can be defined as a function of strain, temperature and ξ_m, the martensitic volume fraction (Liang and Rogers, 1990). The one-dimensional model used to model the stress-strain and shape memory effect is given as

$$\sigma_r - \sigma_0 = D(\varepsilon_r - \varepsilon_0) + \Omega(\xi - \xi_0) + \Theta(T - T_0) \tag{2.1}$$

Where Θ, Ω, and D are the thermoelastic tensor, transformation tensor, and elastic tensor, respectively. For restrained recovery, this equation reduces to

$$\sigma_r - \sigma_0 = \Omega(\xi - \xi_0) + \Theta(T - T_0). \tag{2.2}$$

since the strain remains constant. Also, the unactivated recovery stress is zero for the

58

nitinol fibers in the SMA hybrid composite; therefore $\sigma_0 = 0$, and Eq.(2.2) reduces to

$$\sigma_r = \Omega(\xi - \xi_0) + \Theta(T - T_0). \tag{2.3}$$

For this consideration, the material, when heated to A_s, does not exert any recovery stress. The martensite volume fraction remains constant from A_s through A_f. Essentially very little change is noted in the structure below A_s; hence T_0 can be assumed to equal A_s. At this point, only two unknowns remain to be evaluated for determining recovery stress: ξ and ξ_0. The initial martensite volume fraction, ξ_0 can be determined with the aid of Fig. 2.6 and the following equation:

$$\xi_0 = \frac{\varepsilon_{res}}{\varepsilon_l} \tag{2.4}$$

also, since the fiber is considered to be longitudinally constrained, and the $A \leftarrow M$ transformation has recovered its maximum amount of strain, longitudinal molecular motion ceases, and the martensitic volume fraction does not change with respect to temperature. Hence:

$$\xi = \frac{\varepsilon_r}{\varepsilon_l} \tag{2.5}$$

Thus the recovery stress for an activated SMA fiber embedded in a composite structure can be simply determined by considering the austenite start temperature, the activation temperature and a thermoelastic constant. This final relationship is:

$$\sigma_r = \Theta(T - T_0). \tag{2.6}$$
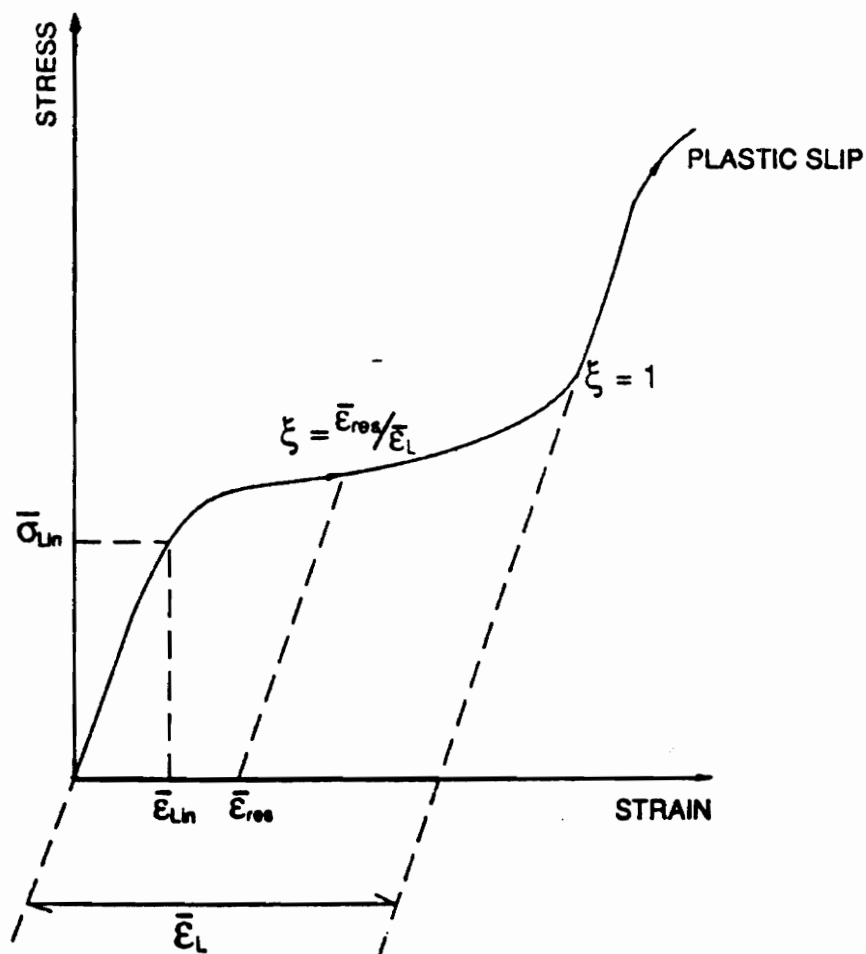
Figure 2.6: Typical Stress-Strain Relationship of an SMA Fiber; after Liang and Rogers, 1990

60

2.3 Constitutive Relations

Stress-strain relations are developed in Section 2.2 for the one-dimensional case. A complete description of these constitutive relations is given by Liang (1990). In this section, the rule of mixtures is used to determine the elastic behavior of an SMA hybrid composite lamina in an arbitrary orientation.

Assumptions

There are three basic assumptions used in the following formulations:

1. The shape memory alloy fibers (actuators) are inelastically elongated before being embedded in the 'matrix'. After the curing process, the external mechanical strain on the material system does not exceed the 'new' elastic limit of the SMA fibers.

2. The SMA and 'matrix' are perfectly bonded together, resulting in strain compatibility across the interfacial boundaries between these fibers and the matrix material.

3. The activation temperature of the fiber is small and does not influence the temperature of the overall material system, thereby resulting in negligible thermal expansion of the matrix material.

Some of these assumptions may in fact prove to be inappropriate for certain applications. For instance, the thermal expansion effects addressed in the third assumption above could very well prove to significantly influence the mechanical behavior of SMA

hybrid composites structures.

Stress-Strain Relationships

Figure 2.7(a) shows the SMA actuator-matrix substructure to be modeled. The stress-strain relations for this substructure containing a single SMA fiber actuator embedded in a matrix will be developed. In Figure 2.7(b), the stresses in a cross section of the substructure are shown. The stress in the matrix, σ_m, is generated by two sources: external forces and the activation-induced SMA fiber recovery stresses. The stresses, σ_r, in the SMA actuators are also induced by two sources, the external mechanical loads and the constriction of the matrix material resulting from fully restrained, activation-induced recovery.

The resultant force in the substructure cross section may be defined as:

$$F = A_m \sigma_m + A_a \sigma_r \tag{2.7}$$

and the average normal stress as

$$\sigma = v_m \sigma_m + v_a \sigma_r. \tag{2.8}$$

The stress-strain relationship derived for the SMA actuators and the linear-elastic 'matrix' components are expressed as

$$\varepsilon = \frac{\sigma_a}{E_a} - \varepsilon_r = \frac{\sigma_m}{E_m}, \tag{2.9}$$

62
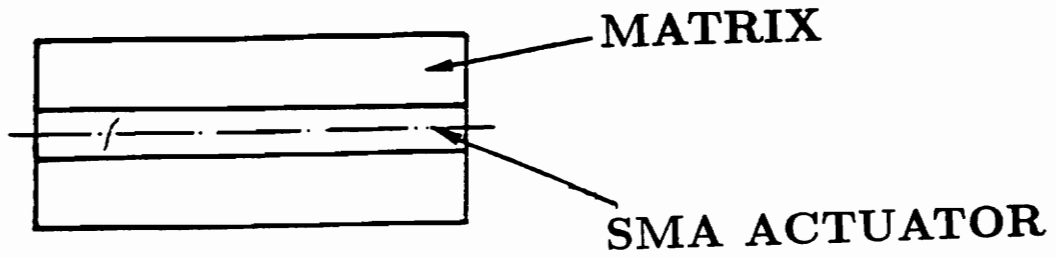
Figure 2.7 a; Actuator-matrix Substructure
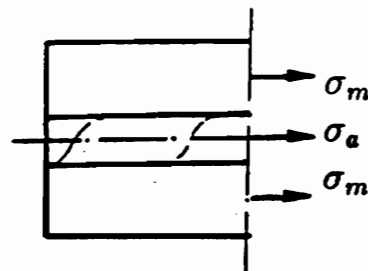
Figure 2.7 b; Cross-sectional Stresses

Figure 2.7: SMA Hybrid Composite Substructure and Cross-sectional Stresses

$$\varepsilon = \frac{\sigma_m}{E_m}. \tag{2.10}$$

The stress-strain relationship for the SMA-matrix system is formulated by substituting Eqs.(2.9) and (2.10) into Eq.(2.8) resulting in

$$\sigma = (v_a E_a + v_m E_m)\varepsilon - v_a \sigma_r, \tag{2.11}$$

This one-dimensional model describes the stress-strain behavior of the actuator-matrix material system in the 'fiber-direction'. This model may then be extended to consider an orthotropic lamina by first referring to the one-dimensional model as predicting the behavior of the lamina in the principal (fiber) direction.

2.3.1 Properties of a Lamina

One of the fundamental needs in formulating a model describing the behavior of an SMA hybrid composite lamina is an appropriate micromechanical constitutive relationship. For this work, the micromechanical law used is the rule of mixtures. Any micromechanical model could be used for future work involving the elastic behavior of SMA hybrid composites; however, the rule of mixtures relates the global mechanical properties of the lamina to its two constituents, namely, the SMA actuators and the 'matrix'. From the rule of mixtures (Jia and Rogers, 1989),

$$
\begin{aligned}
E_1 &= E_{1_m} v_m + E_a v_a \\
E_2 &= \frac{E_{2_m} E_a}{v_m E_a + v_a E_{2_m}} \\
\nu_{12} &= \nu_{12_m} v_m + \nu_a v_a
\end{aligned}
\tag{2.12}
$$

$$G_{12} = \frac{G_{12_m} G_a}{v_m G_a + v_a G_{12_m}}$$

$$\rho = \nu_m \rho_m + \nu_a \rho_a$$

Where E_a is the Young's modulus of the SMA material. Based on these relations, the temperature- and strain-dependent compliance matrix can be written:

$$[S] = \begin{bmatrix} S_{11} & S_{12} & 0 \\ S_{12} & S_{22} & 0 \\ 0 & 0 & S_{66} \end{bmatrix} \tag{2.13}$$

in which

$$S_{11} = \frac{1}{E_1}$$

$$S_{12} = -\frac{\nu_{12}}{E_1} = -\frac{\nu_{21}}{E_2} \tag{2.14}$$

$$S_{22} = \frac{1}{E_2}$$

$$S_{66} = \frac{1}{G_{12}},$$

and the stiffness matrix can be written

$$[Q] = \begin{bmatrix} Q_{11} & Q_{12} & 0 \\ Q_{12} & Q_{22} & 0 \\ 0 & 0 & Q_{66} \end{bmatrix} \tag{2.15}$$

where

$$Q_{11} = \frac{E_1}{1 - \nu_{12}\nu_{21}}$$

$$Q_{12} = \frac{\nu_{12} E_2}{1 - \nu_{12}\nu_{21}} \tag{2.16}$$

$$Q_{22} = \frac{E_2}{1 - \nu_{12}\nu_{21}}$$

$$Q_{66} = G_{12}$$

Considering the lamina properties above, and the stress-strain relations of the previous section, the two-dimensional constitutive relationship can be written for an orthotropic SMA hybrid composite lamina:

$$\left\{ \begin{array}{c} \sigma_1 \\ \sigma_2 \\ \tau_{12} \end{array} \right\} = \left[\begin{array}{ccc} Q_{11} & Q_{12} & 0 \\ Q_{12} & Q_{22} & 0 \\ 0 & 0 & Q_{66} \end{array} \right] \left\{ \begin{array}{c} \varepsilon_1 \\ \varepsilon_2 \\ \gamma_{12} \end{array} \right\} + \left\{ \begin{array}{c} v_a \sigma_r \\ 0 \\ 0 \end{array} \right\}. \tag{2.17}$$

The above equations apply to the principal material coordinate system, in which the fibers are oriented parallel to the 1-axis, and prependicular to the 2-axis, as shown in Fig. 2.8. For cases in which the geometric and material coordinate systems are rotated relative to one another, the following relationship applies; such that when several plies with varying fiber orientation are bonded together to produce a laminate, the stress-strain relations for all plies can be expressed in terms of stress and strain components in a single global coordinate system. In the following formulations, θ is the angle of rotation between the global and material coordinate systems for a single orthotropic layer (or lamina).

$$\left\{ \begin{array}{c} \sigma_x \\ \sigma_y \\ \tau_{xy} \end{array} \right\} = \left[\begin{array}{ccc} \overline{Q}_{11} & \overline{Q}_{12} & \overline{Q}_{16} \\ \overline{Q}_{12} & \overline{Q}_{22} & \overline{Q}_{26} \\ \overline{Q}_{16} & \overline{Q}_{26} & \overline{Q}_{66} \end{array} \right] \left\{ \begin{array}{c} \varepsilon_x \\ \varepsilon_y \\ \gamma_{xy} \end{array} \right\} + \left\{ \begin{array}{c} \sigma_{xr} \\ \sigma_{yr} \\ \tau_{xyr} \end{array} \right\} \tag{2.18}$$
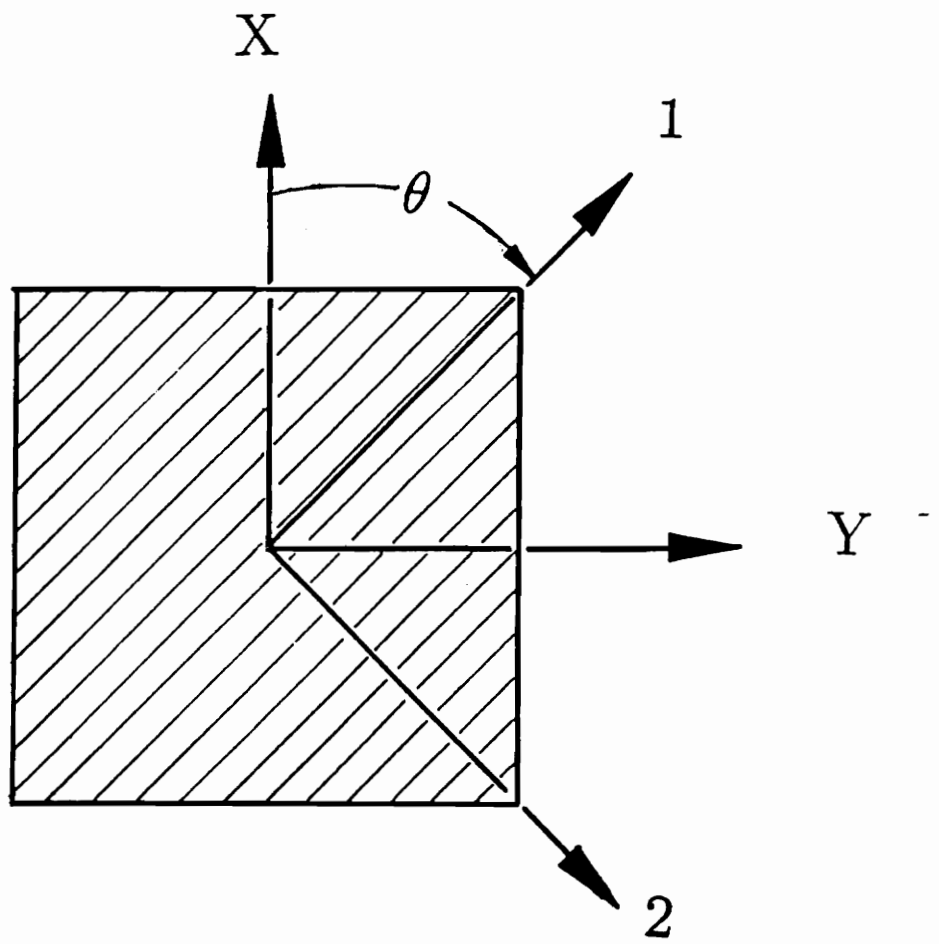
Figure 2.8: Material and Global Coordinate Systems

where by stress and strain tensor transformations (Jones, 1975)

$$
\begin{aligned}
\overline{Q}_{11} &= Q_{11}\cos^4\theta + 2(Q_{12}+2Q_{66})\sin^2\theta\cos^2\theta + Q_{22}\sin^4\theta \\
\overline{Q}_{12} &= (Q_{11}+Q_{22}-4Q_{66})\sin^2\theta\cos^2\theta + Q_{12}(\sin^4\theta+\cos^4\theta) \\
\overline{Q}_{22} &= Q_{11}\sin^4\theta + 2(Q_{12}+2Q_{66})\sin^2\theta\cos^2\theta + Q_{22}\cos^4\theta \qquad (2.19) \\
\overline{Q}_{16} &= (Q_{11}-Q_{12}-2Q_{66})\sin\theta\cos^3\theta + (Q_{12}-Q_{22}+2Q_{66})\sin^3\theta\cos\theta \\
\overline{Q}_{26} &= (Q_{11}-Q_{12}-2Q_{66})\sin^3\theta\cos\theta + (Q_{12}-Q_{22}+2Q_{66})\sin\theta\cos^3\theta \\
\overline{Q}_{66} &= (Q_{11}+Q_{22}-2Q_{12}-2Q_{66})\sin^2\theta\cos^2\theta + Q_{66}(\sin^4\theta\cos^4\theta)
\end{aligned}
$$

and

$$
\left\{
\begin{array}{c}
\sigma_{x_r} \\
\sigma_{y_r} \\
\tau_{xy_r}
\end{array}
\right\}
=
\left\{
\begin{array}{c}
v_a\sigma\cos^2\theta \\
v_a\sigma\sin^2\theta \\
v_a\sigma\sin\theta\cos\theta
\end{array}
\right\}
\qquad (2.20)
$$

Laminate Force and Moment Resultants

So far, this section has presented theoretical formulations for fiber and matrix force and stress components; resolved the elastic behavior of orthotropic laminae in terms of equivalent Young's moduli, shear modulus and Poisson's ratio; and presented the compliance, stiffness and rotated stiffness matrices for single orthotropic SMA hybrid composite layers. The next and final task of this chapter is to establish the elastic behavior of laminated composites in terms of the the forces and moments they exert when deformed by flexure, twisting, or in-plane displacements.

The relationships given above apply for a single orthotropic SMA hybrid composite lamina. Each lamina in a laminate will have its own unique stiffness and stress-strain

behavior depending on its fiber/actuator orientation, its actuator volume fraction, and its state of activation. It is in this way that composite stiffnesses can be tailored to achieve optimal structural performance, both dynamically and statically. In some cases, it is advantageous not to activate all of the SMA fibers in the same way for active structural acoustic control, and other applications as well.

For laminate analysis, each lamina must first be evaluated as described above and then denoted by using the superscript (k) to identify individual plies. The plate theory derived below is an application of the constitutive relation for classical lamination plate theory(CLPT).

For CLPT, the displacements are of the form (see Fig. 2.9):

$$
\begin{aligned}
u &= u^0(x, y, t) - z w_{,x} \\
v &= v^0(x, y, t) - z w_{,y} \\
w &= w(x, y, t).
\end{aligned}
\tag{2.21}
$$

The strain-displacement relationships are

$$
\begin{aligned}
\varepsilon_x &= \varepsilon_x^0 + z \kappa_x \\
\varepsilon_y &= \varepsilon_y^0 + z \kappa_y \\
\gamma_{xy} &= \gamma_{xy}^0 + z \kappa_{xy}
\end{aligned}
\tag{2.22}
$$

69
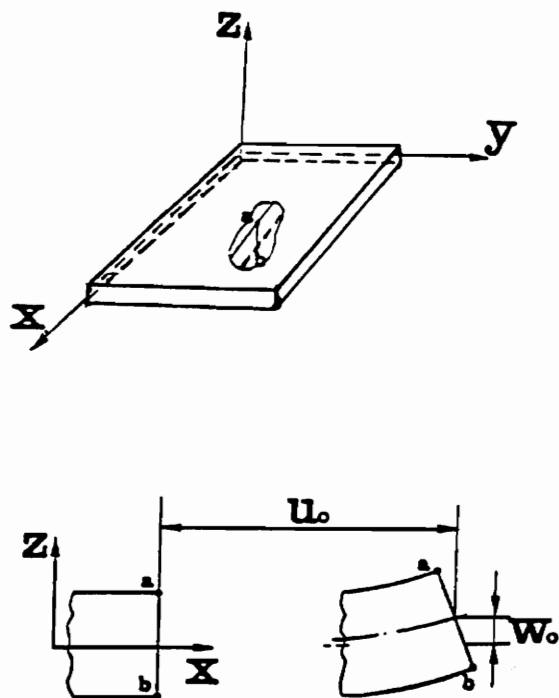
Figure 2.9: CLPT Displacements

where

$$\kappa_x = -w,_{xx}$$

$$\kappa_y = -w,_{yy} \tag{2.23}$$

$$\kappa_{xy} = -2w,_{xy}$$

The stress resultants are defined as follows:

$$(N_x, N_y, N_{xy}) = \int_{-\frac{h}{2}}^{\frac{h}{2}} (\sigma_x^k, \sigma_y^k, \tau_{xy}^k) dz \tag{2.24}$$

$$(Q_x, Q_y) = \int_{-\frac{h}{2}}^{\frac{h}{2}} (\tau_{xz}^k, \tau_{yz}^k) dz \tag{2.25}$$

$$(M_x, M_y, M_{xy}) = \int_{-\frac{h}{2}}^{\frac{h}{2}} (\sigma_x^k, \sigma_y^k, \tau_{xy}^k) z dz \tag{2.26}$$

Using the plane-stress constitutive equation for the kth layer as given by Eq. (2.19) and the force and moment resultants expressed by Eqs.(2.35-2.37), the following constitutive relations for the laminate can be obtained:

$$\begin{Bmatrix} N_x \\ N_y \\ N_{xy} \\ M_x \\ M_y \\ M_{xy} \end{Bmatrix} = \begin{bmatrix} A_{11} & A_{12} & A_{16} & B_{11} & B_{12} & B_{16} \\ A_{12} & A_{22} & A_{26} & B_{12} & B_{22} & B_{26} \\ A_{16} & A_{26} & A_{66} & B_{16} & B_{26} & B_{66} \\ B_{11} & B_{12} & B_{16} & D_{11} & D_{12} & D_{16} \\ B_{12} & B_{22} & B_{26} & D_{12} & D_{22} & D_{26} \\ B_{16} & B_{26} & B_{66} & D_{16} & D_{26} & D_{66} \end{bmatrix} \begin{Bmatrix} \varepsilon_x^0 \\ \varepsilon_y^0 \\ \gamma_{xy}^0 \\ \kappa_x^0 \\ \kappa_y^0 \\ \kappa_{xy}^0 \end{Bmatrix} + \begin{Bmatrix} N_{xr} \\ N_{yr} \\ N_{xyr} \\ M_{xr} \\ M_{yr} \\ M_{xyr} \end{Bmatrix} \tag{2.27}$$

71

where

$$
\begin{aligned}
A_{ij} &= \sum_{k=1}^{N}(\overline{Q}_{ij})_k(z_k - z_{k-1}) \\
B_{ij} &= \sum_{k=1}^{N}\frac{1}{2}(\overline{Q}_{ij})_k(z_k^2 + z_{k-1}^2) \\
D_{ij} &= \sum_{k=1}^{N}\frac{1}{3}(\overline{Q}_{ij})_k(z_k^3 - z_{k-1}^3)
\end{aligned}
\tag{2.28}
$$

and

$$
(N_{x_r}, N_{y_r}, N_{xy_r}) = \int_{\frac{h}{2}}^{\frac{h}{2}}(\sigma_{x_r}^{(k)}, \sigma_{y_r}^{(k)}, \sigma_{xy_r}^{(k)})dz
\tag{2.29}
$$

$$
(M_{x_r}, M_{y_r}, M_{xy_r}) = \int_{-\frac{h}{2}}^{\frac{h}{2}}(\sigma_{x_r}^{(k)}, \sigma_{y_r}^{(k)}, \sigma_{xy_r}^{(k)})z\,dz.
\tag{2.30}
$$

.

In the expressions above, z_k represents the transverse coordinate of upper interface of the kth layer, and z_0 is the transverse coordinate of the bottom face of the laminate.

To determine the laminate mass per unit area,

$$
m_p = \int_{-\frac{h}{2}}^{\frac{h}{2}} \rho^k dz = \sum_{k=1}^{N} \rho^k(z_k - z_{k-1})
\tag{2.31}
$$

The stress-strain relations for a lamina with SMA actuator fibers embedded in a matrix system have been presented, and utilized to describe the force-moment constitutive relationships for a laminated structure of multidirectional orthotropic layers.

72

Chapter 3 utilizes these constitutive relations to formulate analytical models for predicting the structural acoustic response of simply supported, SMA hybrid composite panels.

Chapter 3

Analytical Formulations

This chapter presents and discusses analytical techniques for predicting the structural acoustic response of SMA hybrid composite panels to plane wave acoustic excitation. The chapter begins with a general overview of the analysis of sound transmission through panel-like structures, and introduces the finite panel acoustic radiation analysis of Roussos (1985). It is next shown how this analysis can be applied in conjunction with the Rayleigh-Ritz method and classical laminated plate theory (CLPT) to evaluate thin SMA hybrid composite panels. The chapter concludes with another variation of the finite panel acoustic radiation analysis technique of Roussos, which considers piece-wise evaluation of the Rayleigh-Ritz energy expression for the analysis of elastically discontinuous structures.

3.1 Analysis of Sound Transmission Through Panel-like Structures

Structural dynamics and acoustics involve the response of structural members to dynamic forces. Structural dynamics is primarily concerned with dynamic stresses severe enough to threaten structural integrity. Acoustics considers low-level dynamically ex-

cited waves in structures which are of sufficient strength to radiate unacceptable levels of sound (Ver and Holmer, 1971). When a structure is excited as such, the resulting steady-state vibration field builds up to a level at which the source power balances the losses in the system. These losses include transmitted power to neighboring systems via coupling, and sound waves radiated to the surrounding fluid or air (Ver and Holmer, 1971).

Sound transmission through panels, walls or barriers is usually analyzed by the mass law, infinite panel theory, or finite panel acoustic radiation theory. The mass law is the simplest of the three and can be evaluated in closed form, but it is accurate only where wave effects are unimportant and the transmitted pressure can be assumed to be inversely proportional to the structural mass per unit area (Holmer, 1969).

Non-mass law behavior of single-wall barriers exposed to high frequency acoustic excitation has been observed in experimental results and was explained by Cremer as the wave coincidence effect (Holmer, 1969). Infinite panel theory was put forth as a technique for accurately modelling the coincidence effect by incorporating damping, stiffness, and wave effects into the analysis (Holmer, 1969). Infinite panel theory is accurate when the acoustic wavelength of the incident sound is small compared to the characteristic dimensions of the panel, and boundary effects are not critical to dynamic panel response (Roussos, 1985).

Coincidence occurs when an incident acoustic plane wave produces a standing wave pattern in a panel, and a traveling sound wave which moves across the panel at a speed which matches its free flexural bending wave velocity. At any instant, the

pressure pattern coincides with and reinforces the free wave displacement pattern in the structure as it moves along the plate (Holmer, 1969). This situation, shown graphically in Fig. 3.1, produces pressure waves of high intensity radiating from both surfaces of the panel.

3.2   Finite Panel Acoustic Radiation Theory

For low frequency noise, the dimensions of the transmitting structure are on the order of the incident acoustic wavelength, hence boundary effects are important. The simply supported panel is chosen for this analysis as it closely approxmimates many actual structural configurations (Wallace, 1972). Roussos (1985) developed a method for analyzing sound transmission through a simply supported panel in an infinite baffle. This analysis is beneficial for studying many common noise transmission phenomena which occur in complicated structures that are more easily studied in this simple, idealized form. Where most other analytical methods emphasize solving for radiated noise or radiation efficiency of vibrating plates, the analysis of Roussos addresses the sound transmission problem in its entirety, considering incident noise, panel vibrations, and transmitted noise (Roussos, 1985).

The analysis of sound transmisson through an isotropic plate begins with the following differential equation of motion for an acoustically excited panel:

$$D\nabla^4 w + C_D w_{,t} + m_p w_{,tt} = p_i(x, y, t) + p_r(x, y, t) - p_t(x, y, t) \qquad (3.1)$$
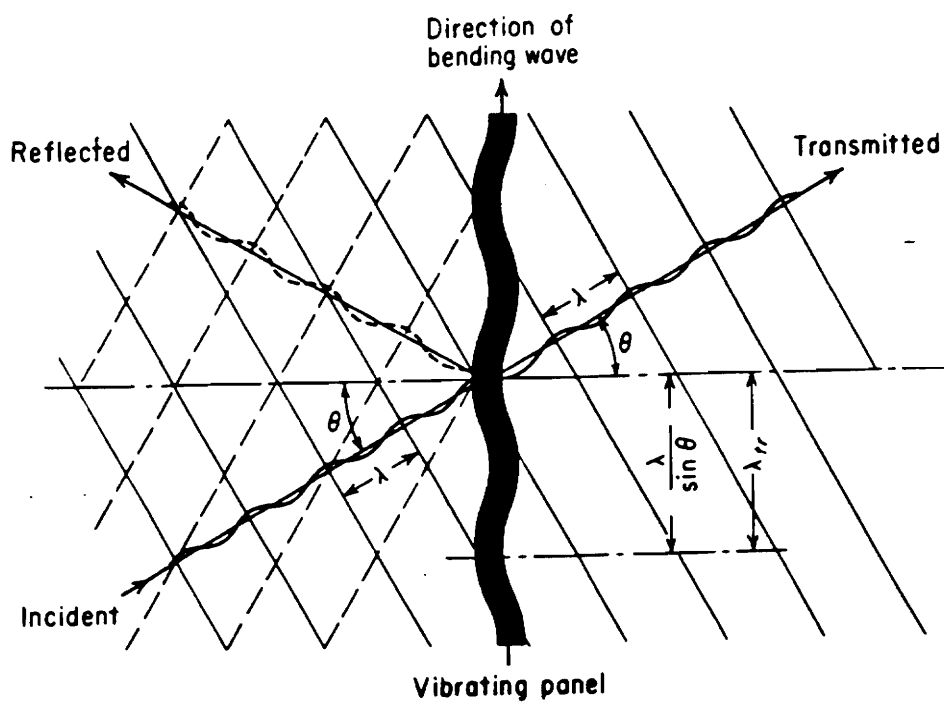
Figure 3.1: The Coincidence Phenomenon

where

$$\nabla^4 = \frac{\partial^4}{\partial x^4} + 2\frac{\partial^4}{\partial x^2 \partial y^2} + \frac{\partial^4}{\partial y^4}.$$

Commas denote partial differentation with respect to the subscripts after them; and p_i, p_r, and p_t are the incident, reflected and transmitted pressures. The geometry of the coordinate system on which this analysis is based is shown in Fig. 3.2. The three pressure components can be written as the sum of the blocked pressure (the pressure on the incident side when the plate is considered infinitely rigid) and the radiated pressure (the pressure that is solely due to plate vibrations). The radiated pressure is an unknown function of plate displacement, w, and the solution of Eq.(3.1) is very complicated. To obtain an accurate solution while avoiding this complexity, it is assumed that the radiated pressure is negligible compared to the blocked pressure in the governing equation for plate motion (Roussos, 1985).

Incorporating this assumption, Eq.(3.1) can be rewritten as:

$$D\nabla^4 w + C_D w_{,t} + m_p w_{,tt} = p_b(x, y, t), \qquad (3.2)$$

where the blocked pressure, p_b, is assumed to equal twice the incident pressure, $(p_b(x, y, t) = 2p_i(x, y, t))$. The assumed incident pressure can now be expressed as an oblique traveling wave:

$$P_i(x, y, t) = P_i \exp[i(\omega t - k_c x \sin\theta_i \cos\phi_i - k_c y \sin\theta_i \sin\phi_i)] \qquad (3.3)$$
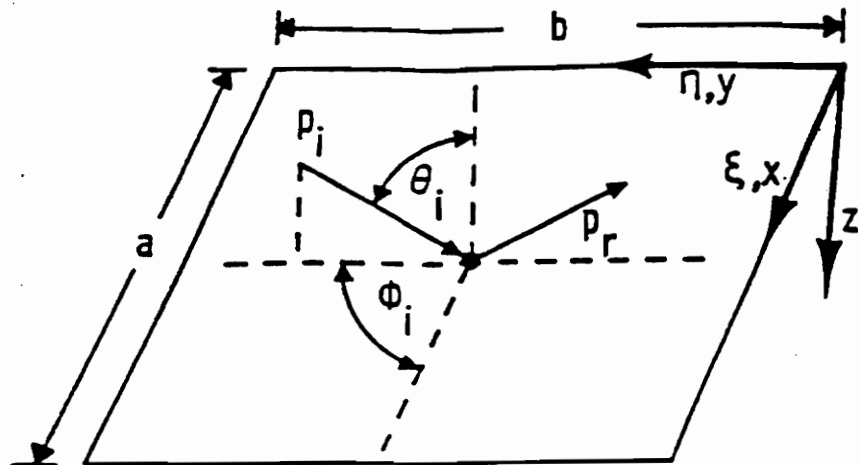
Geometry on Incident Side of Panel
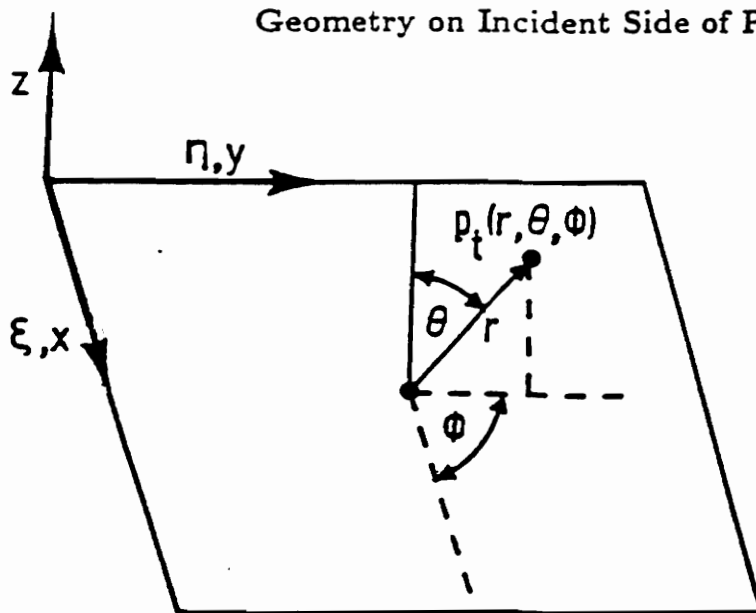
Geometry on Radiating Side of Panel

Figure 3.2: Panel and Acoustic Geometries

where P_i is the incident pressure amplitude and k is the acoustic wave number $(\frac{\omega}{c})$. The panel coordinate system and the acoustic incidence angles are shown in Fig. 3.2. The incident intensity and acoustic power can be determined from the information thus far presented. Since plane wave incidence is considered here, the incident intensity is given by

$$I_i = \frac{(P_i^2 \cos\theta_i)}{2\rho c}, \tag{3.4}$$

and the incident acoustic power is

$$\Pi_i = \frac{(P_i^2 ab \cos\theta_i)}{2\rho c}. \tag{3.5}$$

The steady-state panel vibration is the only response that bears influence on the acoustic transmission solution for this analysis. Because the acoustic forcing function is harmonic, the steady state panel response is harmonic, and can be expressed as

$$W(x,y,t) = W(x,y)\exp(i\omega t). \tag{3.6}$$

Inserting Eqs.(3.3) and (3.6) into Eq.(3.2) and dividing through by the periodic exponential time function yields

$$D\nabla^4 W(x,y) + iC_D\omega W(x,y) - m_p\omega^2 W(x,y) \tag{3.7}$$
$$= 2P_i \exp[-ik_{cp}\sin\theta_i(x\cos\phi_i + y\sin\phi_i)].$$

Since the panel is finite and simply supported on all edges, the boundary conditions

are identically satisfied by the following transverse displacement function:

$$W(x,y) = \sum_{m=1}^{\infty} \sum_{n=1}^{\infty} W_{mn} \sin \frac{m\pi x}{a} \sin \frac{n\pi y}{b} \tag{3.8}$$

Since the steady state solution of Eq.(3.6) must satisfy the boundary conditions also, Eq.(3.8) can be used for the spatial displacement solution assuming the incident pressure can be expanded into an infinite series of the same orthogonal functions. For plane wave sound incidence, the forcing pressure can be expressed as

$$2P_i \exp[-ik_{cp} \sin \theta_i (x \cos \phi_i + y \sin \phi_i)] = \sum_{m=1}^{\infty} \sum_{n=1}^{\infty} p_{mn} \sin \frac{m\pi x}{a} \sin \frac{n\pi y}{b}, \tag{3.9}$$

where p_{mn}, the generalized forcing pressure, is

$$p_{mn} = \frac{8P_i}{ab} \int_{x=0}^{a} \int_{y=0}^{b} \exp[-ik_{cp} \sin \theta_i (x \cos \phi_i + y \sin \phi_i)] \sin \frac{m\pi x}{a} \sin \frac{n\pi y}{b} dy dx. \tag{3.10}$$

Substituting Eqs.(3.8) and (3.9) into Eq.(3.7) produces the general displacement solution

$$W_{mn} = \frac{p_{mn}}{m_p[\omega_{mn}^2 - \omega^2 + (\frac{iC_{Dp}\omega}{m_p})]} \tag{3.11}$$

where

$$\omega_{mn}^2 = (2\pi f_{mn})^2 = \frac{D\pi^4}{m_p} \left(\frac{m^2}{a^2} + \frac{n^2}{b^2} \right)^2 \tag{3.12}$$

Equation (3.10) can be evaluated in closed form to obtain the forcing pressure coef-

81

ficients for characteristic terms of Eq.(3.9).

$$p_{mn} = 8P_i\overline{I}_m\overline{I}_n \tag{3.13}$$

where

$$\overline{I}_m = \begin{cases} -(\frac{i}{2})sgn(\sin\theta_i\cos\theta_i) & , \quad (m\pi)^2 = [sin\theta_i\cos\phi_i(\frac{\omega a}{c})]^2 \\ \frac{m\pi\{1-(-1)^m exp[-i\sin\theta_i\cos\phi_i(\frac{\omega a}{c})]\}}{(m\pi)^2-[\sin\theta_i\sin\phi_i(\frac{\omega a}{c})]^2} & , \quad (m\pi)^2 \neq [\sin\theta_i\cos\phi_i(\frac{\omega a}{c})]^2 \end{cases} , \tag{3.14}$$

and

$$\overline{I}_n = \begin{cases} -(\frac{i}{2})sgn(\sin\theta_i\sin\theta_i) & , \quad (n\pi)^2 = [sin\theta_i\sin\phi_i(\frac{\omega b}{c})]^2 \\ \frac{n\pi\{1-(-1)^n exp[-i\sin\theta_i\sin\phi_i(\frac{\omega b}{c})]\}}{(n\pi)^2-[\sin\theta_i\sin\phi_i(\frac{\omega b}{c})]^2} & , \quad (n\pi)^2 \neq [\sin\theta_i\sin\phi_i(\frac{\omega b}{c})]^2 \end{cases} . \tag{3.15}$$

Knowing the W_{mn} values for a given pressure incidence, θ_i and ϕ_i, the transmitted pressure can be determined by

$$P_t(r,\theta,\phi) = -\frac{\omega^2\rho ab}{2\pi r}\exp\{i\omega[t-\frac{r}{c}-\frac{\sin\theta}{2c}(a\cos\phi+b\sin\phi)]\}\sum_{m=1}^{M}\sum_{n=1}^{N}W_{mn}I_mI_n, \tag{3.16}$$

where

$$I_m = \begin{cases} (-\frac{i}{2})sgn(\sin\theta\cos\theta) & , \quad (m\pi)^2 = [sin\theta\cos\phi(\frac{\omega a}{c})]^2 \\ \frac{m\pi\{1-(-1)^m exp[-i\sin\theta\cos\phi(\frac{\omega a}{c})]\}}{(m\pi)^2-[\sin\theta\sin\phi(\frac{\omega a}{c})]^2} & , \quad (m\pi)^2 \neq [\sin\theta\cos\phi(\frac{\omega a}{c})]^2 \end{cases} , \tag{3.17}$$

and

$$I_n = \left\{ \begin{array}{ll} -(\frac{i}{2})sgn(\sin\theta\sin\theta) & , \quad (n\pi)^2 = [sin\theta\sin\phi(\frac{\omega b}{c})]^2 \\[3mm] \frac{n\pi\{1-(-1)^n exp[-i\sin\theta\sin\phi(\frac{\omega b}{c})]\}}{(n\pi)^2-[\sin\theta\sin\phi(\frac{\omega b}{c})]^2} & , \quad (n\pi)^2 \neq [\sin\theta\sin\phi(\frac{\omega b}{c})]^2 \end{array} \right\}. \tag{3.18}$$

Here, r is the radial distance from the panel centroid to a point in the far field, and θ and ϕ are the polar and azimuthal transmission angles, as shown in Figure 3.2. These equations are described in greater detail by Roussos (1985). The far field velocity is next obtained from

$$U_r = \frac{P_t}{\rho c}. \tag{3.19}$$

Considering U_r^* to be the complex conjugate of U_r, the transmitted acoustic intensity is defined as

$$I_t(r,\theta,\phi) = \frac{1}{2}Re[P_t U_r^*]. \tag{3.20}$$

The transmitted intensity, from which the directivity pattern can be determined, is a function of the polar and azimuthal angles. Finally, the transmitted acoustic power, Π_t, can be calculated from

$$\Pi_t = \int_{\phi=0}^{2\pi} \int_{\theta=0}^{\frac{\pi}{2}} I_t r^2 \sin\theta d\theta d\phi. \tag{3.21}$$

This integration can be solved by 100-point Gauss quadrature. The incident acoustic

power, Π_i, is defined as

$$\Pi_i = \frac{(P_i^2 ab \cos \theta_i)}{2\rho c}. \tag{3.22}$$

The ratio of the transmitted to incident power is referred to commonly as the transmission coefficient, and the transmission loss is defined as the log of its inverse,

$$TL = 10 \log(\frac{\Pi_i}{\Pi_t}). \tag{3.23}$$

To illustrate the difference between the predicted mass law response and infinite panel theory, analytical results from Ver and Holmer (1971) are included in Fig. 3.3. Comparing the transmisson loss versus normalized frequency curves, two key observations can be made. The predicted transmission loss values at and around the critical frequency (where coincidence occurs) diverge considerably for the two theories. Also, the transmission loss 'dip' at coincidence decreases as structural damping is increased.

To compare finite panel acoustic radiation theory with the infinite panel theory, results are shown in Fig. 3.4. The apparent transmission loss differences between these theories at very low frequencies illustrate the importance of boundary effects in the low-frequency range. It is interesting that, in Fig. 3.4, the results for the two analyses agree in the frequency range near coincidence. Referring to Eq.(3.16), for the finite panel analysis to be sensitive to the coincidence effect, the series expansion must be carried out a sufficient number of terms to include the characteristic standing wave in its range of solutions.
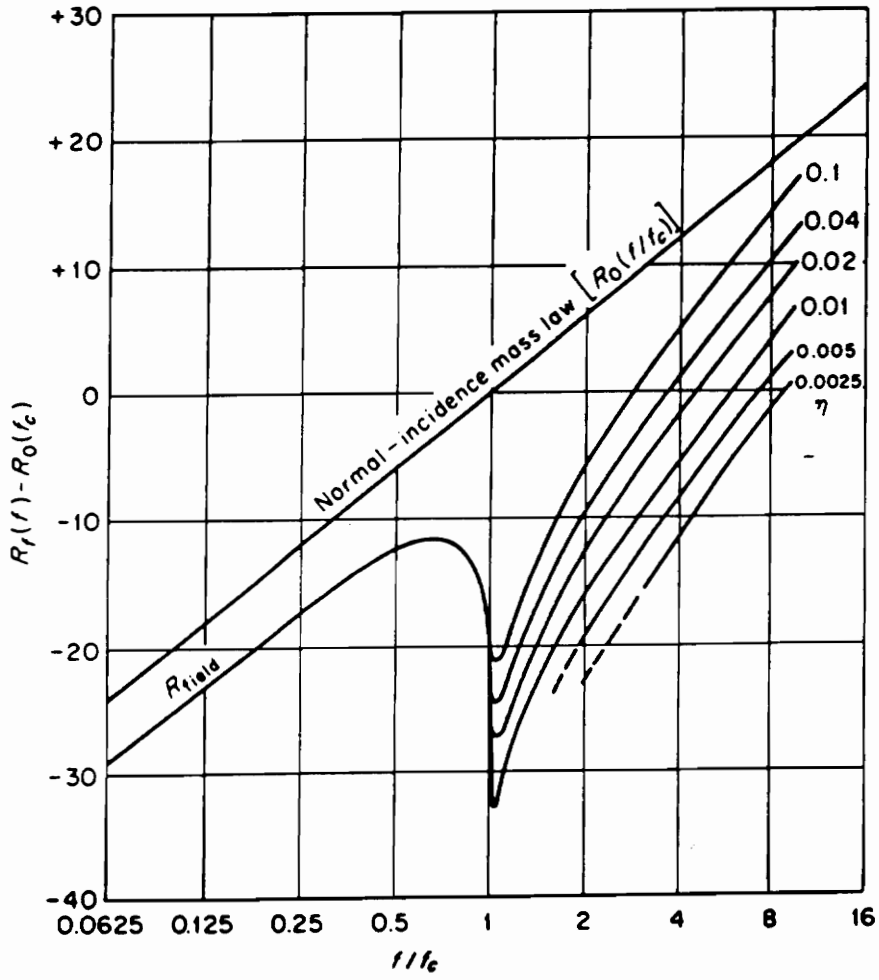
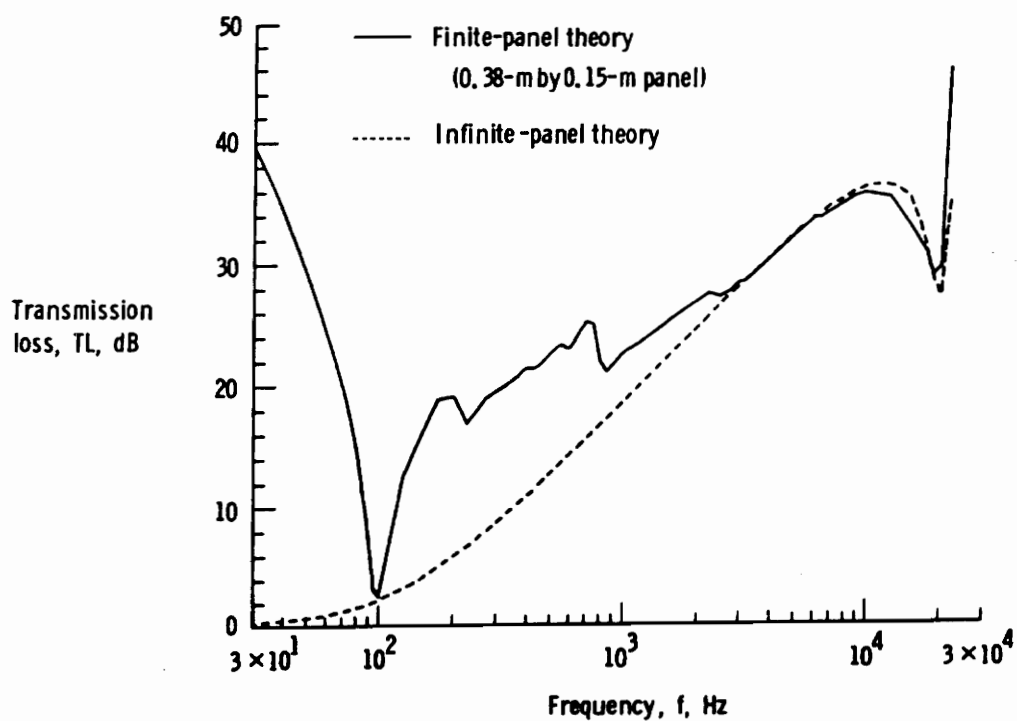Figure 3.3: Mass Law and Infinite Panel Theory Comparison; after Ver and Holmer,1971

85

Figure 3.4: Comparison of Infinite and Finite Panel Theories; after Roussos, 1985

3.3 Rayleigh-Ritz Formulation Using CLPT

Acoustic radiation of isotropic simply supported panels is usually studied assuming the vibration can be described by mode shapes corresponding to single characteristic terms from a double sine series expansion in x and y. The study of composite panels has revealed that harmonic excitation of anisotropic plates excites several of these characteristic mode shapes simultaneously, such that rather than having geometric mode shapes conveniently defined by a single product of orthogonal functions in x and y, displacement solutions for anisotropic panels require simultaneous consideration of several series terms and their associated amplitude coefficients (Rogers, Liang, and Fuller 1990).

This section introduces an analytical method for determining sound transmission through anisotropic simply-supported panels using the Rayleigh-Ritz method, classical laminated plate theory, and the finite panel acoustic radiation theory presented in the previous section. This formulation is limited to simply supported, symmetrically laminated panels that are sufficiently thin that the assumptions of Classical Laminated Plate Theory (CLPT) apply. At at the expense of added mathematical complexity and computing time, the model can be expanded to consider non-symmetrical laminates and various combinations of fixed, simply supported and free boundary conditions.

The assumptions governing CLPT (Whitney, 1987) are given below:

1. The plate is constructed of an arbitrary number of orthotropic layers perfectly

bonded together. The orthotropic axes of material symmetry do not neccesarily coincide with the x-y axes of the plate.

2. The plate is thin such that its thickness, h, is much smaller than its other dimensions.

3. The displacements u, v, and w are small compared to the plate thickness.

4. In-plane strains ε_x, ε_y and γ_{xy} are small compared to unity.

5. To include in-plane effects, nonlinear terms in the equations of motion involving products of stresses and plate slopes are retained. All other nonlinear terms are neglected.

6. The transverse shear strains γ_{xz} and γ_{yz} are negligible.

7. Tangential displacements u, and v are linear functions of the transverse (z) coordinate.

8. The transverse normal stress and strain (σ_z and ε_z) are negligible.

9. Hooke's law governs the stress-strain behavior of each ply.

10. The plate is of constant thickness.

11. Rotary inertia effects are negligible.

12. No body forces act on the plate.

13. Transverse shear stresses σ_{xz} and σ_{yz} vanish at the upper and lower surfaces of the plate.

Liang, Rogers and Fuller (1990) applied the analysis of Roussos (1985) to evaluate thin, symmetrically laminated, simply supported, generally activated SMA hybrid composite panels. The boundary conditions given for a simply supported panel are:

at $x = 0$ and $x = a$;

$$w = m_x = -D_{11}W_{,xx} - 2D_{16}W_{,xy} - D_{12}W_{,yy} = 0 \qquad (3.24)$$

and at $y = 0$ and $y = b$;

$$w = m_y = -D_{12}W_{,xx} - 2D_{16}W_{,xy} - D_{22}W_{,yy} = 0 \qquad (3.25)$$

Based on these prescribed boundary conditions, the assumed transverse displacement solution is

$$W(x,y,t) = \sum_{m=1}^{M} \sum_{n=1}^{N} W_{mn} \sin \frac{\pi m x}{a} \sin \frac{\pi n y}{b} e^{i\omega t}. \qquad (3.26)$$

where a and b are the panel dimensions in the x and y directions as shown in Fig. 3.5, and ω is the angular freqency of the applied periodic acoustic forcing function

$$q(x,y,t) = \sum_{m=1}^{M} \sum_{n=1}^{N} q_{mn} \sin \frac{\pi m x}{a} \sin \frac{\pi n y}{b} e^{i\omega t}. \qquad (3.27)$$

The total energy functional for a thin, symetrically laminated composite panel can
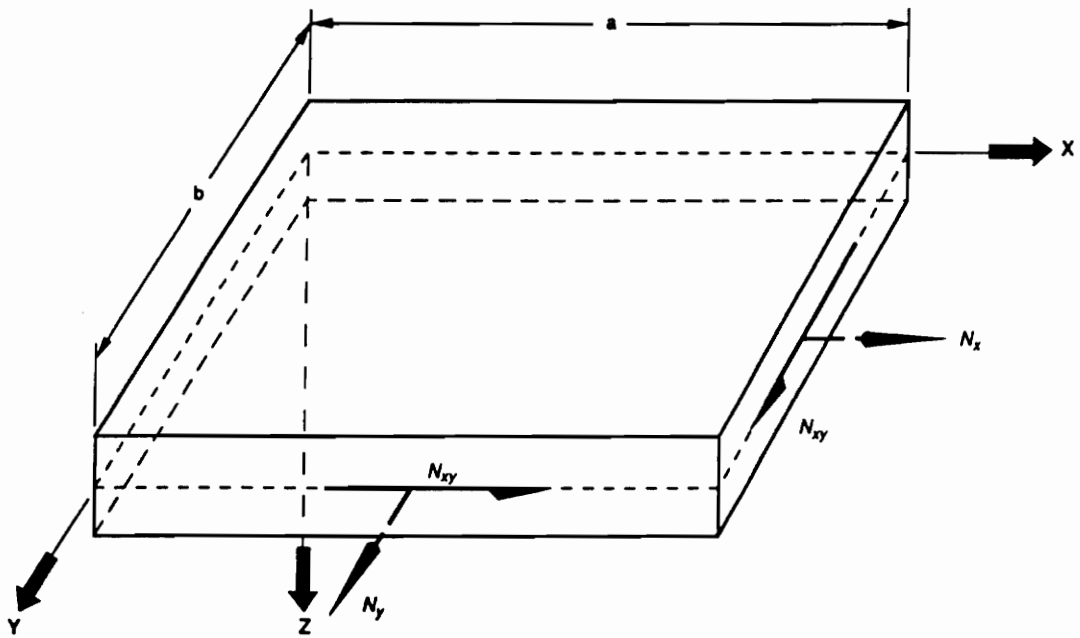
Figure 3.5: Panel Geometry and In-Plane Force Resultants

90

be written:

$$\Pi = \frac{1}{2} \int_0^a \int_0^b \{D_{11}W_{,xx}^2 + 2D_{12}W_{,xx}W_{,yy} + D_{22}W_{,yy}^2 + 4D_{66}W_{,xy}^2 + N_x W_{,x}^2$$
$$+ N_y W_{,y}^2 + 2N_{xy}W_{,x}W_{,y} - 2qW + C_D i\omega W^2 - m_p\omega^2 W^2\}dxdy, \quad (3.28)$$

where the D_{ij} variables represent the flexural stiffness coefficients of the composite material; the subscripted N's are the applied in-plane loads shown in Fig. 3.5; m_p is plate mass per unit area; and C_D is the damping coefficient expressed in this case as

$$C_D = 2m_p\xi, \quad (3.29)$$

where ξ is the mass-proportional damping constant. For most cases in this study, ξ is assumed to be 0.05.

Combining Eqs.(3.22) through (3.24) and minimizing with respect to the amplitude coefficients (W_{mn}) produces M by N linear equations defined by:

$$\Pi_{,W_{mn}} = 0 = \sum_{i=1}^{M} \sum_{j=1}^{N} \int_0^a \int_0^b \{D_{11}(X_{i,xx}X_{m,xx})(Y_jY_n)$$

$$+D_{12}[(X_mX_{i,xx})(Y_jY_{n,yy}) + (X_iX_{m,xx})(Y_nY_{j,yy})]$$

$$+D_{22}(X_iX_m)(Y_{j,yy}Y_{n,yy}) + 4D_{66}(X_{i,x}X_{m,x})(Y_{j,y}Y_{n,y})$$

$$+2D_{16}[(X_{i,xx}X_{m,x})(Y_jY_{n,y}) + (X_{m,xx}X_{i,x})(Y_nY_{j,y})]$$

$$+2D_{26}[(X_mX_{i,x})(Y_{j,y}Y_{n,yy}) + (X_iX_{m,x})(Y_{j,yy}Y_{n,y})]$$

$$+N_x(X_{m,x}X_{i,x})(Y_jY_n) + N_y(X_iX_m)(Y_{j,y}Y_{n,y})$$

$$+N_{xy}[(X_{i,x}X_m)(Y_jY_{n,y}) + (X_iX_{m,x})(Y_{j,y}Y_n)]$$

$$+C_D i\omega(X_i X_m)(Y_j Y_n) - m_p\omega^2(X_i X_m)(Y_i Y_n)\}dxdyW_{mn}$$

$$-\int_0^a \int_0^b q_{mn} X_m Y_n dxdy \qquad (3.30)$$

where;

$$m, i = 1, 2, 3, ...M$$

$$n, j = 1, 2, 3, ...N$$

$$X_i = \sin\frac{\pi i x}{a}$$

$$X_m = \sin\frac{\pi m x}{a}$$

$$Y_j = \sin\frac{\pi j y}{b}$$

$$Y_n = \sin\frac{\pi n y}{b}$$

Equation (3.25) can be written in matrix form to evaluate forced dynamic and static response as:

$$[K_{st}]\{W_t\} = \{q_s\} \qquad (3.31)$$

where

$$t = (i - 1)N + j$$

$$s = (m - 1)N + n$$

or to determine the eigenvalues and natural frequencies as

$$([\overline{K}_{st}] - [V_{st}]\omega^2)\{W_t\} = 0 \qquad (3.32)$$

where the damping terms and forcing function are set equal to zero.

The stiffness terms, $\overline{K}_{st}$ can be expressed as:

$$\overline{K}_{st} = \sum_{i=1}^{M}\sum_{j=1}^{N} \int_0^a \int_0^b D_{11}(X_{i,xx}X_{m,xx})(Y_jY_n)$$

$$+D_{12}[(X_mX_{i,xx})(Y_nY_{j,yy}) + (X_iX_{m,xx})(Y_jY_{n,yy})]$$

$$+D_{22}(X_iX_m)(Y_{j,yy}Y_{n,yy}) + 4D_{66}(X_{i,x}X_{m,x})(Y_{j,y}Y_{n,y})$$

$$+2D_{16}[(X_{i,xx}X_{m,x})(Y_jY_{n,y}) + (X_{m,xx}X_{i,x}(Y_nY_{j,yy})]$$

$$+2D_{26}[(X_mX_{i,x})(Y_{j,y}Y_{n,yy}) + (X_iX_{m,x})(Y_{j,yy}Y_{n,y})]$$

$$+N_x(X_{m,x}X_{i,x})(Y_jY_n) + N_y(X_iX_m)(Y_{j,y}Y_{n,y})$$

$$+ N_{xy}[(X_{i,x}X_m)(Y_jY_{n,y}) + (X_iX_{m,x})(Y_{j,y}Y_n)]dxdy \qquad (3.33)$$

The mass terms V_{st} are determined by:

$$V_{st} = \sum_{i=1}^{M}\sum_{j=1}^{N} \int_0^a \int_0^b m_p\omega^2(X_iX_m)(Y_jY_n)dxdy \qquad (3.34)$$

To analyze sound transmission through the panel, the technique of Roussos (1985) is utilized. For this analysis, an acoustic plane wave is considered to excite one side of the panel, causing it to vibrate, and reradiate (or transmit) acoustic energy to the other side. For light acoustic media such as air, the forcing function function $q(x,y,t)$ can be expressed as the blocked pressure:

$$q(x,y) = 2P_i \exp[-(\omega/c)i(x\sin\theta_i\cos\phi_i + y\sin\theta_i\cos\phi_i)], \qquad (3.35)$$

where c is the speed of sound, θ_i is the polar incidence angle, and ϕ_i is the azimuth of the incident sound wave. The distributed forcing function can be rewritten in the form

$$q_s = 2P_i\overline{I}_m\overline{I}_n, \qquad (3.36)$$

93

where $\bar{I}_m$ and $\bar{I}_n$ are defined in Eqs.(3.14) and (3.15).

By solving the set of simultaneous equations produced by combining Eqs.(3.24) and (3.28), the displacement coefficients (W_{mn}) can be determined. Knowing the W_{mn} values for a given pressure incidence, θ_i and ϕ_i, the transmitted pressure can be determined using the Rayleigh integral approach as

$$P_t(r,\theta,\phi) = -\frac{\omega^2 \rho ab}{2\pi r} \exp\{i\omega[t - \frac{r}{c} - \frac{\sin\theta}{2c}(a\cos\phi + b\sin\phi)]\} \sum_{m=1}^{m} \sum_{n=1}^{N} W_{mn} I_m I_n, \quad (3.37)$$

where I_m and I_n are given in Eqs.(3.17) and (3.18). Here, r is the radial distance from the panel centroid to a point in the far field, and θ and ϕ are the polar and azimuthal transmission angles, as shown in Fig. 3.2. The far field velocity is next obtained from

$$U_r = \frac{P_t}{\rho c}. \quad (3.38)$$

Considering U_r^* to be the complex conjugate of U_r, the transmitted acoustic intensity is defined as

$$I_t(r,\theta,\phi) = \frac{1}{2} Re[P_t U_r^*]. \quad (3.39)$$

The transmitted intensity, from which the directivity pattern can be determined, is a function of the polar and azimuthal angles. Finally, the transmitted acoustic power, Π_t, can be determined as

$$\Pi_t = \int_{\phi=0}^{2\pi} \int_{\theta=0}^{\frac{\pi}{2}} I_t r^2 \sin\theta d\theta d\phi. \quad (3.40)$$

This integration can be solved by 100-point Gauss quadrature. The incident acoustic

power, Π_i, is defined as

$$\Pi_i = \frac{(P_i^2 ab \cos \theta_i)}{2\rho c}. \tag{3.41}$$

The ratio of the transmitted to incident power is referred to commonly as the transmission coefficient, and the transmission loss is defined as the log of its inverse,

$$TL = 10 \log(\frac{\Pi_i}{\Pi_t}). \tag{3.42}$$

At low frequencies, sound transmission through a panel is highly dependent on its stiffness and modal response characteristics. For finite panels, Wallace (1972) nondimensionalized the ratio of the acoustic power radiated by characteristic mode shapes to the product of the spatial average panel velocity squared and the characteristic impedance of the surrounding fluid in terms of modal radiation efficiency. The radiation efficiency for a given mode is

$$\overline{S}_{mn} = \frac{\overline{\Pi}_t^{mn}}{\rho cab < |\overline{U}_{mn}|^2 >}, \tag{3.43}$$

where $< |\overline{U}_{mn}|^2 >$ is the spatial time-average panel velocity squared, when the panel is vibrating at the m,n characteristic mode shape with a modal amplitude of unity; $\overline{\Pi}_t^{mn}$ is the power transmitted by the panel vibrating at the homogeneous mode shape characterized by m and n, ρ is the density of the surrounding acoustic medium, c is the speed of sound in that medium, and a and b are the respective panel dimensions in the x and y directions.

To graphically describe the acoustic behavior of characteristic mode shapes vibrating over a broad range of frequencies, Wallace (1972) has plotted radiation efficiency as

95

a function of the dimensionless parameter, γ, for various panel aspect ratios where:

$$\gamma = \frac{K_{cp}}{K_p},\tag{3.44}$$

in which K_{cp} is the wave number of the acoustic medum expressed by

$$K_{cp} = \frac{\omega}{c},\tag{3.45}$$

K_p is the panel wave number defined by

$$K_p = \left[\left(\frac{\pi m}{a}\right)^2 + \left(\frac{\pi n}{b}\right)^2\right]^{\frac{1}{2}},\tag{3.46}$$

ω is the frequency of vibration, and m and n characterize the mode shape of the panel. More information regarding radiation efficiency is available in Wallace (1972).

The mode shapes of anisotropic panels can be mathematically represented as the superposition of numerous characteristic mode shapes (Liang, Rogers and Fuller, 1989). The kth normalized mode shape, Φ^k, can be expressed as

$$\Phi^k = \sum_{m=1}^{M}\sum_{n=1}^{N} \overline{A}_{mn}^k \sin\frac{m\pi x}{a} \sin\frac{n\pi y}{b},\tag{3.47}$$

where $\overline{A}_{mn}^k$ values are normalized modal amplitude coefficients.

Modal radiation efficiency for the kth geometric or composite mode shape can be numerically determined as a function of frequency by numerical solution as

$$\overline{S}_k = \frac{\overline{\Pi}_t^k}{\rho cab <|\overline{U}_{mn}|^2>},\tag{3.48}$$

but the panel wave number, K_p, cannot be determined by Eq.(3.46). The geometric mode shapes, Φ^k consist of several characteristic modes and their associated modal

amplitude coefficents. To determine the wave number for a the kth geometric (or composite) mode shape, Φ_k, the following expression is introduced:

$$K_p^k = \left\{ \sum_{m=1}^{M} \sum_{n=1}^{N} \overline{A}_{mn}^{k}{}^2 \left[\left(\frac{m\pi}{a}\right)^2 + \left(\frac{n\pi}{b}\right)^2 \right] \right\}^{\frac{1}{2}} \qquad (3.49)$$

For any composite mode shape which can be expressed in terms of Eq.(3.47), the panel wave number can now be determined by Eq.(3.49), the medium wave number can be determined from Eq.(3.45), and radiation efficiency can be determined by Eq.(3.48).

3.4 Analysis of Thin, Elastically Discontinuous Panels

The procedure formulated in this section can be used to determine sound transmission through piece-wise 'homogeneous' simply-supported panels. A segmented Rayleigh-Ritz technique is used, in which the kinetic, potential and strain energies of discrete panel sections are minimized, individually integrated, and summed. The formulation presented is limited to simply supported, symmetrically laminated panels that are sufficiently thin that the assumptions of Classical Laminated Plate Theory (CLPT) apply, however thick plates could be analyzed by extending this technique to higher-order plate theories. At at the expense of added mathematical complexity and computing time, the analysis can also be expanded to consider unsymmetric laminates and various combinations of fixed, simply supported and free boundary conditions.

Section 3.3 presents a finite panel acoustic radiation analysis formulation by CLPT

which can be used to evaluate thin, symmetrically laminated, simply supported, spatially homogeneous SMA hybrid composite panels. The theory of Section 3.3 can be expanded to consider non-spatially homogeneous panels as follows:

The assumed displacement solution for a simply supported panel is

$$W(x,y,t) = \sum_{m=1}^{M} \sum_{n=1}^{N} W_{mn} \sin\frac{\pi m x}{a} \sin\frac{\pi n y}{b} e^{i\omega t}. \tag{3.50}$$

The assumed applied periodic acoustic forcing function is

$$q(x,y,t) = \sum_{m=1}^{M} \sum_{n=1}^{N} q_{mn} \sin\frac{\pi m x}{a} \sin\frac{\pi n y}{b} e^{i\omega t}. \tag{3.51}$$

The total energy functional for a thin, symetrically laminated composite panel is:

$$
\begin{aligned}
\Pi = & \frac{1}{2} \int_0^a \int_0^b \{ D_{11} W_{,xx}^2 + 2D_{12} W_{,xx} W_{,yy} + D_{22} W_{,yy}^2 + 4D_{66} W_{,xy}^2 + N_x W_{,x}^2 \\
& + N_y W_{,y}^2 + 2N_{xy} W_{,x} W_{,y} - 2qW + C_D i\omega W^2 - m_p \omega^2 W^2 \} dx\,dy,
\end{aligned} \tag{3.52}
$$

Which is minimized with respect to the amplitude coefficient to produce M by N linear governing differential equations of motion defined by:

$$
\begin{aligned}
& \sum_{i=1}^{M} \sum_{j=1}^{N} \int_0^a \int_0^b \{ D_{11}(X_{i,xx} X_{m,xx})(Y_j Y_n) \\
& + D_{12}[(X_m X_{i,xx})(Y_j Y_{n,yy}) + (X_i X_{m,xx})(Y_n Y_{j,yy})] \\
& + D_{22}(X_i X_m)(Y_{j,yy} Y_{n,yy}) + 4D_{66}(X_{i,x} X_{m,x})(Y_{j,y} Y_{n,y}) \\
& + 2D_{16}[(X_{i,xx} X_{m,x})(Y_j Y_{n,y}) + (X_{m,xx} X_{i,x})(Y_n Y_{j,y})] \\
& + 2D_{26}[(X_m X_{i,x})(Y_{j,y} Y_{n,yy}) + (X_i X_{m,x})(Y_{j,yy} Y_{n,y})] \\
& + N_x(X_{m,x} X_{i,x})(Y_j Y_n) + N_y(X_i X_m)(Y_{j,y} Y_{n,y}) \\
& + N_{xy}[(X_{i,x} X_m)(Y_j Y_{n,y}) + (X_i X_{m,x})(Y_{j,y} Y_n)] - m_p \omega^2 (X_i X_m)(Y_i Y_n)
\end{aligned}
$$

$$+ C_D i\omega(X_i X_m)(Y_j Y_n)\} dx\, dy\, W_{mn} = \int_0^a \int_0^b q_{mn} X_m Y_n dx\, dy \tag{3.53}$$

where;

$$
\begin{aligned}
m, i &= 1, 2, 3, ... M \\
n, j &= 1, 2, 3, ... N \\
X_i &= \sin\frac{\pi i x}{a} \\
X_m &= \sin\frac{\pi m x}{a} \\
Y_j &= \sin\frac{\pi j y}{b} \\
Y_n &= \sin\frac{\pi n y}{b}
\end{aligned}
$$

The same theory can be applied to locally activated adaptive panels by integrating the minimized energy functional over each spatially homogeneous section and summing these integrals over the x-y surface of the panel.

The following expression can be used to analyze locally activated panels:

$$\sum_{l=1}^{L}\sum_{i=1}^{M}\sum_{j=1}^{N} \int_{x_1{}^l}^{x_2{}^l} \int_{y_1{}^l(x)}^{y_2{}^l(x)} \{D_{11}{}^l(X_{i,xx}X_{m,xx})(Y_j Y_n)$$

$$+ D_{22}{}^l(X_i X_m)(Y_{j,yy}Y_{n,yy}) + 4D_{66}{}^l(X_{i,x}X_{m,x})(Y_{j,y}Y_{n,y})$$

$$+ D_{12}{}^l[(X_m X_{i,xx})(Y_j Y_{n,yy}) + (X_i X_{m,xx})(Y_n Y_{j,yy})]$$

$$+ 2D_{16}{}^l[(X_{i,xx}X_{m,x})(Y_j Y_{n,y}) + (X_{m,xx}X_{i,x})(Y_n Y_{j,yy}]$$

$$+ 2D_{26}{}^l[(X_m X_{i,x})(Y_{j,y}Y_{n,yy}) + (X_i X_{m,x})(Y_{j,yy}Y_{n,y})]$$

$$+ N_x{}^l(X_{m,x}X_{i,x})(Y_j Y_n) + N_y{}^l(X_i X_m)(Y_{j,y}Y_{n,y})$$

$$+ N_{xy}{}^l[(X_{i,x}X_m)(Y_j Y_{n,y}) + (X_i X_{m,x})(Y_{j,y}Y_n)] + C_D{}^l i\omega(X_i X_m)(Y_j Y_n)$$

$$- m_p{}^l \omega^2(X_i X_m)(Y_i Y_n)\} dx\, dy\, W_{mn} = \int_0^a \int_0^b q_{mn} X_m Y_n dx\, dy \tag{3.54}$$

Where L is the number of spatially homogeneous panel sections, and the "l" super-scripts represent properties or loads assigned to these sections. Figure 3.6 shows an example of a locally activated panel, and how it can be resolved into spatially homogeneous sections. Locally activated panels may be resolved into quadrilateral or triangular regions for analysis. This is handled by integrating Eq.(3.54) between limits in y which are defined as linear functions of x rather than constants.

Equation (3.54) can be written in matrix form to evaluate forced dynamic and static response as:

$$[K_{st}]\{W_t\} = \{q_s\} \tag{3.55}$$

where;

$$t = (i-1)N + j$$
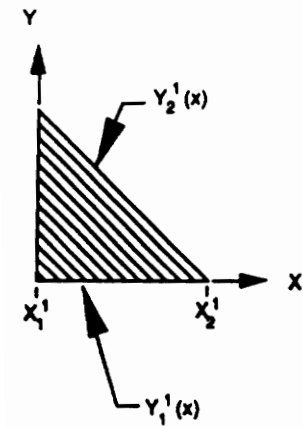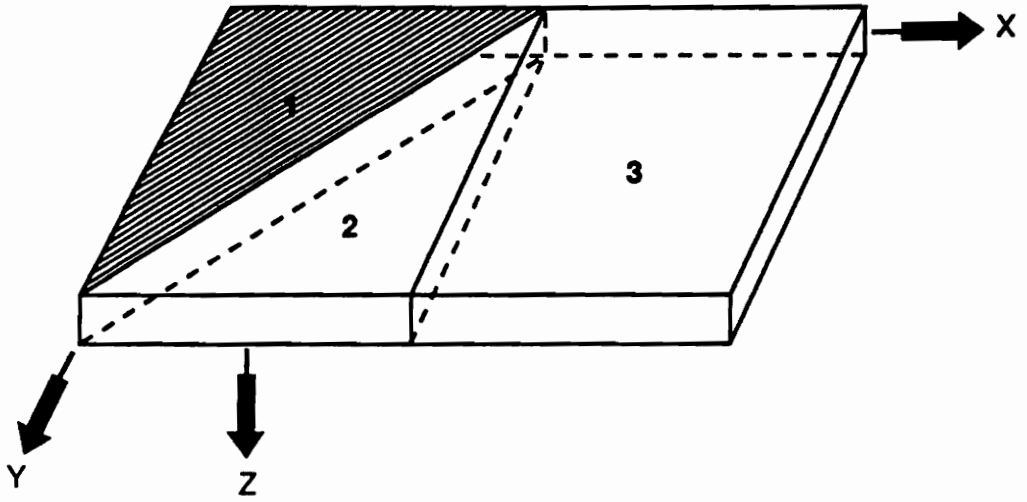$$s = (m-1)N + n$$

or to determine the eigenvalues and natural frequencies using this form:

$$([\overline{K}_{st}] - [V_{st}]\omega^2)\{W_t\} = 0 \tag{3.56}$$

where the damping terms and forcing function are set equal to zero.

The stiffness terms, $\overline{K}_{st}$ can be expressed as:

$$\overline{K}_{st} = \sum_{l=1}^{L} \sum_{i=1}^{M} \sum_{j=1}^{N} \int_{x_1{}^l}^{x_2{}^l} \int_{y_1{}^l(x)}^{y_2{}^l(x)} \{D_{11}{}^l(X_{i,xx}X_{m,xx})(Y_jY_n)$$
$$+ D_{22}{}^l(X_iX_m)(Y_{j,yy}Y_{n,yy}) + 4D_{66}{}^l(X_{i,x}X_{m,x})(Y_{j,y}Y_{n,y})$$

100
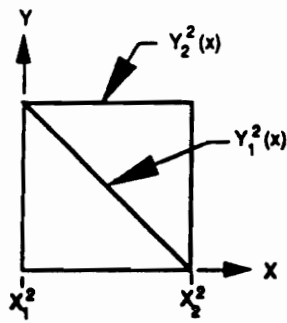
Figure 3.6: A Locally Activated Panel Resolved into Sections

$$+D_{12}{}^l[(X_mX_{i,xx})(Y_nY_{j,yy}) + (X_iX_{m,xx})(Y_jY_{n,yy})]$$

$$+2D_{16}{}^l[(X_{i,xx}X_{m,x})(Y_jY_{n,y}) + (X_{m,xx}X_{i,x}(Y_nY_{j,yy}]$$

$$+2D_{26}{}^l[(X_mX_{i,x})(Y_{j,y}Y_{n,yy}) + (X_iX_{m,x})(Y_{j,yy}Y_{n,y})]$$
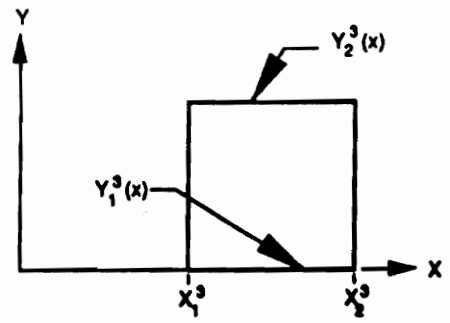
$$+N_x{}^l(X_{m,x}X_{i,x})(Y_jY_n) + N_y{}^l(X_iX_m)(Y_{j,y}Y_{n,y})$$

$$+ N_{xy}^l[(X_{i,x}X_m)(Y_jY_{n,y}) + (X_iX_{m,x})(Y_{j,y}Y_n)]dxdy \qquad (3.57)$$

The mass terms V_{st} are determined by:

$$V_{st} = \sum_{l=1}^{L}\sum_{i=1}^{M}\sum_{j=1}^{N}\int_{x_1{}^l}^{x_2{}^l}\int_{y_1{}^l(x)}^{y_2{}^l(x)} m_p{}^l\omega^2(X_iX_m)(Y_jY_n)dxdy \qquad (3.58)$$

To analyze sound transmission through the panel, the technique of Roussos (1985) is again utilized. The acoustic plane wave considered in Sections 3.2, and 3.3 is assumed to excite one side of the panel, causing it to vibrate, and transmit acoustic energy to the other side. For light acoustic media such as air, the forcing function function $q(x, y, t)$ can be expressed as the blocked pressure

$$q(x, y) = 2P_i \exp[-(\omega/c)i(x \sin \theta_i \cos \phi_i + y \sin \theta_i \cos \phi_i)], \qquad (3.59)$$

The distributed forcing function can be rewritten in the form

$$q_s = 2P_i\overline{I}_m\overline{I}_n, \qquad (3.60)$$

By solving the set of simultaneous equations produced by combining Eq.(3.60) and (3.55), the displacement coefficients (W_{mn}) can be determined. Knowing the W_{mn} values for a given pressure incidence, θ_i and ϕ_i, the transmitted pressure can be

102

determined using the Rayleigh integral approach as

$$P_t(r,\theta,\phi) = -\frac{\omega^2 \rho ab}{2\pi r} \exp\{i\omega[t - \frac{r}{c} - \frac{\sin\theta}{2c}(a\cos\phi + b\sin\phi)]\} \sum_{m=1}^{m} \sum_{n=1}^{N} W_{mn} I_m I_n, \quad (3.61)$$

The far field velocity is next obtained from

$$U_r = \frac{P_t}{\rho c}. \quad (3.62)$$

Considering U_r^* to be the complex conjugate of U_r, the transmitted acoustic intensity is defined as

$$I_t(r,\theta,\phi) = \frac{1}{2} Re[P_t U_r^*]. \quad (3.63)$$

The transmitted acoustic power, Π_t, can be determined as

$$\Pi_t = \int_{\phi=0}^{2\pi} \int_{\theta=0}^{\frac{\pi}{2}} I_t r^2 \sin\theta d\theta d\phi. \quad (3.64)$$

The incident acoustic power, Π_i, is

$$\Pi_i = \frac{(P_i^2 ab \cos\theta_i)}{2\rho c}, \quad (3.65)$$

Finally, the transmission loss is

$$TL = 10\log\left(\frac{\Pi_i}{\Pi_t}\right). \quad (3.66)$$

3.5   Summary

Two analytical models have been formulated in this chapter for the structural acoustic and modal analysis of thin, simply supported, symmetrically laminated SMA hybrid

composite panels. The second model is presented as an enhancement of the first, as it provides the same analytical capabilities with the added feature of piece-wise analysis capability for elastically discontinuous structures. At the expense of added mathematical complexity and computing time, these models can be further enhanced to consider unsymmetric laminates, thick panels, and various combinations of simply supported, clamped, and free boundary support conditions. A finite panel acoustic radiation analysis model is formulated for thick SMA hybrid composite panels by first-order shear deformation theory in Appendix A.

Chapter 4

Results and Discussion

This chapter presents and discusses results obtained using the analytical models formulated in Chapter 3. These results are organized into seven sections. Section 4.1 compares CLPT and FSDT transmission loss results obtained for quasi-isotropic fiberglass panels of given spatial dimensions and various thicknesses to determine how the effects of rotary inertia and transverse shear deformation affect the response of simply supported composite panels to incident plane wave acoustic excitation.

In Section 4.2, the CLPT analysis formulated in Section 3.3 is used to investigate the effects of panel thickness on adaptive tuning capability. Section 4.3 includes an evaluation of the influence of structural damping on acoustic transmisson loss. Dimensionless studies of panel aspect ratio and laminate stacking sequence (for symmetric angle ply laminates) are presented in Section 4.4.

The results of two case studies considering locally activated SMA hybrid composite panels analyzed by the the model formulated in Section 3.5 are presented in Section 4.5. Two concepts of adaptive structural acoustic control by alternate resonance tuning are demonstrated in Section 4.6 considering a single panel; and two adjacent

105

simply supported, elastically coupled panels. This chapter concludes with Section 4.7, which summarizes the analytical results of Sections 4.1 through 4.6, reiterating key observations made during the course of this research.

4.1   CLPT and FSDT Comparison

Finite panel acoustic radiation analysis models are formulated in Chapter 3 using two plate theories: CLPT (Section 3.3) and FSDT (Appendix A). CLPT is accurate for analyzing thin structures, where the effects of transverse shear deformation and rotary intertia are negligible. FSDT takes these effects into account, and therefore can be used to accurately model the static, modal and dynamic response of thick laminated structures, where the assumptions of CLPT are not valid. The purpose of this section is not to provide a complete, comprehensive comparison of the two theories, but to investigate the effects of transverse shear deformation and rotary inertia on structural acoustic response.

Comparing the acoustic transmission analysis models formulated by CLPT and FSDT, it is obvious that the accuracy of FSDT realized for thicker panels is gained at the expense of mathematical complexity and computing time. In fact, comparing Eqs.(3.31) and (A.22), the rank of a matrix required to solve for a given number of series terms (and thus that same given number of characteristic modes: M,N) is three times greater for FSDT than for CLPT. For example, expanding the orthogonal transverse displacement functions to M=N=10 terms, the coefficient matrix for analysis by CLPT requires a 100 by 100 matrix, whereas analysis by FSDT requires a 300 by 300 matrix.

106

Because the purpose of this work is to investigate physical trends and capabilties, the analyses of subsequent sections are done by CLPT only. Sufficient information is included in Appendix A, however, to expand any analysis of this thesis to accurately model thick panels by FSDT. Furthermore, future sections show that active structural tuning capability is generally higher for thin panels, therefore CLPT is sufficient for fulfilling the goals of this research.

The principal objective of this section is to determine where CLPT is valid for finite panel acoustic radiation analysis, and how the combined effects of shear deformation and rotary inertia affect the transmission of sound through panel-like structures. The analysis of this section considers quasi-isotropic panels of given spatial dimensions, with width-to-thickness ($\frac{b}{h}$) ratios of 100, 50, 25 and 10. Fixed parameters for his analysis are specified in Table 4.1.

The first ten natural frequencies for each $\frac{b}{h}$ ratio considered are presented in Table 4.2. The results show that the presence of shear deformation, even for very thin panels with $\frac{b}{h}$ ratios as large as 100, adds some compliance to the structure by introducing additional degrees of freedom and rotary inertia, thereby reducing the computed natural frequencies. The influence of these effects becomes increasingly evident as the width-to-thickness ratio is reduced. Eventually, as $\frac{b}{h}$ approaches 10, the effects of shear deformation and rotary inertia affect the natural frequencies such that they significantly depart from CLPT behavior.

Transmission loss is plotted versus frequency for four $\frac{b}{h}$ ratios in Figs. 4.1 through 4.4.

Table 4.1: Panel Specifications for CLPT/FSDT Comparison Study

Spatial Geometry and Stacking Sequence	
Stacking Sequence	$[90/\pm 45/0]_s$
Panel Length (a)	1.2m
Panel Width (b)	0.8m

Material Specifications	
Material	Fiberglass
Material Nomenclature	GFRP
E_1	38.6 GPa
E_2	8.3 GPa
G_{12}	4.1 GPa
ν_{12}	0.26
ρ	1800 $\frac{kg}{m^3}$
Laminate Properties	
E_x	18.9 GPa
E_y	18.9 GPa
G_{xy}	7.45 GPa
ν_{xy}	0.27

Table 4.2: Natural Frequencies Computed by CLPT and FSDT

$\frac{b}{h} = 100$				$\frac{b}{h} = 50$		
	CLPT	FSDT			CLPT	FSDT
ω_1 (Hz)	29.4	29.4		ω_1 (Hz)	58.9	58.7
ω_2 (Hz)	48.9	48.9		ω_2 (Hz)	98.9	97.5
ω_3 (Hz)	81.6	81.4		ω_3 (Hz)	163.3	162.4
ω_4 (Hz)	98.5	98.3		ω_4 (Hz)	197.0	195.6
ω_5 (Hz)	117.7	117.5		ω_5 (Hz)	235.5	233.7
ω_6 (Hz)	127.2	126.9		ω_6 (Hz)	254.9	252.6
ω_7 (Hz)	150.3	150.0		ω_7 (Hz)	300.8	298.0
ω_8 (Hz)	184.8	184.0		ω_8 (Hz)	370.2	365.4
ω_9 (Hz)	197.3	197.0		ω_9 (Hz)	395.1	390.7
ω_{10} (Hz)	213.7	212.9		ω_{10} (Hz)	427.4	421.2

$\frac{b}{h} = 25$				$\frac{b}{h} = 10$		
	CLPT	FSDT			CLPT	FSDT
ω_1 (Hz)	117.7	116.8		ω_1 (Hz)	294.3	281.1
ω_2 (Hz)	195.7	193.3		ω_2 (Hz)	489.2	457.3
ω_3 (Hz)	326.7	320.4		ω_3 (Hz)	816.6	738.0
ω_4 (Hz)	394.0	383.7		ω_4 (Hz)	985.0	854.5
ω_5 (Hz)	471.1	457.1		ω_5 (Hz)	1177	1005
ω_6 (Hz)	509.8	495.3		ω_6 (Hz)	1274	1103
ω_7 (Hz)	601.6	580.4		ω_7 (Hz)	1504	1250
ω_8 (Hz)	740.4	710.7		ω_8 (Hz)	1851	1523
ω_9 (Hz)	790.2	808.8		ω_9 (Hz)	1975	1586
ω_{10} (Hz)	854.9	212.9		ω_{10} (Hz)	2137	1636

Panel Dimensions (meters)		
a	b	h
1.200	0.800	0.008

LEGEND: —— CLPT ------ FSDT

Figure 4.1: Transmission Loss Versus Frequency ($\frac{b}{h}=100$)

110
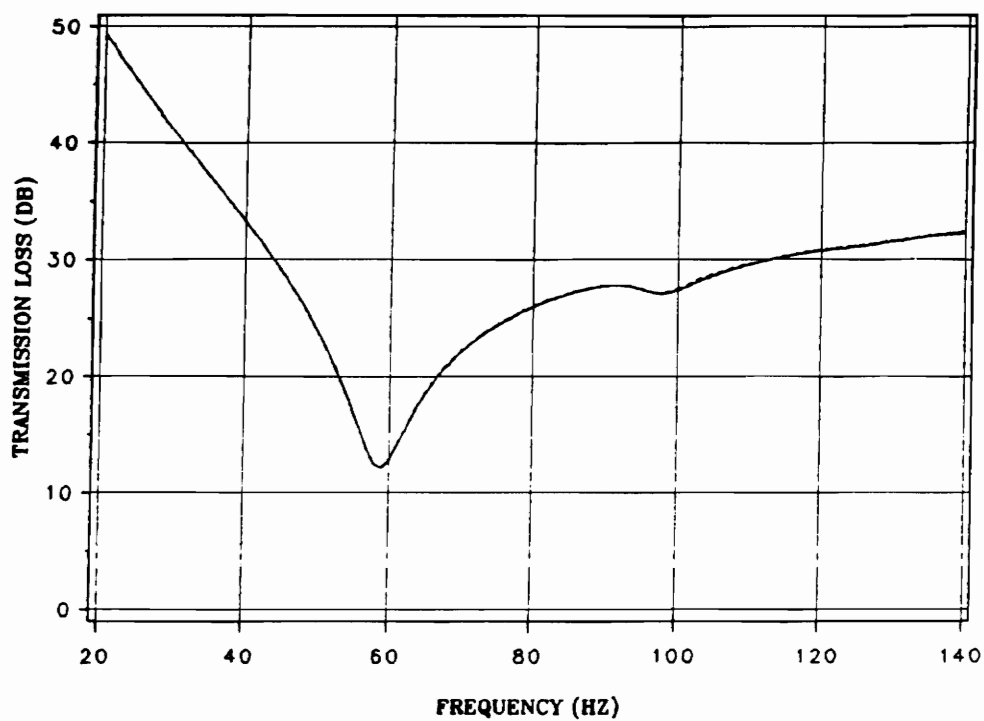
Panel Dimensions (meters)		
a	b	h
1.200	0.800	0.016

LEGEND: ———— CLPT ------- FSDT

Figure 4.2: Transmission Loss Versus Frequency ($\frac{b}{h}$=50)
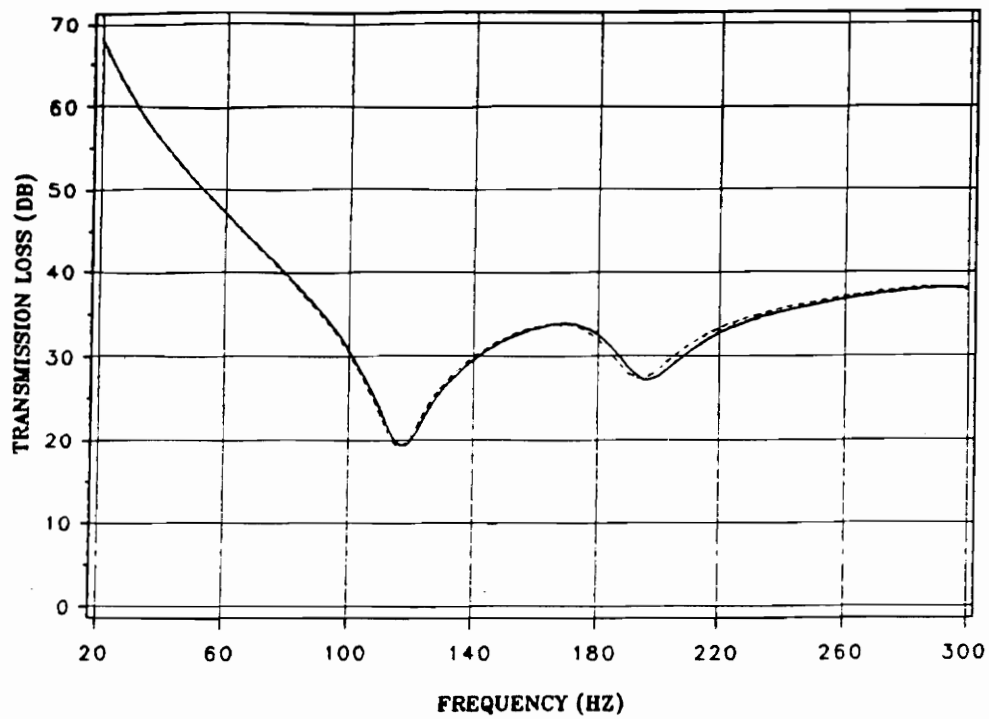
Panel Dimensions (meters)		
a	b	h
1.200	0.800	0.032

LEGEND: ——— CLPT - - - - - FSDT

Figure 4.3: Transmission Loss Versus Frequency ($\frac{b}{h}$=25)

112
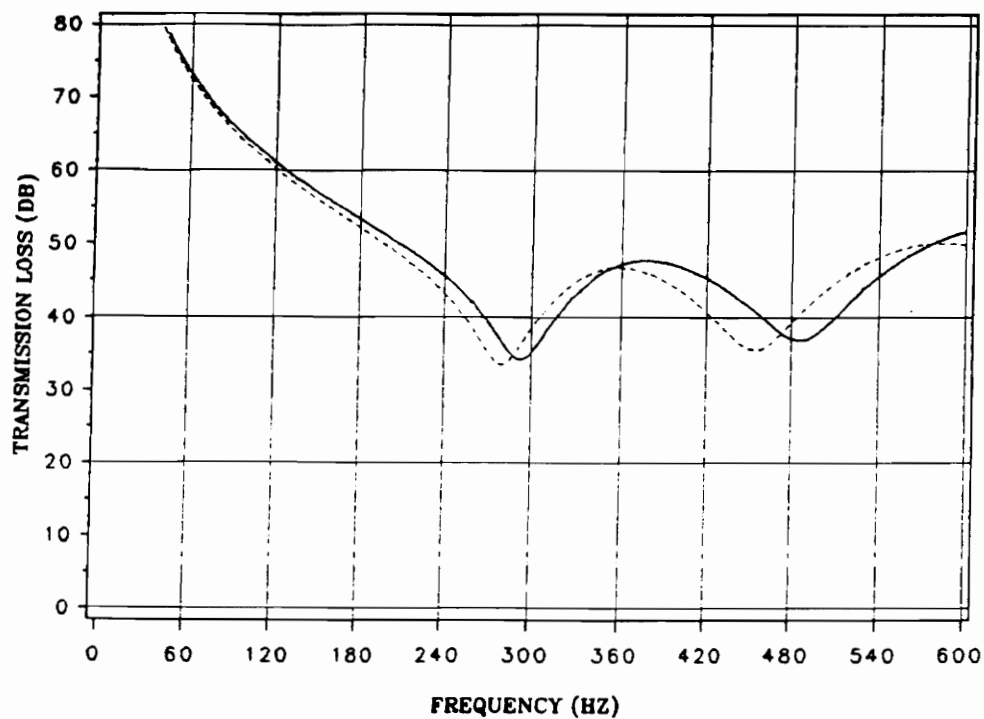
Panel Dimensions (meters)		
a	b	h
1.200	0.800	0.080

LEGEND: ———— CLPT ······· FSDT

Figure 4.4: Transmission Loss Versus Frequency ($\frac{b}{h}=10$)

113

For the thinnest case, where $\frac{b}{h} = 100$, the transmission loss versus frequency curves analyzed by FSDT and CLPT of Fig. 4.1 are virtually identical. The two theories agree very closely in the lower frequency range for the panel with $\frac{b}{h} = 50$ in Fig. 4.2, and diverge slightly as frequency increases. For the $\frac{b}{h} = 25$ case shown in Fig. 4.3, the two theories are fairly consistent off-resonance, however a moderate inconsistency is apparent at and around the first two modes. The theories significantly diverge in Fig. 4.4 for the $\frac{b}{h} = 10$ case. The fact that FSDT predicts a more compliant panel with added rotary inertia explains why the natural frequencies determined by this theory are lower than those obtained by the CLPT analysis. This also explains why, for the thicker panels, the FSDT transmission loss curves appear shifted to the left relative to the the CLPT curves.

To proceed in an efficient manner from the standpoint of mathematical simplicity and computing time, all subsequent analyses are done by CLPT. The key objective of this work is to diagnose trends and physical tendancies which enhance structural acoustic control capabilities; therefore, utilizing the more efficient technique within its limits does not degrade the quality of the analysis or its accuracy, but rather enables a broader scope and a more thorough investigation. By this resolution, only panels with $\frac{b}{h}$ equal to or greater than 25 are considered henceforth; and where possible, thin panels with $\frac{b}{h}$ of 100 are considered.

4.2 Panel Thickness Effects

In the previous section, finite panel acoustic radiation analysis results obtained using CLPT and FSDT are compared. These studies show that transmission loss versus frequency curves diverge as $\frac{b}{h}$ decreases, due to the effects of transverse shear deformation and rotary inertia. The issue of how panel thickness influences the adaptive structural tuning capabilities of SMA hybrid composite structures requires additional investigation. In this section, the acoustic transmission control capabilities of SMA hybrid composite panels are evaluated based on panel thickness within the width-to-thickness ratio range where CLPT can be applied with reasonable accuracy.

For this study, nitinol/fiberglass (NiTi/GFRP) panels are sized to have identical unactivated resonant frequencies by considering the relationships:

$$\frac{ab}{h} = constant \tag{4.1}$$

and

$$a = \frac{4b}{3}. \tag{4.2}$$

For consistency, each panel evaluated conforms to the specifications of Table 4.3, and a baseline geometry is established as:

$$a = 1.200m.$$

$$b = 0.800m.$$

$$h = 0.008m.$$

Table 4.3: Specifications for Panel Thickness Study

Material Specifications	
Material	nitinol/fiberglass
Material Nomenclature	NiTi/GFRP
Stacking Sequence	$[90/\pm 45/0]_s$
NiTi volume fraction	20%
GFRP volume fraction	80%
Material Properties (unactivated)	
E_1	36.5 GPa
E_2	9.6 GPa
G_{12}	4.7 GPa
ν_{12}	0.28
ρ	2730 $\frac{kg}{m^3}$
Membrane Stress σ_1	0.0 MPa
Laminate Properties (unactivated)	
E_x	19.2 GPa
E_y	19.2 GPa
G_{xy}	7.6 GPa
ν_{xy}	0.27
Material Properties (activated)	
E_1	47.3 GPa
E_2	10.1 GPa
G_{12}	5.0 GPa
ν_{12}	0.28
ρ	2730 $\frac{kg}{m^3}$
Membrane Stress σ_1	68.9 MPa
Laminate Properties (activated)	
E_x	23.2 GPa
E_y	23.2 GPa
G_{xy}	9.1 GPa
ν_{xy}	0.28

The thickness dimension, h is then progressively doubled such that 0.016m, 0.032m, and 0.064m panels are evaluated, and their spatial dimensions, a and b, are determined using Eqs. (4.1) and (4.2). The geometric dimensions for each of these panels are presented in Table 4.4. To evaluate the contributions of APT and ASET to the overall structural tuning authority of each panel, the first ten natural frequencies for each panel are computed with only the effects of APT and compared with the results obtained considering also the activation-induced membrane stresses, by which ASET occurs in SMA hybrid composite structures. The results of these analyses are presented in Tables 4.5 through 4.8.

The panel dimensions for each case were determined using Eqs. (4.1) and (4.2) such that when a particular set of material properties and a specific laminate ply stacking sequence are considered, the natural frequencies for each case will be identical in the absence of strain energy effects. This uniformity was established by considering the relationship used to normalize the natural frequencies of anisotropic plates. The first ten natural frequencies listed in the third columns of Tables 4.5 through 4.8 correspond to panel activation scenarios in which only the effects of properties transformation (APT) are considered to be present; hence the APT-activated natural frequencies for each of the four panels are identical. These results indicate that the effects of APT do not vary with the thickness of a structure, and that natural frequencies are increased by approximately 10 % for the SMA hybrid composite material evaluated. More adaptive structural tuning authority by APT can be incorporated into the material by either increasing the SMA volume fraction, using a more compliant matrix material, or both.

117

Table 4.4: Panel Geometries for Thickness Analysis

Thickness (h) (m)	Length (a) (m)	Width (b) (m)
0.008	1.200	0.800
0.016	1.697	1.131
0.032	2.400	1.600
0.064	3.394	2.263

Table 4.5: Natural Frequencies for Laminate Thickness Analysis (h=0.008m)

Mode	ω_u (Hz)	ω_a (APT) (Hz)	ω_a (APT+ASET) (Hz)	$\frac{\omega_a}{\omega_u}$ (APT) (dimensionless)	$\frac{\omega_a}{\omega_u}$ (APT+ASET) (dimensionless)
1	23.8	26.5	88.5	1.11	3.72
2	40.4	44.0	125.1	1.09	3.10
3	68.1	73.4	172.6	1.08	2.52
4	79.2	88.6	173.5	1.11	2.19
5	95.5	106.0	199.4	1.11	2.09
6	106.9	114.5	230.6	1.07	2.16
7	123.1	135.3	240.6	1.10	1.95
8	155.4	166.2	289.0	1.07	1.86
9	163.3	177.5	291.7	1.09	1.79
10	171.5	192.3	298.2	1.12	1.74

Panel Dimensions (m)		
h	a	b
0.008	1.200	0.800

119

Table 4.6: Natural Frequencies for Laminate Thickness Analysis(h=0.016m)

Mode	ω_u (Hz)	ω_a (APT) (Hz)	ω_a (APT+ASET) (Hz)	$\frac{\omega_a}{\omega_u}$ (APT) (dimensionless)	$\frac{\omega_a}{\omega_u}$ (APT+ASET) (dimensionless)
1	23.8	26.5	65.3	1.11	2.74
2	40.4	44.0	93.8	1.09	2.32
3	68.1	73.4	133.2	1.08	1.96
4	79.2	88.6	137.3	1.11	1.73
5	95.5	106.0	159.7	1.11	1.67
6	106.9	114.5	182.0	1.07	1.70
7	123.1	135.3	195.2	1.10	1.59
8	155.4	166.2	238.3	1.07	1.53
9	163.3	177.5	244.5	1.09	1.50
10	171.5	192.3	245.8	1.12	1.43

Panel Dimensions (m)		
h	a	b
0.016	1.697	1.131

120

Table 4.7: Natural Frequencies for Laminate Thickness Analysis (h=0.032m)

Mode	ω_u (Hz)	ω_a (APT) (Hz)	ω_a (APT+ASET) (Hz)	$\frac{\omega_a}{\omega_u}$ (APT) (dimensionless)	$\frac{\omega_a}{\omega_u}$ (APT+ASET) (dimensionless)
1	23.8	26.5	49.8	1.11	2.09
2	40.4	44.0	73.3	1.09	1.81
3	68.1	73.4	107.5	1.08	1.58
4	79.2	88.6	115.5	1.11	1.46
5	95.5	106.0	135.5	1.11	1.42
6	106.9	114.5	152.1	1.07	1.42
7	123.1	135.3	167.9	1.10	1.36
8	155.4	166.2	205.6	1.07	1.32
9	163.3	177.5	213.5	1.09	1.31
10	171.5	192.3	220.6	1.12	1.29

Panel Dimensions (m)		
h	a	b
0.032	2.400	1.600

Table 4.8: Natural Frequencies for Laminate Thickness Analysis (h=.064m)

Mode	ω_u (Hz)	ω_a (APT) (Hz)	ω_a (APT+ASET) (Hz)	$\frac{\omega_a}{\omega_u}$ (APT) (dimensionless)	$\frac{\omega_a}{\omega_u}$ (APT+ASET) (dimensionless)
1	23.8	26.5	39.9	1.11	1.68
2	40.4	44.0	60.4	1.09	1.50
3	68.1	73.4	92.1	1.08	1.35
4	79.2	88.6	102.9	1.11	1.30
5	95.5	106.0	121.6	1.11	1.27
6	106.9	114.5	134.6	1.07	1.26
7	123.1	135.3	152.4	1.10	1.24
8	155.4	166.2	187.0	1.07	1.20
9	163.3	177.5	196.3	1.09	1.20
10	171.5	192.3	206.9	1.12	1.21

Panel Dimensions (m)		
h	a	b
0.064	3.394	2.263

The natural frequencies presented in the fourth columns of Tables 4.5 through 4.8 correspond to panels considered to be activated such that the combined effects of APT and ASET are present. These values vary substantially from case-to-case. The fundamental frequency of the thinnest (0.008m) panel is shown to increase from 23.8 Hz to 88.5 Hz (Table 4.5) by active structural tuning with the combined effects of APT and ASET: an increase of 272%. The fundamental frequency of the 0.064m panel is shown to increase from 23.8 Hz to 39.9 Hz (Table 4.8) when activated similarly; which constitutes a change of only 68%. This decrease in tuning authority with increasing panel thickness can be theoretically confirmed by the explanation that the in-plane force resultants (which are directly related to ASET control authority) are linearly proportional to laminate thickness; whereas the flexural stiffness coefficients (D_{ij}) vary cubically with laminate thickness. By this rational, the overall control authority of SMA hybrid composite structures is largely due to the high membrane stresses induced by the fully-constrained recovery of the embedded SMA fibers. The greatest structural tuning authority for SMA hybrid composites exists in thin members.

Transmission loss versus frequency plots are presented in Figs. 4.5 and 4.6 for the thinnest (0.008m) and thickest (0.064m) panels, considering polar and azimuthal plane-wave incidence angles of 45° and 0°, respectively. The effects of increased panel thickness and reduced strain energy tuning capability on structural acoustic response and control authority can be readily seen by comparing these two figures. For the thinner panel (h=0.008m), the transmission loss at and around the first unactivated resonance (23.8 Hz), is shown in Fig. 4.5 to increase by more than 40dB due to the presence of ASET. For the thicker panel (h=0.064m), ASET is shown in Fig. 4.6 to

123
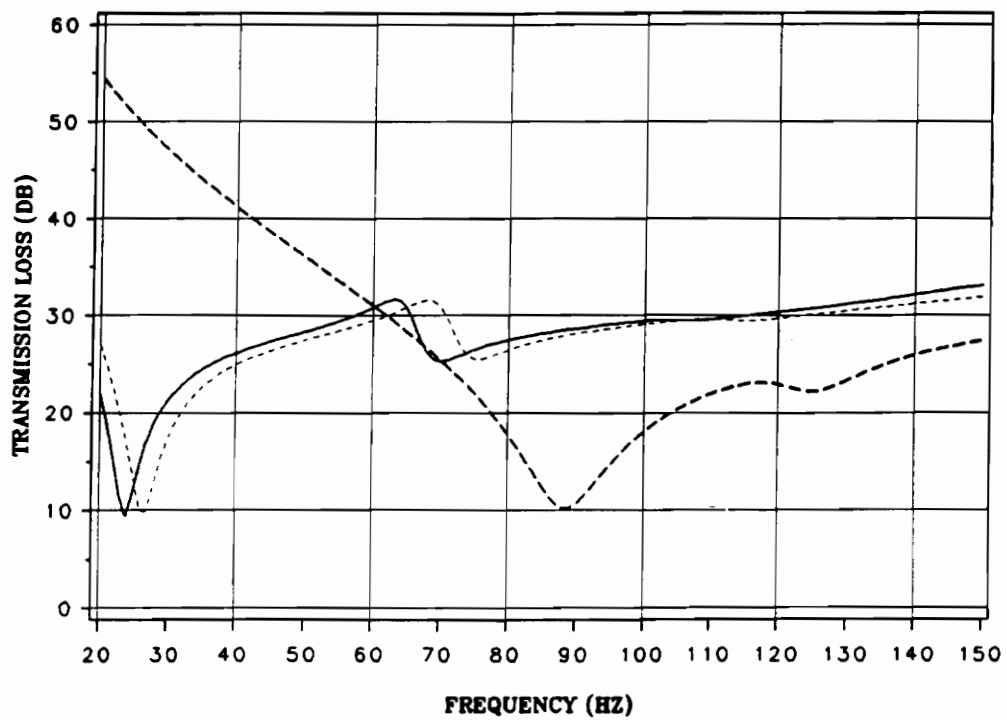
Panel Dimensions (meters)		
a	b	h
1.200	0.800	0.008

LEGEND: —————— UNACTIVATED
········· APT-ACTIVATED
—————— APT/ASET-ACTIVATED

Figure 4.5: Transmission Loss Versus Frequency for a Thin Panel (h=0.008m: Unactivated, APT-Activated, and Activated with ASET)

124
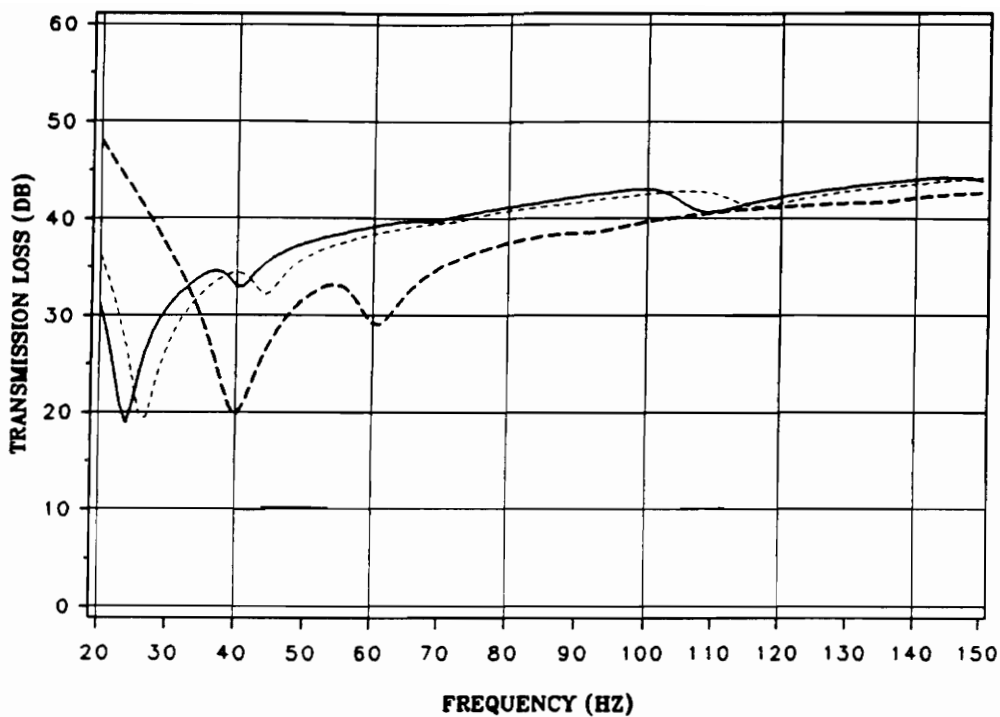
Panel Dimensions (meters)		
a	b	h
3.394	2.263	0.064

LEGEND:	————	UNACTIVATED
	--------	APT−ACTIVATED
	− − − − −	APT/ASET−ACTIVATED

Figure 4.6: Transmission Loss Versus Frequency for a Thick Panel (h=0.064m: Unactivated, APT-Activated, and Activated with ASET)

125

increase the transmission loss around the first unactivated panel resonance (23.8Hz) by less than 25dB.

4.3 Structural Damping Analysis

In this section, the influence of structural damping on structural acoustic behavior is studied considering the quasi-isotropic GFRP panel construction specified in Table 4.9. For this analysis, mass-proportional damping coefficients (ξ) of 0.025, 0.05, 0.10 and 0.20 are considered, and results are presented as transmission versus frequency curves corresponding to incident plane wave sound at 0° azimuthal and 45° polar incidence angles.

The transmission loss curves of Fig. 4.7 show an interesting trend. When acoustic incidence causes the panel to resonate (particularly at efficient sound-radiating modes), the amount of damping strongly influences structural acoustic response. For example, at and around the first natural frequency, increasing the damping coefficient from 0.025 to 0.20 raises transmission loss by nearly 15 dB between 70 and 80 Hz, where high off-resonance transmission loss diminishes with increased structural damping. For this analysis, a 5 dB tranmission loss reduction is evident as the damping coefficient increases from 0.025 to 0.20. This trend suggests that increased structural damping can either raise or lower the transmission of low-frequency sound through a panel, depending on the modal response of the structure and the excitation frequency.

Table 4.9: Panel Specifications

Ply Layup	$[90/\pm 45/0]_s$
Material	GFRP
Panel Length (a)	1.2 m
Panel Width (b)	0.8 m
Ply Thickness	0.001 m
Panel Thickness	0.008 m
E_x	18.9 GPa
E_y	18.9 GPa
G_{xy}	7.45 GPa
ν_{xy}	0.27
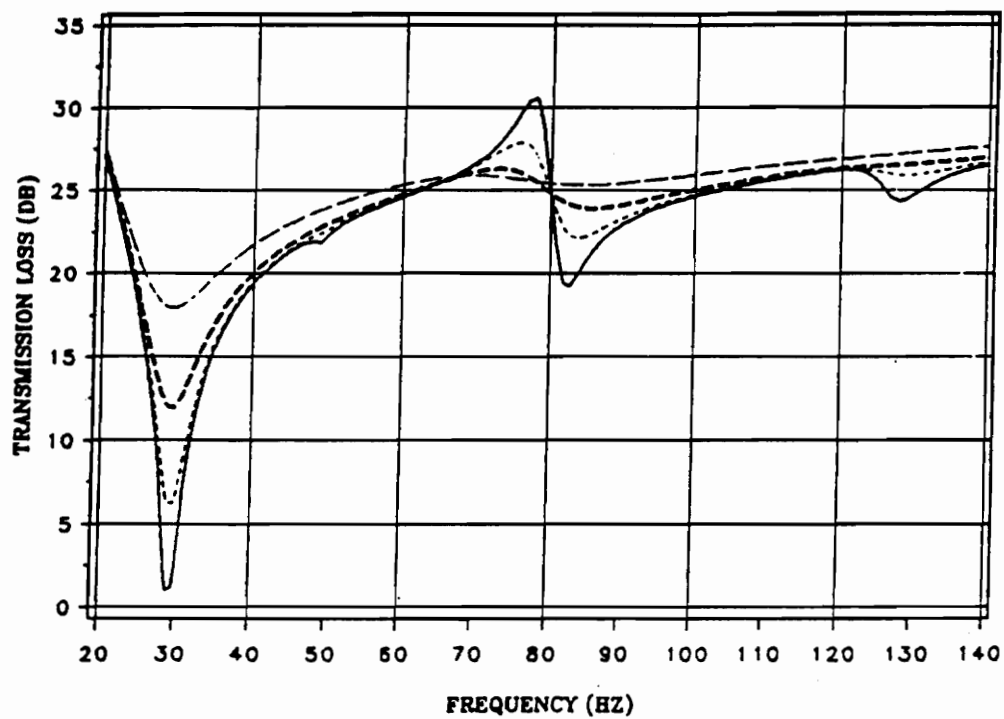
Panel Dimensions (meters)		
a	b	h
1.200	0.800	0.008

LEGEND: ——— CD=0.025 ········ CD=0.050
        ----- CD=0.100 ——— CD=0.200

Figure 4.7: Transmission Loss Versus Frequency for Various Mass Proportional Damping Coefficients

4.4 Nondimensionalized Parametric Studies

Previous sections discuss panel thickness and damping. Two additional parameters, ply lay-up and spatial dimensions are evaluated and discussed in this section. To study these parameters effectively, structural tuning of SMA hybrid composite panels is again decomposed to isolate and evaluate the effects of ASET and APT. For these analyses, normalized fundamental panel frequencies are plotted versus ply angle (θ) considering families of 8-layer, balanced symmetric, angle-ply laminates (ie. $[\pm\theta/\pm\theta]_s$).

The normalized fundamental frequency parameter chosen for this analysis is

$$\overline{\omega}_1 = \omega_1 ab \left[\frac{m_p}{(ELU)h^3} \right]^{\frac{1}{2}}. \tag{4.3}$$

where ω_1 represents the fundamental panel frequency, ELU is the unactivated Young's modulus in the longitudinal fiber direction of the material, h is the panel thickness, a and b are the respective length and width of the panel, and m_p is the panel mass per unit area.

To characterize the transformation of elastic properties induced by the SMA fiber activation, the ratio of activated to unactivated longitudinal Young's modulus ($\frac{ELA}{ELU}$) is considered. This ratio is determined for five levels of elastic properties transformation corresponding to 0% ($E_1 = 36.5 GPa$ for the unactivated laminate specified in Table 4.3), 25% ($E_1 = 39.2 GPa$), 50% ($E_1 = 41.9 GPa$), 75% ($E_1 = 44.6 GPa$) and 100% ($E_1 = 47.3 GPa$ for the fully activated laminate specified in Table 4.3). These properties are obtained by linear interpolation, considering the amount of activation assumed for each 25% properties transformation increment. The other laminate elas-

tic properties, E_2 and G_{12}, are interpolated in a similar manner for this analysis considering the activated and unactivated elastic properties listed in Table 4.3.

To evaluate the effects of aspect ratio ($\frac{a}{b}$) and ply orientation, the results of three analytical studies are presented. For these analyses, the panel length-to-width ratios are 1.0, 2.0 and 4.0, and five states of transformed elastic properties are considered. The $\frac{ELA}{ELU}$ values range from 1.0 to 1.3 considering 0%, 25%, 50%, 75% and 100% activation based on the material properties specified in Table 4.3. Figure 4.8 shows the variation of normalized fundamental panel frequency with ply angle considering $\frac{a}{b} = 1$. The maximum normalized frequency for each APT scenario in this figure corresponds to $\theta = 45°$. The influence of APT is shown in Fig.4.8 to increase the fundamental panel frequency of square angle-ply panels by 6.25% when $\theta = 45°$, and by 17% when $\theta = 0°$ or $90°$.

Figure 4.9 shows results for the same analysis repeated for a panel with $\frac{a}{b} = 2.0$. These results show that as θ increases, so does panel stiffness (and thus $\bar{\omega}_1$). Also, the curves disperse as θ approaches $90°$. These results suggest that the maximum structural tuning authority of APT in these circumstances is greatest at $90°$, where a 12% increase in fundamental frequency occurs, and is least at $0°$ where a 5% increase occurs.

For the analysis considering $\frac{a}{b} = 4$, the results (Fig. 4.10) are similar, but the fundamental frequency increase at $90°$ increases to 17%, and where $\theta = 0°$, very little structural tuning capability (5% increase in fundamental frequency) is apparent. The results of the three analyses suggest that APT control authority is greatest for panels

Figure 4.8: Dimensionless APT Study ($\frac{a}{b} = 1$)

Figure 4.9: Dimensionless APT Study ($\frac{a}{b} = 2$)

Panel Dimensions (meters)		
a	b	h
3.200	0.800	0.008

LEGEND:		
———	ELA/ELU= 1.00 ELA	
········	ELA/ELU= 1.07 ELA	
-----	ELA/ELU= 1.15 ELA	
— — —	ELA/ELU= 1.22 ELA	
— —	ELA/ELU= 1.30 ELA	

Figure 4.10: Dimensionless APT Study ($\frac{a}{b} = 4$)

with large in-plane aspect ratios, and fibers oriented parallel to the shortest spatial panel dimension.

The same basic analytical procedure is followed to isolate and evaluate the effects of structural tuning by ASET based on the in-plane panel dimensions and the laminate ply stacking sequence. For this evaluation, however, activation-induced stiffening is characterized by the ratio of recovery stress to activated longitudinal Young's modulus. Because in-plane stresses and flexural stiffnesses do not vary consistently relative to one-another with panel thickness, the nondimensional ASET analysis of this section is valid for only one width-to-thickness ratio (in this case, $\frac{b}{h} = 100$). Another subtle difference is that rather than considering the unactivated elastic longitudinal Young's modulus, the activated Young's modulus is considered, such that

$$\bar{\omega}_2 = \omega_1 ab \left[\frac{m_p}{(ELA)h^3} \right]^{\frac{1}{2}}. \tag{4.4}$$

Results for the analysis discussed above are presented in Fig. 4.11 for $\frac{a}{b} = 1$, in Fig. 4.12 for $\frac{a}{b} = 2$, and in Fig. 4.13 for $\frac{a}{b} = 4$. These results follow the same trend noted in the APT analysis: maximum structural tuning authority is achievable with high $\frac{a}{b}$ panel ratios where the fibers are oriented parallel to the shortest in-plane dimension. In Fig. 4.11, the normalized fundamental frequency is shown to increase by 183% and 233% for ply angles of 45° and 0 or 90°, respectively. The structural tuning authority increases for the $\frac{a}{b} = 2$ panel such that the maximum and minimum normalized fundamental frequency changes are 200% and 300% for $\theta = 0°$ and 90°, respectively. The structural tuning authority increases even more for the $\frac{a}{b} = 4$ panel such that the maximum and minimum normalized fundamental frequency changes are 180% and
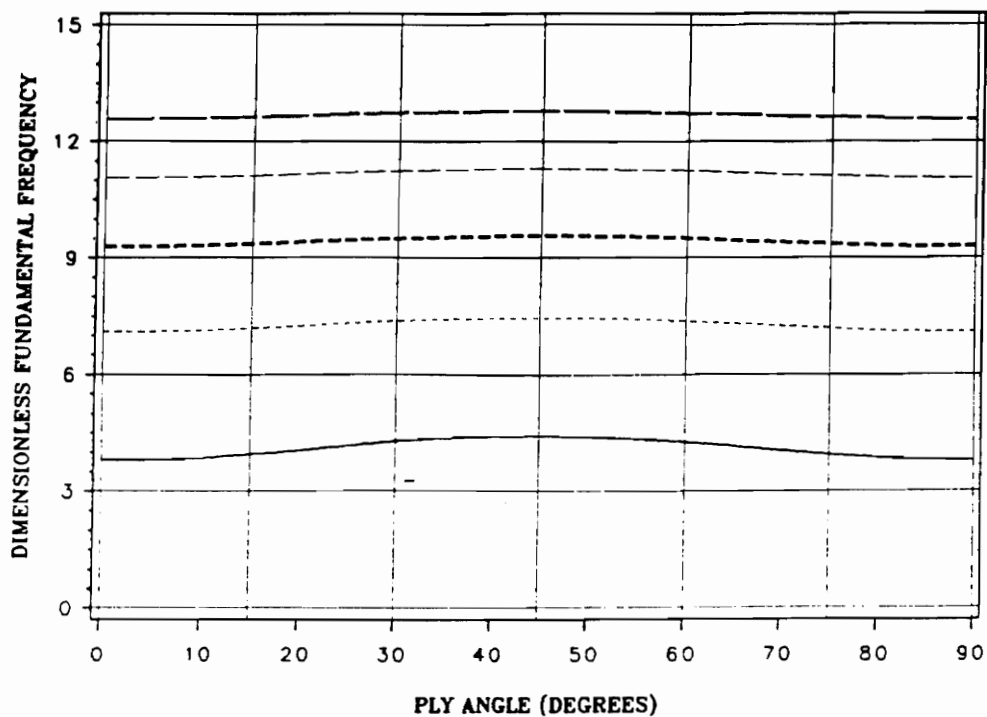
Figure 4.11: Dimensionless ASET Study ($\frac{a}{b} = 1$)

Figure 4.12: Dimensionless ASET Study ($\frac{a}{b} = 2$)
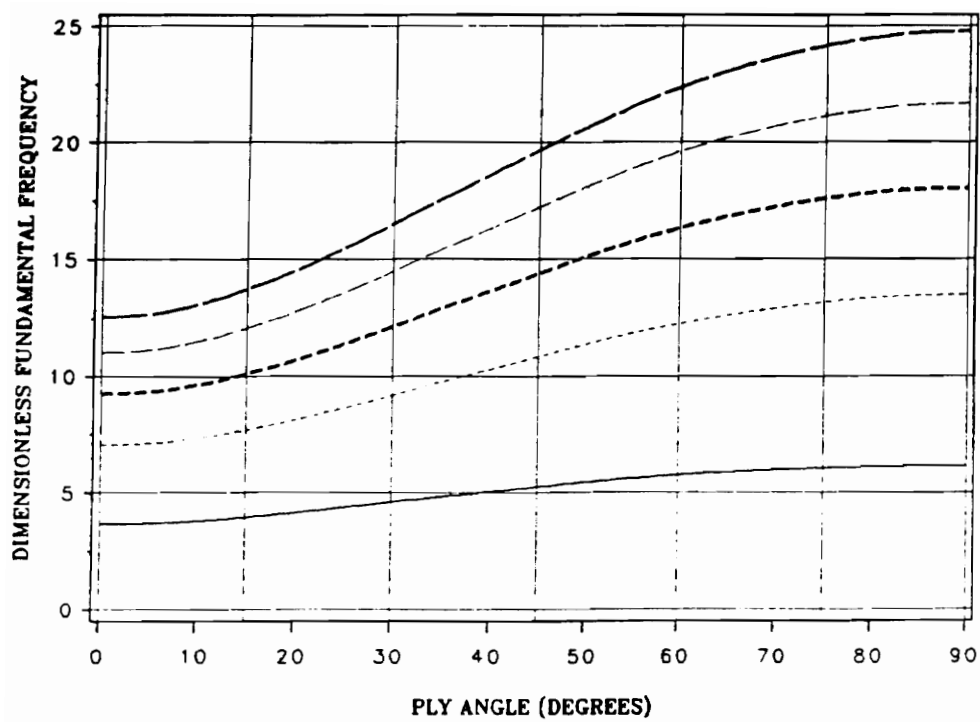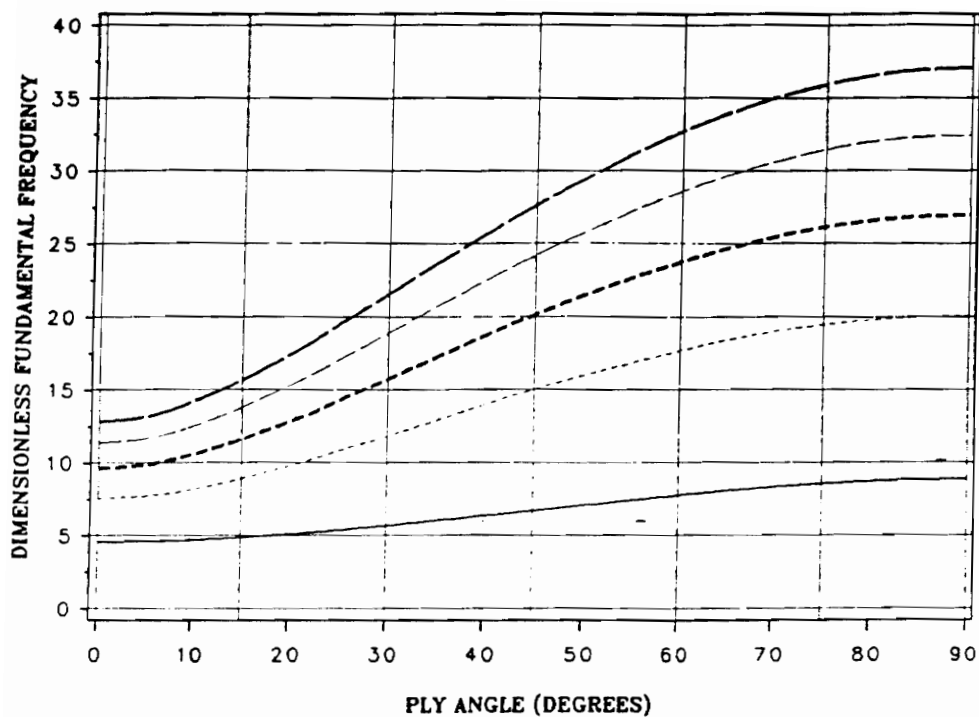
Panel Dimensions (meters)		
a	b	h
1.600	0.800	0.008

LEGEND:
——————— RECOVERY STRESS = 0.0000 ELA
·········· RECOVERY STRESS = 0.0004 ELA
— — — — RECOVERY STRESS = 0.0007 ELA
— — — RECOVERY STRESS = 0.0011 ELA
———— — RECOVERY STRESS = 0.0015 ELA

DIMENSIONLESS FUNDAMENTAL FREQUENCY vs PLY ANGLE (DEGREES)

Panel Dimensions (meters)		
a	b	h
3.200	0.800	0.008

LEGEND:		
———	RECOVERY STRESS = 0.0000 ELA
········	RECOVERY STRESS = 0.0004 ELA
– – – –	RECOVERY STRESS = 0.0007 ELA
— – —	RECOVERY STRESS = 0.0011 ELA
—— ——	RECOVERY STRESS = 0.0015 ELA

Figure 4.13: Dimensionless ASET Study ($\frac{a}{b} = 4$)

137

328% for $\theta = 0°$ and 90°, respectively. The normalized frequency dispersion for all values of θ is greater for the ASET results than for the APT results. This supports the theory that, depending on the recovery stress of the SMA material and the SMA volume fraction, for a thin panel (in this case $\frac{b}{h} = 100$), stiffness control authority of ASET can be considerably higher than APT control authority. This depends, of course, on the SMA recovery stress and volume fraction.

4.5 Locally Activated Panel Studies

Comprehensive studies investigating acoustic transmission through SMA hybrid adaptive composite panels with uniformly distributed activation have been conducted and published by Rogers, Liang and Fuller (1990). The results of this work indicate that general activation can effectively alter the transmission of low frequency sound over broad frequency ranges by changing the critical frequencies and altering mode shapes. To gain more insight into optimizing this capability, the study of locally activated SMA hybrid adaptive composite panels was initiated.

The results published by Liang, Rogers and Fuller (1990) demonstrate how natural frequencies, mode shapes and acoustic transmission loss through generally activated SMA hybrid composite panels can be controlled by active structural tuning. Analytical results for two case studies are presented in this section to demonstrate the effects of structural tuning by locally activating SMA fibers to stiffen discrete panel sections. Each of these case studies considers five panel activation scenarios which include global activation, no activation, and three cases of localized activation. Panel specifications for the first case study are provided in Table 4.10.

138

Table 4.10: First Case Study Panel Specifications

Panel Length (a)	1.1 m.
Panel Width (b)	0.8 m.
Damping Coefficient (ξ)	0.05
Ply Layup	$[90_{NiTi/Ep}/\pm 45_{GFRP}/0_{GFRP}]_s$
Ply Thickness	0.001 m
E_x (activated)	31.64 GPa
E_y (activated)	28.12 GPa
G_{xy} (activated)	12.00 GPa
ν_{xy} (activated)	0.30
E_x (unactivated)	30.50 GPa
E_y (unactivated)	22.62 GPa
G_{xy} (unactivated)	11.73 GPa
ν_{xy} (unactivated)	0.26
Nitinol/Epoxy	
Notation	NiTi/Ep
Density	$2350 \frac{Kg}{m^3}$
Composition	NiTi(40%) Epoxy(60%)
E_1 (activated)	41.36 GPa
E_2 (activated)	20.69 GPa
G_{12} (activated)	7.54 GPa
ν_{12} (activated)	0.30
E_1 (unactivated)	19.31 GPa
E_2 (unactivated)	17.25 GPa
G_{12} (unactivated)	6.43 GPa
ν_{12} (unactivated)	0.30
Activated Ply Stress	0.138 Gpa
Fiberglass	
Notation	GFRP
Density	$1790 \frac{Kg}{m^3}$
E_1	53.78 GPa
E_2	17.93 GPa
G_{12}	8.96 GPa

The adaptive SMA hybrid composite material considered for the first case study is a balanced-symmetric laminate. The generated force is assumed to be uniformly distributed throughout the 90 degree layers and symmetric about the midplane of the panel such that N_x, N_{xy}, and all applied moments are zero. The five activation scenarios and their first four mode shapes are shown with their associated natural frequencies in Figure 4.14.

These results show that all first and second modes are dominated by the characteristic 1,1 and 2,1 mode shapes, respectively. The first modes for Cases 3, 4 and 5 show some modification, as amplitudes are reduced for these cases in areas where the panel is considered to be activated. Comparing the first natural frequencies for Cases 3 and 4, the first mode of the centrally activated (Case 4) panel occurs at a considerably higher frequency, because the activation-induced stiffening is concentrated where the maximum bending curvature occurs for the characteristic 1,1 mode shape. A similar situation is apparent for the second modes with the Case 3 second mode occuring at a slightly higher frequency than the Case 4 second mode, because of concentrated activation-induced stiffening about the panel region of maximum curvature associated with the characteristic 2,1 mode shape. These results demonstrate how SMA hybrid adaptive composite materials can be locally tuned to alter the dynamic behavior of vibrating panel-like structures. Furthermore, it is evident that the effectiveness of a specific local activation scheme for controlling panel vibration at a given frequency is strongly dependent on the dominant modal characteristics of the structure at that frequency.

The third and fourth mode shapes in Fig. 4.14 illustrate the utility of active modal

140

Mode	Case 1: Unactivated	Case 2: Activated	Case 3: Left Half Activated	Case 4: Center Half Activated	Case 5: Left & Right Quarters Activated
1st mode shape (freq.)	(32.0 Hz)	(87.7 Hz)	(51.1 Hz)	(77.9 Hz)	(44.1 Hz)
2nd mode shape (freq.)	(64.7 Hz)	(99.7 Hz)	(92.7 Hz)	(83.7 Hz)	(83.5 Hz)
3rd mode shape (freq.)	(93.3 Hz)	(126.9 Hz)	(114.5 Hz)	(123.0 Hz)	(107.3 Hz)
4th mode shape (freq.)	(117.4 Hz)	(172.7 Hz)	(123.4 Hz)	(158.3 Hz)	(124.2 Hz)
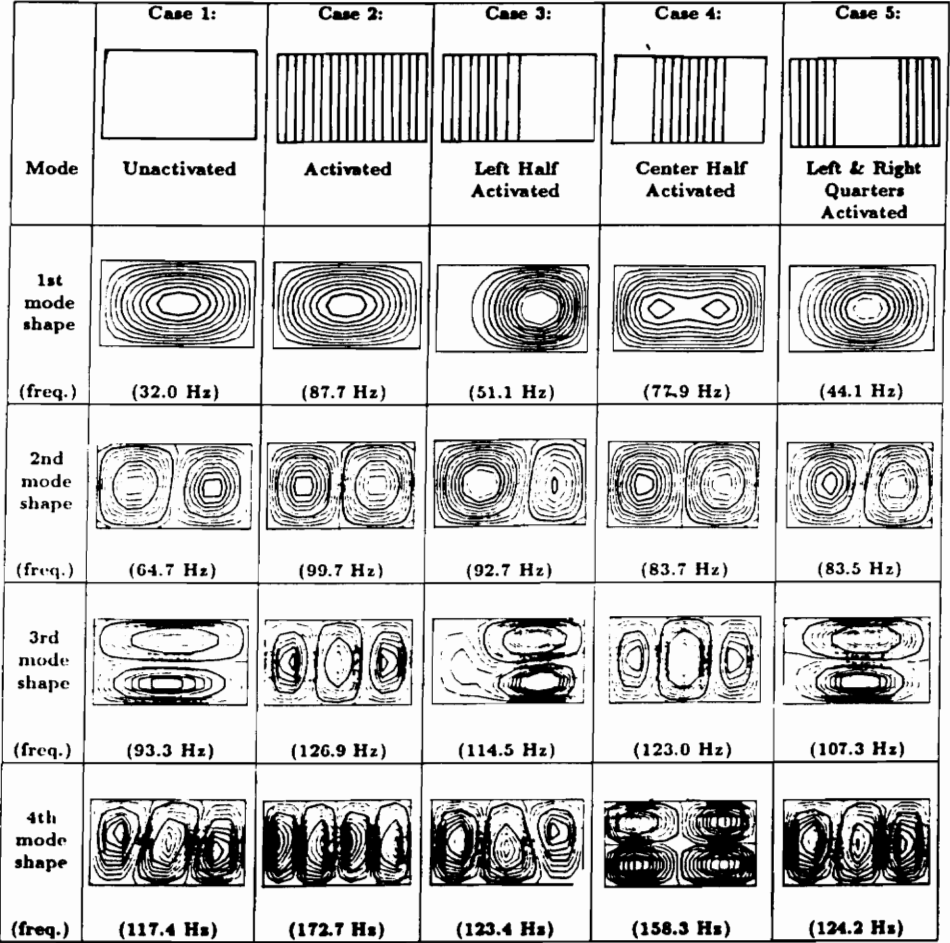
Figure 4.14: Activation and Modal Analysis Summary for First Case Study

141

modification for low frequency structural acoustic control. These modes are dominated by the 1-2, 3-1, 2-2 and 4,1 characteristic mode shapes, of which the 3,1 characteristic mode is the most efficient acoustic radiator because of unbalanced pairing of convex and concave lobes in the radiating surfaces of the panel. The 1-2, 2-2, and 4,1 characteristic mode shapes radiate sound less efficiently because of their even number of lobes, which produces lower volume velocity, and therefore less net acoustic power radiation to the far field. Selectively activating the SMA fibers to produce panel vibration with inefficient acoustic radiation can enhance acoustic transmission control capability over particular frequency ranges.

To evaluate the structural acoustic performance of the five panel activation scenarios, transmission loss was analyzed as a function of frequency considering incident plane-wave acoustic excitation. The respective polar and azimuthal incidence angles for this analysis are 45° and 0°, respectively. Transmission loss in dB is plotted versus frequency from 20 to 150 Hz in Fig. 4.15; which suggests that for this case study, general activation produces higher transmisson loss at frequencies below 65 Hz, because the structural acoustic behavior of the panel below its first resonance is stiffness dominated. From 65 to 120 Hz however, localized activation offers up to 5 dB transmission loss benefit over the generally activated or unactivated scenarios.

Comparing the modal analysis results of Fig. 4.14 with the transmisson loss versus frequency curves of Fig. 4.15; the first modes, which are dominated by the characteristic 1,1 mode shape, produce low transmission loss at and around the first resonance for all cases analyzed.

142
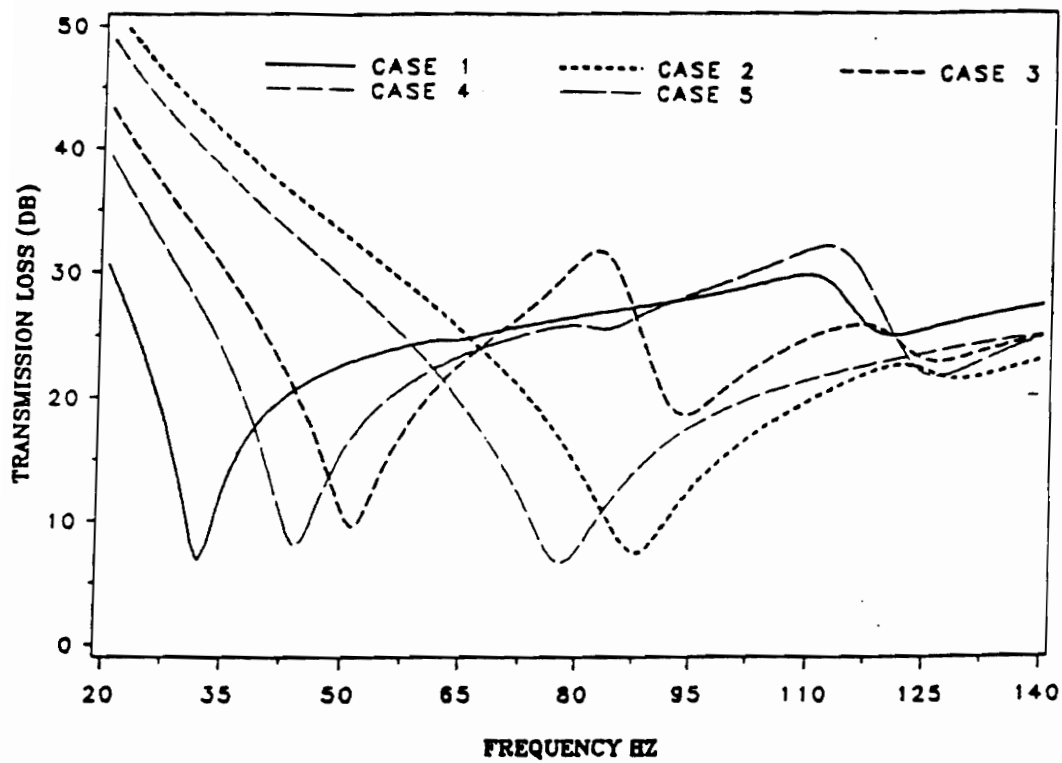
Panel Dimensions (meters)		
a	b	h
1.200	0.800	0.008

Figure 4.15: First Case Study Transmisson Loss Frequency Curves

Transmission loss for Case 3 is slightly higher at the first resonance because locally activating half of the panel causes the panel to behave like two adjacent structures which are elastically coupled at the interface. At first resonance, the more compliant section dominates the response, whereby the stiffer section is primarily stimulated by coupling at the interface. This produces less volume velocity for Case 3 at the first resonance than for the other cases; therefore less sound is transmitted through the panel. At and around second resonance, the transmission loss versus frequency curve for Case 3 exhibits a profound drop. This is explained by the second mode shape, which is now dominated by the stiffer panel section, with the more compliant section oscillating less vigorously such that the volume velocity is greater at second resonance for Case 3 than for the other scenarios.

At the third and fourth resonances, transmission loss is also very mode shape dependent. For each situation where the excitation frequency corresponds to a resonance dominated by a characteristic 3,1 mode shape, a frequency range characterized by low transmission loss appears. An exception to this observation is Case 4. Referring to the third mode shape (Fig. 4.14) for this case; the resonance is dominated by the stiffened central region, such that the center lobe of the mode shape is oscillating with greater amplitude than the outer lobes. The volume velocity for this case is lower than the 3,1 modes for the other cases; hence for Case 4, the radiation efficiency for the third mode is fairly low. Referring again to Fig. 4.15, Case 5 produces considerable transmission loss reduction at and around the fourth resonance. The fourth mode shape for Case 5 shown in Fig. 4.14 is dominated by the outer lobes, which oscillate with greater magnitude than the central lobe. This produces higher volume velocity and therefore reduces transmission loss at and around that resonance.

144

The utility of using SMA hybrid composites for adaptive low frequency structural acoustic control is demonstrated in Fig. 4.15, as the minimum transmission loss for any single case alone is less than 10 dB. Considering all 5 activation scenarios, the transmission loss attainable over the frequency range evaluated can be controlled to always exceed 25 dB by choosing an activation scheme - localized, general or unactivated - to most effectively reduce the transmission of incident sound at a given frequency.

A second case study was performed considering the laminate specified in Table 4.11. Figure 4.16 summarizes the five activation scenarios considered for this analysis, and their first four mode shapes and natural frequencies. The previous study considered activation that could be resolved into rectangular panel sections. For this case study, the 45° plies rather than the 90° plies are nitinol epoxy layers. This produces N_x, N_y and N_{xy} force resultants in the activated sections of the panel. Also, localized activated scenarios must be resolved into quadrilateral and triangular regions for analysis. This is handled by integrating Eqs.(3.54), (3.57) and (3.58) between limits in y which are defined as linear functions of x rather than constants.

Transmission loss curves are presented for these cases in Figure 4.17. As in the first analysis, structural acoustic control advantages are realized above 60 Hz; however none of the cases considered is clearly advantageous over the others throughout the low frequency spectrum.

Summarizing the results of this section, midplane-symmetric panel activation applies in-plane force resultants that produce material stiffening effects capable of altering

145

Table 4.11: Second Case Study Panel Specifications

Panel Length (a)	1.1 m.
Panel Width (b)	0.8 m.
Damping Coefficient (ξ)	0.05
Ply Layup	$[90_{GFRP}/45_{NiTi/Ep}/-45_{GFRP}/0_{GFRP}]_s$
Ply Thickness	0.001 m
E_x (activated)	31.64 GPa
E_y (activated)	28.12 GPa
G_{xy} (activated)	12.00 GPa
ν_{xy} (activated)	0.30
E_x (unactivated)	30.50 GPa
E_y (unactivated)	22.62 GPa
G_{xy} (unactivated)	11.73 GPa
ν_{xy} (unactivated)	0.26
Nitinol Epoxy	
Notation	NiTi/Ep
Density	2350 $\frac{Kg}{m^3}$
Composition	NiTi(40%) Epoxy(60%)
E_1 (activated)	41.36 GPa
E_2 (activated)	20.69 GPa
G_{12} (activated)	7.54 GPa
ν_{12} (activated)	0.30
E_1 (unactivated)	19.31 GPa
E_2 (unactivated)	17.25 GPa
G_{12} (unactivated)	6.43 GPa
ν_{12} (unactivated)	0.30
Activated Ply Stress	1.38 Gpa
Fiberglass	
Notation	GFRP
Density	1790 $\frac{Kg}{m^3}$
E_1	53.78 GPa
E_2	17.93 GPa
G_{12}	8.96 GPa
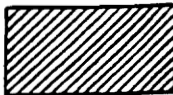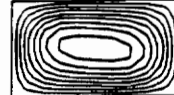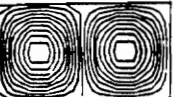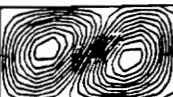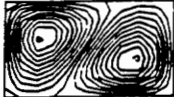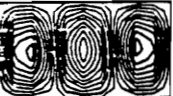
Mode	Case 1: Unactivated	Case 2: Activated	Case 3: Left Half Activated	Case 4: Center Half Activated	Case 5: Left & Right Quarters Activated
1st mode shape (freq.)	(34.9 Hz)	(79.1 Hz)	(52.8 Hz)	(64.5 Hz)	(61.6 Hz)
2nd mode shape (freq.)	(62.9 Hz)	(116.3 Hz)	(91.5 Hz)	(86.2 Hz)	(97.0 Hz)
3rd mode shape (freq.)	(111.1 Hz)	(170.3 Hz)	(129.2 Hz)	(134.4 Hz)	(138.3 Hz)
4th mode shape (freq.)	(113.3 Hz)	(185.1 Hz)	(148.5 Hz)	(156.2 Hz)	(152.0 Hz)

Figure 4.16: Activation and Modal Analysis Summary for Second Case Study

147
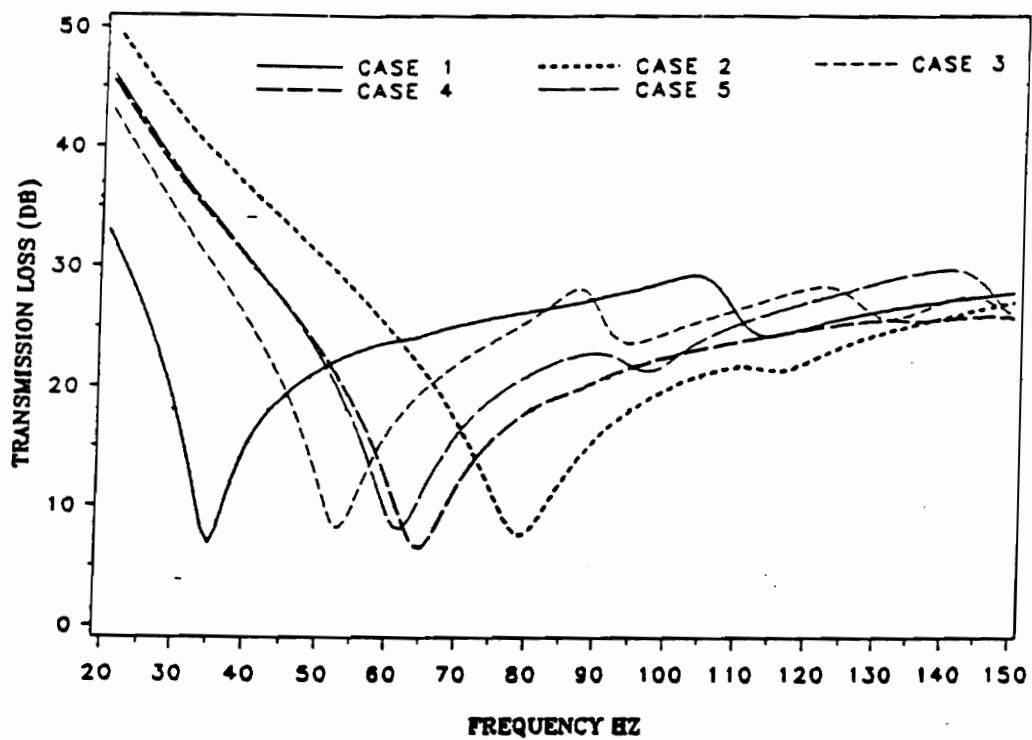
Figure 4.17: Transmisson Loss Versus Frequency Plots for Second Case Study

Panel Dimensions (meters)		
a	b	h
1.200	0.800	0.008

resonant frequencies and mode shapes. Resonant frequencies can be increased if activation-induced stiffening is concentrated about the areas where maximum bending curvature occurs, which are strongly mode shape dependent. For the balanced symmetric adaptive laminates considered, the third and fourth mode shapes were successfully modified; however, the dominant characteristic 1,1 first mode shapes were not significantly altered, resulting in low transmission loss at and around the first natural frequencies. By selectively activating fibers throughout the low frequency range such that maximum transmission loss is achieved at discrete frequencies, minimum transmission loss through adaptive SMA hybrid composite panels can be increased from less than 10 dB to approximately 25 dB.

A technique was presented in Section 3.5 and demonstrated in this section for analyzing the modal and structural acoustic behavior of locally activated, simply supported, thin, anisotropic, adaptive composite panels with mid-plane symmetric elastic properties and applied in-plane force resultants. The application of this technique is not limited to SMA hybrid composite panels, as the same theory can be applied to analyze panels locally stiffened by ribs or struts.

Analytical results for two case studies are presented to demonstrate how various localized and general activation schemes affect critical frequencies, mode shapes, and transmission loss from 20 to 150 Hz. These results indicate that localized panel activation can enhance the structural acoustic control capabilities of SMA hybrid composite structures in the low-frequency range. Activating SMA fibers embedded in a composite structure consumes electrical energy. Localized activation requires less energy than general activation, enabling adaptive structural acoustic control with reduced

power consumption.

Acoustic transmission control capabilities were identified in the stiffness-controlled frequency range. These capabilities can be improved by more effectively modifying the first mode shape, which for all cases evaluated in this paper is dominated by the characteristic 1,1 mode shape. Section 4.6 presents a technique by which the first and second mode shapes can be effectively modified, and demonstrates how this affects the structural acoustic panel behavior. This concept, adaptive alternate resonance tuning can be implemented to strategically, purposefully and adaptively tune SMA hybrid composite panels to effectively control low-frequency sound transmission through panel-like structures.

4.6 Adaptive Alternate Resonance Tuning of SMA Hybrid Composite Panels

When adjacent sound-transmitting panels in a structure are tuned to resonate above and below a particular frequency such that they oscillate and radiate sound with equal source strength and opposite phase, radiated sound is readily attenuated by the structure at and near the frequency to which the panels are tuned. This concept is known as alternate resonance tuning (ART). The amplitude and phase characteristics of two adjacent panels tuned for ART are shown in Figure 4.18.

 A simply supported SMA hybrid composite panel can be locally stiffened by selectively activating embedded SMA fibers to achieve ART adaptively, thereby enabling the panel to attenuate sound over several activation-dependent frequency ranges. Sections 4.6.1 and 4.6.2 include analytical studies of this adaptive ART concept consider-
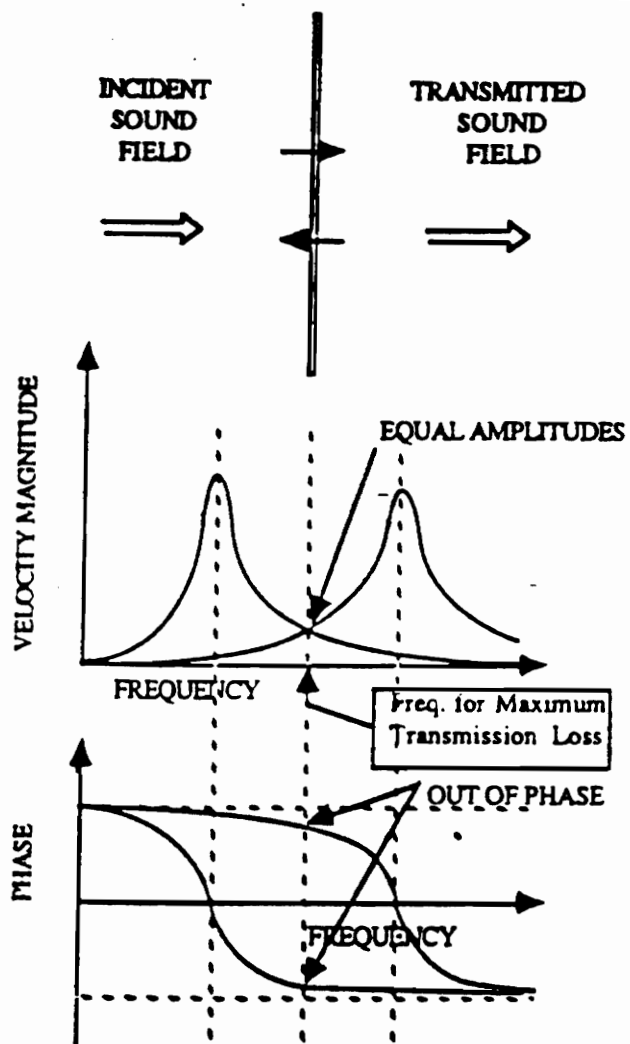
150

Figure 4.18: Amplitude and Phase Relations of Adjacent Panels Tuned for ART

ing localized activation of SMA hybrid composite panels, and identify some physical trends and characteristics which influence its capabilities.

Bliss and Gottwald (1990) experimentally demonstrated the concept of alternate resonance tuning by arranging panel arrays with adjacent panels tuned to resonate above and below a given operating frequency. Acoustic incidence at that frequency was observed to excite the panels to oscillate with nearly equal amplitude and opposite phase, thereby radiating sound with comparable source strength but opposite phase; causing high near-field acoustic interaction, and effective reduction of sound transmission to the far-field. The concept of ART was devised as a passive technique for reducing sound transmission through a panel-like structure when excited by incident sound at or near a particular frequency. The following sections present and analytically demonstrate the concept of adaptive ART by localized activation of SMA hybrid composite panels.

4.6.1 Adaptive ART of a Single Simply Supported Panel

An investigation of the utility and performance of adaptive ART by localized activation of SMA hybrid composites was initiated to address the issue of low frequency structural acoustic control. Selectively activating the SMA fibers embedded near the center of a panel induces localized stiffening and produces a "rigid" section interposed between two compliant sections. The stiffened section may be regarded as a pseudo-stiffener or support which couples the two adjacent 'compliant' panel sections, ie. the complete panel is adapted into sub-panel regions. This coupling influences the modal and structural acoustic behavior of the panel as a whole. The concept of adap-

tive ART using a single panel differs significantly from the passive control concept using an array of indepenently supported panels introduced by Bliss and Gottwald, as dynamic and structural acoustic panel behavior can be actively tuned to exploit the advantages of ART over several frequency ranges by strategic placement of the activated SMA fiber region in order to adapt the panel configuration in response to changing input disturbances.

Previous investigations considering locally and globally activated panels showed no significant modification of the first and second mode shapes. Analytical results for a unidirectional SMA hybrid fiberglass (NiTi/GFRP) panel with a narrow band of fibers considered activated at its center to demnstrate the capability of effectively modify the first two mode shapes, such that the two unactivated panel sections appear to assume their own separate modal identities, with a finite amount of coupling introduced in the activated region.

Displacing the region of activation-induced stiffening from the center of the panel introduces a stiffness inbalance between the two unactivated sections, thereby tuning them to resonate at different frequencies. Moving the activated section about the central region of the panel changes the modal response of the entire panel and the stiffnesses of the unactivated panel sections; stiffening one section, making the other more compliant, and retuning the alternate resonance behavior. Sound transmission through SMA hybrid composite panels can be adaptively mimimized by strategically activating fibers to best attenuate incident sound over a range of frequencies by exploiting the concept of ART thus providing broad-band structural acoustic control capability.

To demonstrate the concept of adaptive ART, a 0.8m by 1.2m unidirectionally laminated panel composed of 60% fiberglass by volume and 40% nitinol (nickel-titanium shape memory alloy) was analyzed. The material and geometry specifications for this panel are listed in Table 4.12.

The structure, shown in Fig. 4.19, has all fibers (glass and nitinol) oriented parallel to the shorter spatial panel dimension for maximum structural tuning authority. The activation-induced recovery stress in the nitinol fibers is assumed to be 344 MPa (50 Ksi, which corresponds to 5% initial strain and an SMA fiber activation temperature of 127° per Fig. 2.3); thus the internally distributed stress throughout the laminate, where activated, is 138 MPa by Eq.(2.8). The magnitude and sign of this stress are determined by the initial inelastic strain of the SMA fibers; the recovery stress-strain behavior of the SMA material; and the laminate cure cycle. These effects are are currently being investigated in detail (Rogers, Fuller and Liang, 1990).

The mechanism by which adaptive ART is achieved using a single SMA hybrid composite panel is best described as follows. Activating a narrow band of SMA fibers in the central region of the panel (see Fig. 4.19) applies a strong, unidirectional tension, alters the local state of strain energy, and produces an activation-induced pseudo-rib or stiffener. The presence of this pseudo-rib divides the panel into three sub-structures: two larger unactivated sub-panel sections with the pseudo-rib between them. The pseudo-rib causes the unactivated sub-panels to vibrate as two elastically coupled structures, and thereby changes the vibratory response of the overall structure.

154

Table 4.12: SMA Hybrid Composite Panel for Adaptive ART

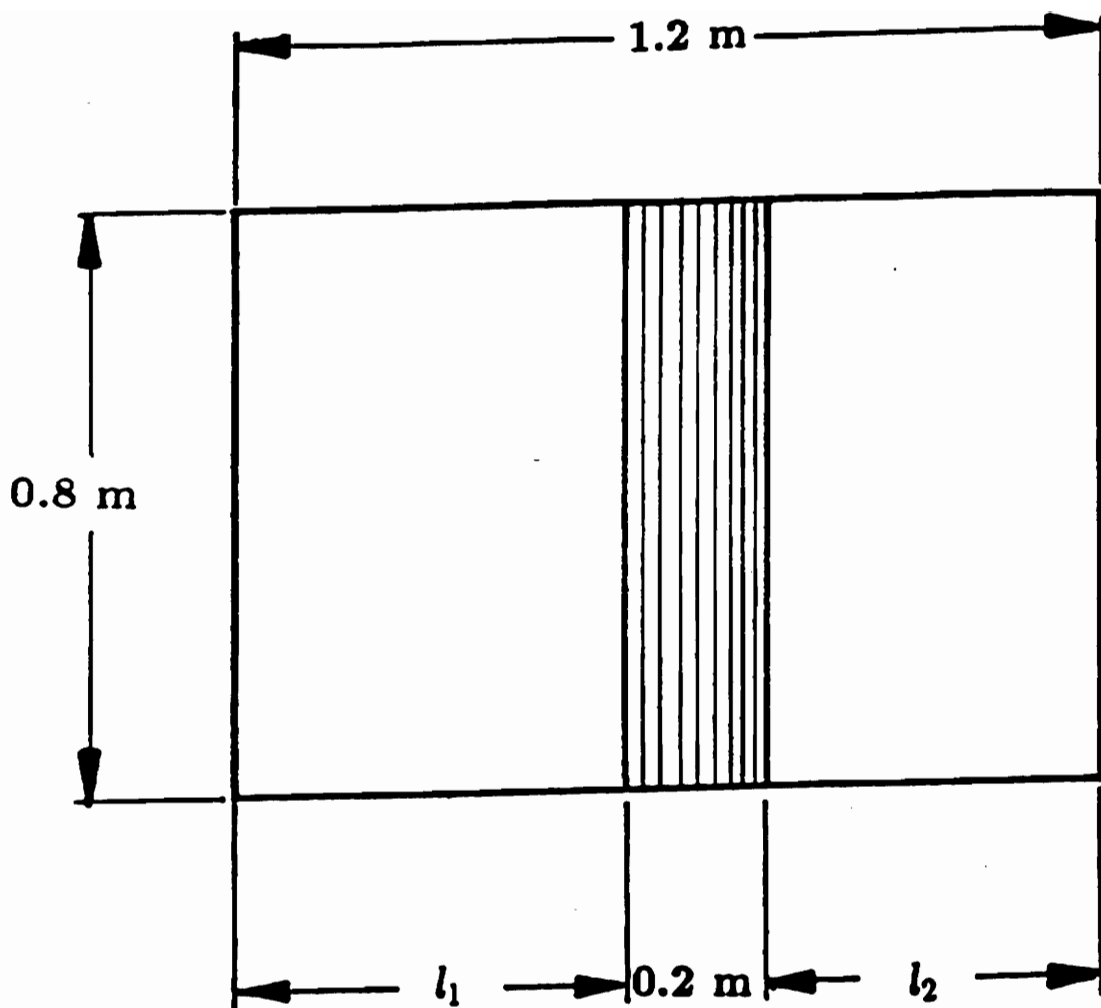| Panel Length (a)	1.2 m.
Panel Width (b)	0.8 m.
Ply Layup	$[90_{NiTi/GFRP}]$
Nitinol/Fiberglass	
Notation	NiTi/GFRP
Density	2680 $\frac{Kg}{m^3}$
Composition	NiTi(40%) Fiberglass(60%)
E_1 (activated)	56.24 GPa
E_2 (activated)	49.10 GPa
G_{12} (activated)	5.47 GPa
E_1 (unactivated)	34.2 GPa
E_2 (unactivated)	33.30 GPa
G_{12} (unactivated)	5.47 GPa
Thickness	0.008 m
Activated Ply Stress	.138 Gpa

Figure 4.19: Activation Scheme for Adaptive ART

To demonstrate this concept, four ART activation scenarios are analyzed considering the parameters of Table 4.12 and the panel geometry of Fig. 4.19. The variable $\frac{l_1}{l_2}$ is introduced to characterize each ART activation scheme in terms of the widths of the unactivated panel sections. The $\frac{l_1}{l_2}$ ratios chosen for this analysis are 0.7, 0.8, 0.9 and 1.0. To demonstrate the effectiveness of adaptive ART, an unactivated panel was also analyzed for comparison. The plane wave acoustic excitation for this analysis is oriented at 45° polar (θ_i) and 0° degree azimuthal (ϕ_i) incidence angles.

Figure 4.20 summarizes the modal analysis results along with transmisson loss values corresponding to the first and second resonances for each case. These results show that the first two modes can be actively modified by this adaptive structural tuning technique. Comparing the first mode shapes indicates that the the activation-induced pseudo-rib causes the panel to vibrate as two coupled sub-structures, and the first mode shapes can be altered somewhat by moving the pseudo-rib about the central panel region (changing the $\frac{l_1}{l_2}$ ratio), thus altering vibrational balance between the two modal lobes. Two physical effects influence the modal response of the activated panels considered. The presence of the pseuo-rib causes the subpanels to oscillate out-of-phase at the first panel resonance. The location of the pseudo-rib also simultaneously tunes the sub-panels such that the larger, more compliant sub-panel dominates the first panel resonance; and the smaller, stiffer sub-panel dominates the second resonance.

Considering the first resonance transmission loss results of Fig. 4.20, the activated cases demonstrate effective sound transmission reduction at first resonance by active
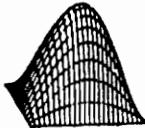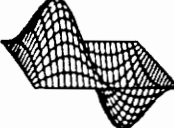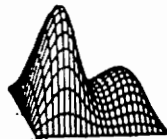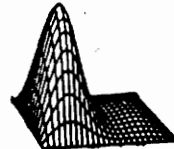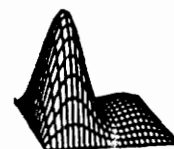
ACTIVATION	FIRST MODE SHAPE	FREQUENCY (TL)	SECOND MODE SHAPE	FREQUENCY (TL)
Unactivated		27.7 Hz (9.3 dB)		52.6 Hz (26.8dB)
$\frac{l_1}{l_2} = 1.0$		57.3 Hz (17.8 dB)		64.3 Hz (9.2 dB)
$\frac{l_1}{l_2} = 0.9$		56.2 Hz (21.2 dB)		65.9 Hz (10.7 dB)
$\frac{l_1}{l_2} = 0.8$		53.6 Hz (18.5 dB)		69.6 Hz (12.6 dB)
$\frac{l_1}{l_2} = 0.7$		50.8 Hz (16.3 dB)		75.0 Hz (14.0 dB)

Figure 4.20: Modal Analysis Summary

158

modal modification. The transmission loss values at second resonance for these cases, however, do not compare favorably with the unactivated case. At second resonance, the coupling introduced by the pseudo-rib adversely effects the structural acoustic behavior of the ART-activated panels because it causes the unactivated sub-panels to oscillate in-phase. The second mode shapes in Fig. 4.20 show how the smaller, stiffer, unactivated sub-panels dominate the second panel resonances.

To further evaluate the effects of active modal modification, radiation efficiency is plotted versus nondimensionalized frequency (γ) in Figs. 4.21 and 4.22. Comparing the first mode radiation efficiencies for the cases considered, the low frequency radiation efficiency for the $\frac{l_1}{l_2} = 1.0$ scenario is significantly lower than the low-frequency radiation efficiencies for the first mode shapes associated with the other scenarios. This is because the 2,1 characteristic first mode shape for the $\frac{l_1}{l_2} = 1.0$ case produces lower volume velocity at a given frequency than the other cases considered. As the $\frac{l_1}{l_2}$ ratios are decreased, the lobes of the first mode shape become less balanced, the volume velocities increase, and the radiation efficiency increases as well.

In Fig. 4.22, radiation efficiencies for the second mode shapes are plotted versus non-dimensionalized frequency. For the second modes, the unactivated panel radiates sound more efficiently at a given frequency, where $\gamma < 1$, than the adaptive cases. Referring again to Fig. 4.20, the second mode for the unactivated panel is dominated by the characteristic 2,1 mode shape, which produces lower panel volume velocity at a given frequency than the adaptive ART scenarios.

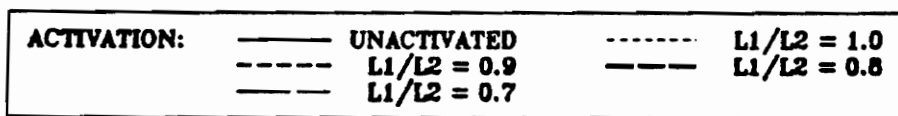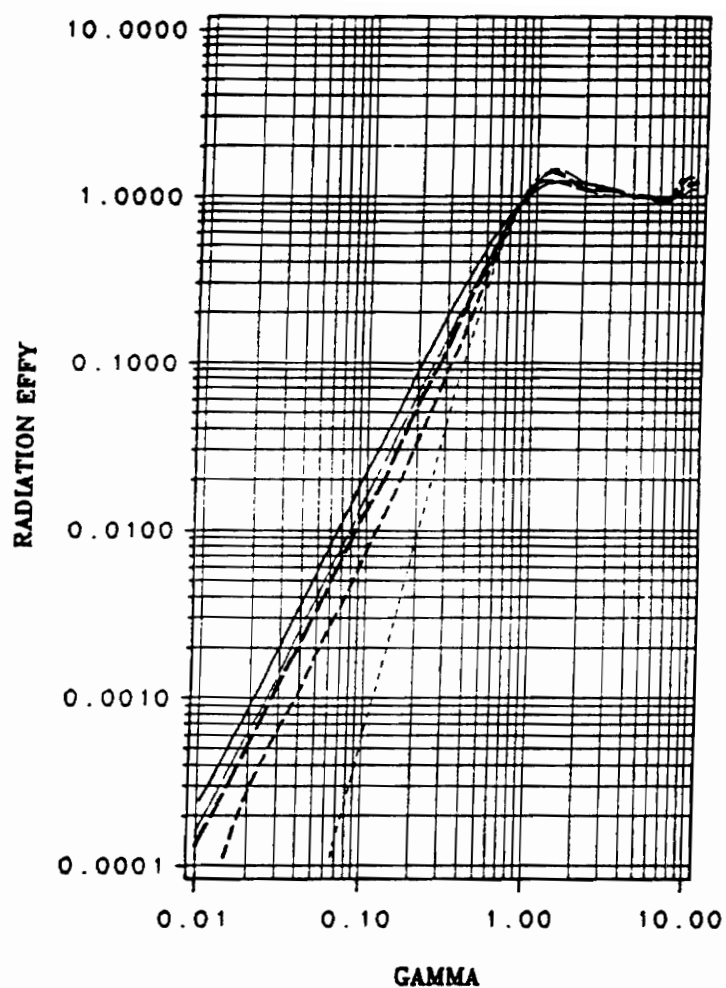The results presented in Figs. 4.20 through 4.22 indicate that adaptive structural

159

Figure 4.21: First Mode Radiation Efficiencies Versus Frequency
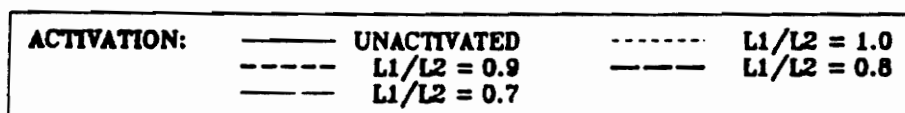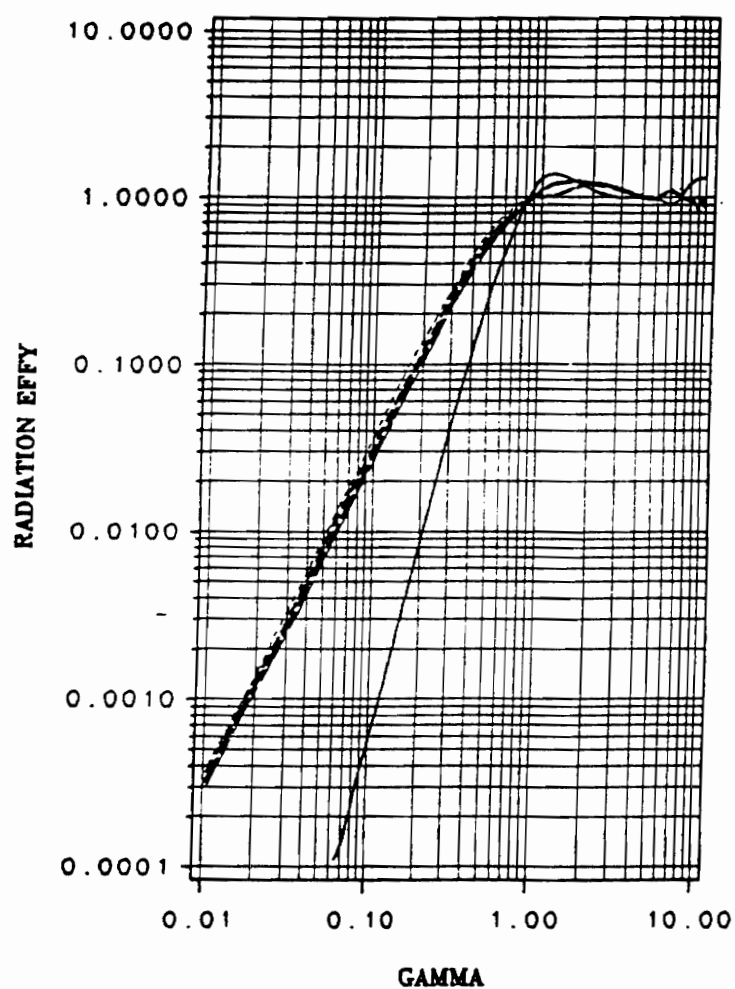
Figure 4.22: Second Mode Radiation Efficiencies Versus Frequency

acoustic control by active modal modification alone does not necessarily guarantee effective broad-band low-frequency control capability. In fact, the concept of ART was formulated considering off-resonance structural acoustic behavior; therefore, adaptive ART is best studied by evaluating transmission loss as a function of frequency.

Acoustic transmission loss is plotted in Fig. 4.20 versus frequency from 20 to 100 Hz for each of the activation scenarios. The effects of active modal modification by adaptive ART are most evident at and around the first two resonances for the activated cases. The results shown in Fig. 4.23 are consistent with the radiation efficiency curves of Figs. 4.21 and 4.22 and the mode shapes shown in Fig. 4.20. The first resonance transmission loss magnitudes for the activated cases are greater than the transmission loss levels at and around the second resonances. This illustrates how active modal modification can be used to effectively change the radiation efficiency and transmission loss at and around the first and second natural frequencies. To most effectively increase sound attenuation at a particular frequency by adaptive ART, Fig. 4.22 indicates that the off-resonance behavior is more critical for adaptive structural acoustic control than the on-resonance response.

For the activated panels, high off-resonance transmission loss peaks occur between the first and second natural frequencies. This behavior is the key mechanism behind the concept of ART: tuning adjacent panels to resonate above and below the particular frequency to which the system is tuned. The benefit of adaptive ART is that the stiffnesses of two adjacent panel sections can be actively and simultaneously modified by moving the activated SMA fiber band to reduce the radiated sound such that the off-resonance transmission loss peaks are tuned to occur at a given frequency.
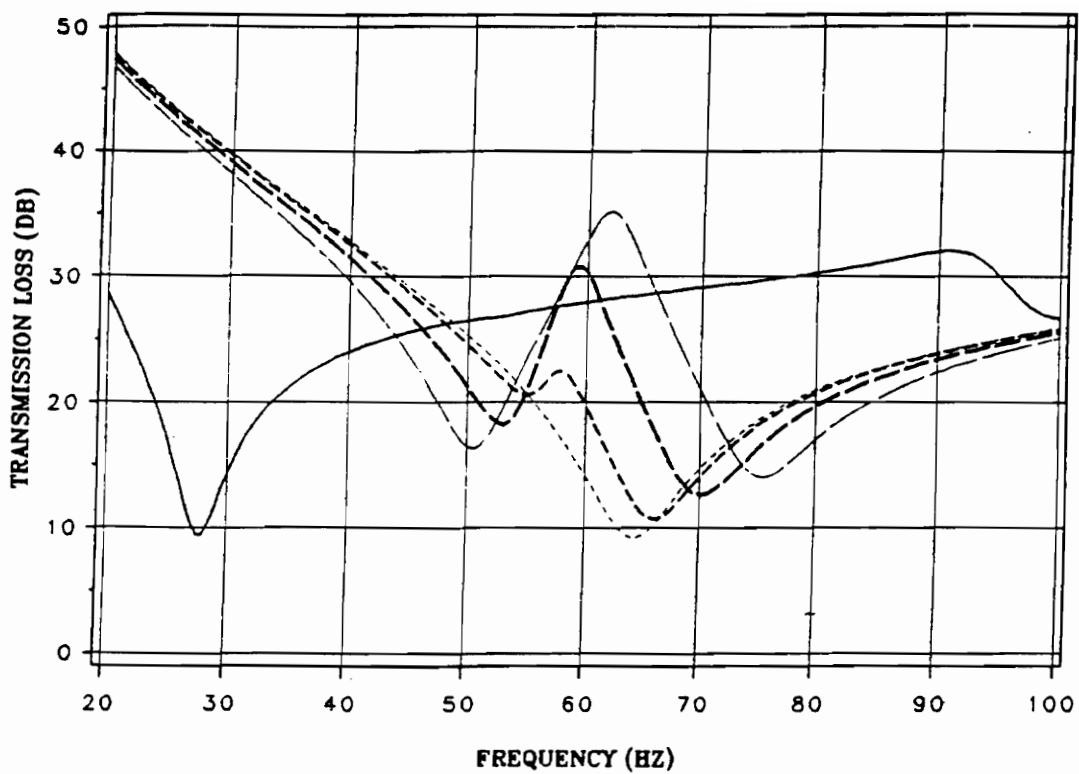
162

Figure 4.23: Transmisson Loss Versus Frequency (unactivated and $\frac{l_1}{l_2} = 0.7$ through 1.0)

Figure 4.23 shows an off-resonance transmission loss peak for the $\frac{l_1}{l_2} = 0.7$ panel that attenuates up to 7 dB more acoustic power than the unactivated panel near 62 Hz. Considering $\frac{l_1}{l_2}$ ratios ranging from 0.4 to 0.7 in increments of 0.1. Figure 4.24 shows how this control capability can be exploited from 55 to 88 Hz. Over the frequency ranges of 20 to 48 Hz and 58 to 88 Hz, active structural acoustic control advantages have been demonstrated considering only 6 panel activation scenarios. The panel considered for this study can be actively tuned in a nearly infinite number of localized fiber activation arrangements; thus further investigation can certainly further enhance the structural acoustic control capability for this particular panel.

Analytical results are presented in this section for a thin, unidirectional SMA fiber reinforced laminate to demonstrate how SMA hybrid composite panels can be locally activated in various arrangements to modify mode shapes, modal radiation efficiencies and sound transmission loss at and around the first two resonant frequencies. The concept of adaptive alternate resonance tuning was analytically demonstrated considering a nitinol reinforced fiberglass panel to effectively attenuate sound between the first and second resonant frequencies.

Numerous possibilities exist for implementing the concept of adaptive ART using SMA hybrid composites. For example, an array of independently supported SMA fiber reinforced composite panels can be selectively activated - either locally, generally, or with varying degrees of fiber activation - to further enhance the structural acoustic control capabilities demonstrated for alternate resonance tuning.
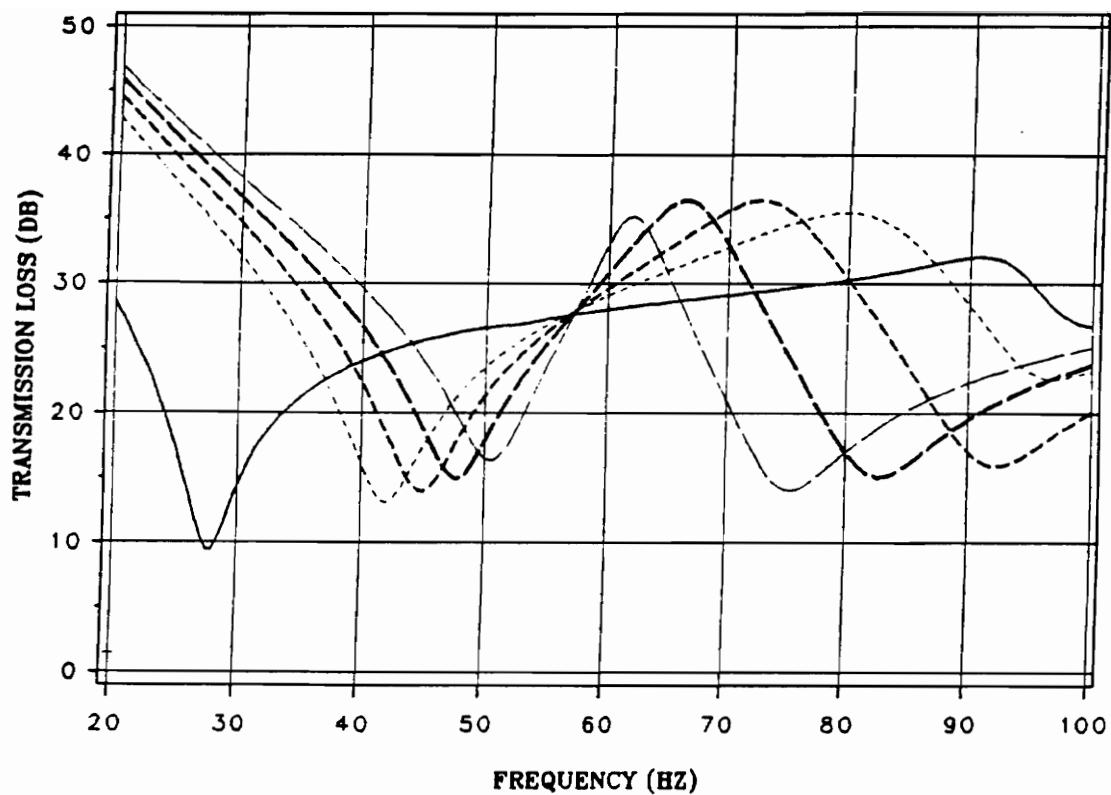
Panel Dimensions (meters)		
a	b	h
1.200	0.800	0.008

ACTIVATION:
——— UNACTIVATED   ········· L1/L2 = 0.4
- - - - - L1/L2 = 0.5   — — — L1/L2 = 0.6
— — L1/L2 = 0.7

Figure 4.24: Transmisson Loss Versus Frequency ($\frac{l_1}{l_2}$= 0.4 through 0.7.0)

4.6.2 The Effects of Damping on Adaptive ART

In Section 4.3, the effects of damping on structural acoustic behavior are evaluated and discussed. The results of this evaluation suggest that transmission loss tends to increase with increased damping at and near resonant frequencies. At certain off-resonance conditions, however, it is apparent that transmission loss tends to decrease as damping increases. The purpose of this subsection is to determine how structural damping affects structural acoustic control by adaptive ART.

The analysis of this section considers the $\frac{l_1}{l_2} = 0.6$ activation scenario for the adaptive ART strategy discussed in the previous section. The same acoustic incidence is considered for this study ($\theta_i = 45°$ and $\phi_i = 0°$). The mass proportional damping coefficients, ξ, evaluated are 0.010, 0.025, 0.050, and 0.100. The results of this analysis are presented in Fig. 4.25. As seen in the previous damping study, the transmission loss at and near the first and second panel resonances is very sensitive to damping. Contrary to the notion that off-resonance transmission loss should diminish with increased structural damping, this analysis predicts that increased damping tends have little effect on, and in fact increases transmission loss in the frequency range where ART is effective.

4.6.3 Adaptive ART of a Centrally Supported Panel

The concept of adaptive ART using a single SMA hybrid composite panel presented earlier in this section requires an activation-induced pseudo-rib or stiffener to cause the panel to vibrate as two coupled substructures. This concept is very sensitive to laminate ply stacking sequence, which limits the amount of tailoring versatility which

166
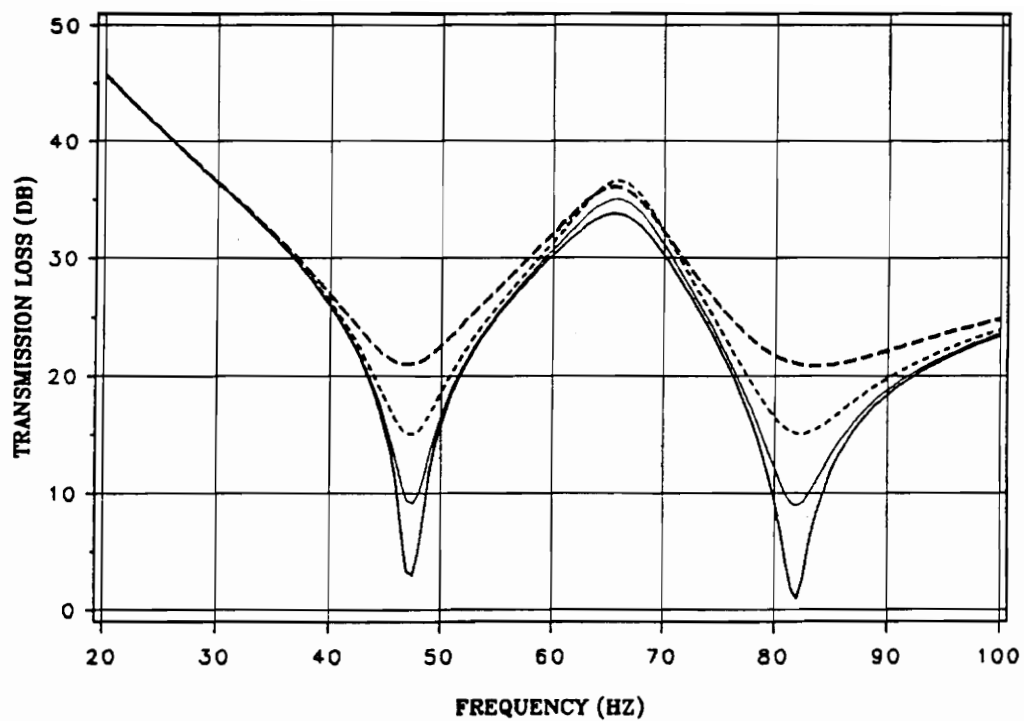
Panel Dimensions (meters)			
a	b	h	$\frac{l_1}{l_2}$
1.200	0.800	0.008	0.60

DAMPING COEFFICIENT:		
	———	0.010
	———	0.025
	··········	0.050
	— — —	0.100

Figure 4.25: ART Damping Analysis

may be required to optimize the strength and stiffness of a panel like structure. Another drawback of this approach is that the strength of the structure may be locally reduced due to the inclusion of a large concentration of SMA fibers when unactivated, and the composite itself may be locally weakened by the presence by highly concentrated heat energy at the location of the activation-induced pseudo-rib.

This section presents another arrangement which includes two adjacent simply supported panels with an elastically coupled common boundary. This arrangement enables the panels to be tuned independently without the need for an activation-induced pseudo-stiffener; thus allowing decreased concentrated heat energy, and laminate ply stacking sequence flexibility.

The case study presented in this section considers a similar arrangement to the panel evaluated previously for for the single panel ART studies, the ply stacking sequence is quasi-isotropic (rather than unidirectional), and the structure is divided into two identical separate panels with a simple support introduced at their common boundary (or edge) as illustrated in Fig. 4.26.

The support is modeled as a very narrow rib that is slighlty displaced from the center of the panel. The elastic properties of this rib are sveral orders of magnitude greater than the elastic properties condidered for the rest of the panel, which introduces high stiffness in its longitudinal direction. This high stiffness supresses transverse deformation in the region of the panel near the rib, such that the two adjacent panel sections vibrate as two separate structures. The rib is modeled as being slightly offset from the panel center to eliminate the analytical occurance of degenerative modes.
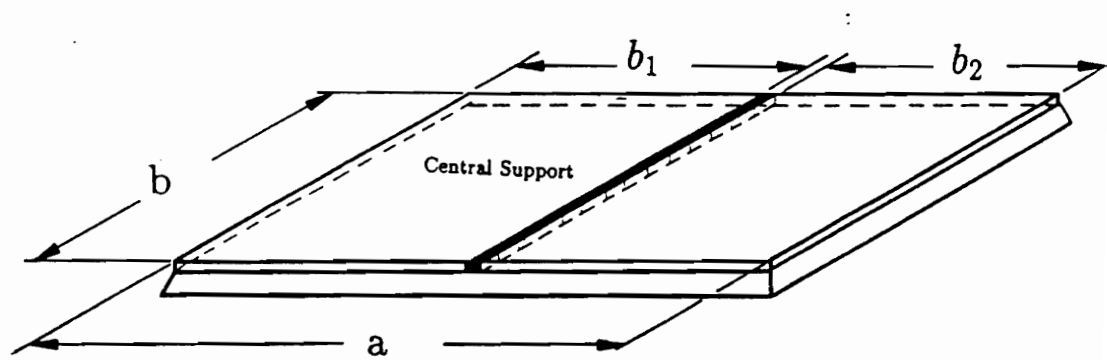
Figure 4.26: Centrally supported Adaptive ART Panel Geometry

The dynamic characteristics of the two adjacent panels when activated in the same manner are very similar, but not identical.

Specifications for the panels evaluated in this case study are presented in Table 4.13. The activation scenarios are summarized in Table 4.14, and with the mode shapes and natural frequencies in Figs. 4.26 through 4.31.

Modal analysis results for the unactivated, Case A and Case B panel scenarios (Figs. 4.31, 4.32 and 4.33) are similar to the results for the unidirectional panel study of Section 4.6.1, in the sense that the first two mode shapes show two adjacent panel sections oscillating out-of-phase at first resonance and in-phase at second resonance. All of these mode shapes include a single lobe per panel section.

By definition, ART is a technique for reducing sound transmission through panel-like structures by tuning adjacent panels such that their fundamental resonances fall above and below a given frequency; thereby oscillating with approximately equal amplitudes and near-opposite phase, reducing acoustic coupling between the structure and the transmitted soundfield when excited at that given frequency.

Figures 4.30 and 4.31 represent cases in which the second resonance of one panel occurs near or below the first resonance of the other panel. This behavior differs from the modal characteristics noted in the cases studied in Section 4.6.1, as higher-order modes occur in one panel at frequencies below the fundamental resonance of the other panel. For example, the second mode shape for Case C includes a characteristic 1,2 mode shape on one side of the panel, and very little oscillation on the other side.

Table 4.13: Panel Specifications for Two Panel Adaptive ART Study

Spatial Geometry and Stacking Sequence	
Stacking Sequence	$[90/\pm 45/0]_s$
Structure Length (a)	1.2m
Structure Width (b)	0.8m
Panel 1 Width (b_1)	0.597m
Panel 2 Width (b_2)	0.598m
Support Width (w_r)	0.005m
Material Specifications	
Material Nomenclature	NiTi(20%)/GFRP(80%)
E_1(unactivated)	36.5 GPa
E_2(unactivated)	9.6 GPa
G_{12}(unactivated)	4.7 GPa
ν_{12}	0.28
E_1 (activated)	47.3 GPa
E_2 (activated)	10.1 GPa
G_{12} (activated)	5.0 GPa
$\nu_{12}(activated)$	0.28
ρ	2730 $\frac{kg}{m^3}$
Laminate Properties	
E_x (unactivated)	19.2 GPa
E_y (unactivated)	19.2 GPa
G_{xy} (unactivated)	7.5 GPa
ν_{xy} (unactivated)	0.27
E_x (activated)	23.2 GPa
E_y (activated)	23.2 GPa
G_{xy} (activated)	9.1 GPa
ν_{xy} (activated)	0.28
Recovery Stress	68.9 MPa

Table 4.14: Two Panel Adaptive ART Activation Scenarios

Scenario	Activation Summary
Unactivated	no plies activated
Case A	0° and 90° plies of panel 1 activated only
Case B	90° plies of panel 1 activated only
Case C	all plies of panel 1 activated only
Case D	all plies of panel 1 and 90° plies of panel 2 activated

Left Panel:
No Plies
Activated

Right Panel:
No Plies
Activated
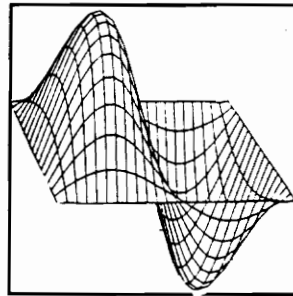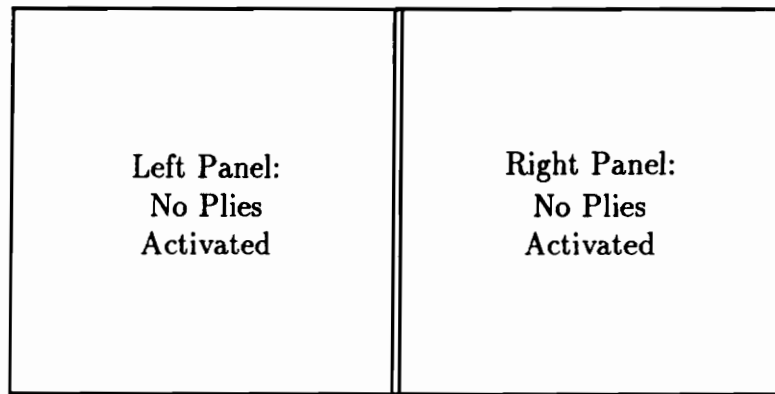
Mode 1 (43.1 Hz)
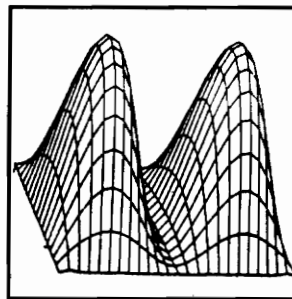
Mode 2 (49.8 Hz)

Figure 4.27: Unactivated Panel Modal Analysis and Activation Summary

173

Left Panel:
0° and 90° Plies
Activated

Right Panel:
No Plies
Activated
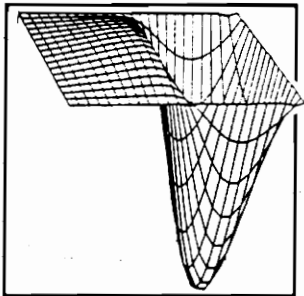
Mode 1 (47.1 Hz)
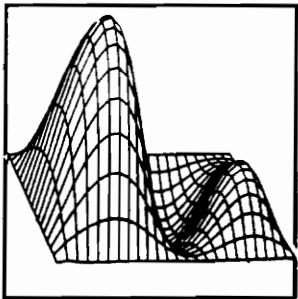
Mode 2 (95.7 Hz)

Figure 4.28: Case A Panel Modal Analysis and Activation Summary

174

Left Panel:
90° Plies
Activated

Right Panel:
No Plies
Activated

Mode 1 (46.2 Hz)

Mode 2 (68.7 Hz)

Figure 4.29: Case B Panel Modal Analysis and Activation Summary

175
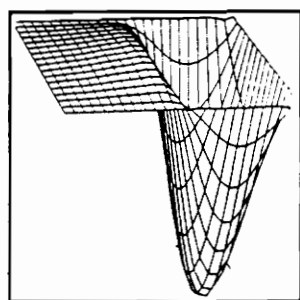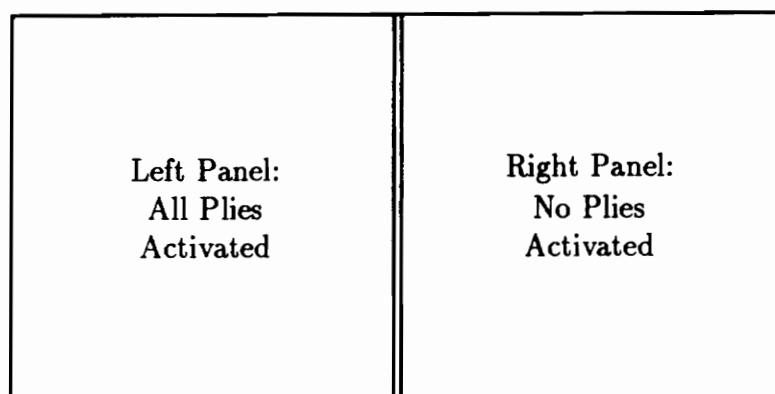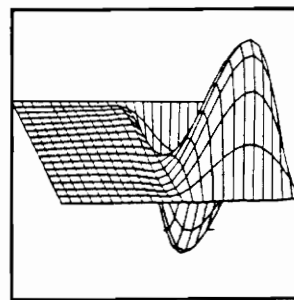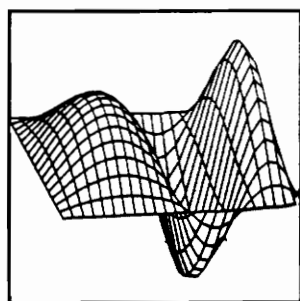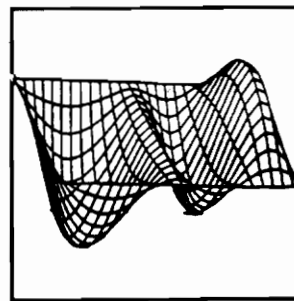
Figure 4.30: Case C Panel Modal Analysis and Activation Summary

Left Panel:
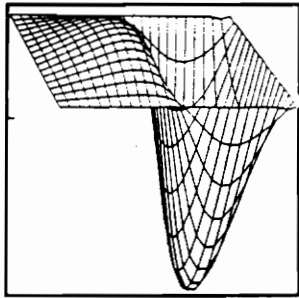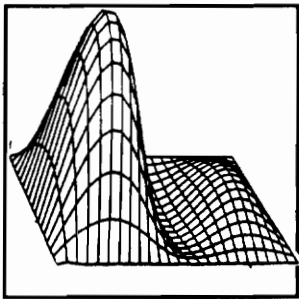All Plies
Activated

Right Panel:
90° Plies
Activated
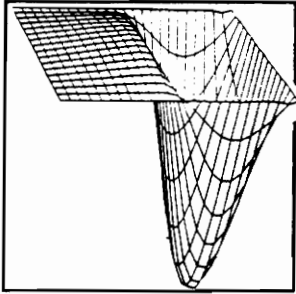
Mode 1 (69.6 Hz)
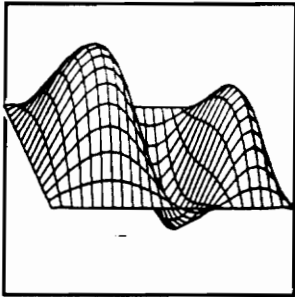
Mode 2 (125.3 Hz)

Figure 4.31: Case D Panel Modal Analysis and Activation Summary

Referring to the transmission loss curves of Fig. 4.32, at the second structural reso-
nance (100.2 Hz) for Case C, the transmisson loss exceeds 30 dB; and in fact remains
consistently above 30 dB from 60 to 110 Hz. This trend suggests structural acoustic
control of adjacent adaptive panels is not limited to the first two structural modes;
but, in fact, the concept can be extended to consider numerous combinations of mode
shapes. Additionally, Fig. 4.32 shows that sound tranmsission loss can be effectively
controlled by adaptivly tuning this centrally supported panel from 0 to 110 Hz, with
minimum transmission loss exceeding 30dB.

4.7 Discussion of Results

The analytical results obtained using the techniques formulated in Chapter 3 are pre-
sented in this Chapter to demonstrate some of the key physical trends, limitations
and capabilities of low frequency structural acoustic control of SMA hybrid composite
panels.

Acoustic transmission analysis results by CLPT and FSDT are compared in Section
4.1, showing that the two theories agree very well for thin panels with width-to-
thickness ratios $(\frac{b}{h})$ greater than or equal to 50. These theories also agree fairly well
for panels as thick as $\frac{b}{h} = 25$, and diverge significantly as $\frac{b}{h}$ approaches 10, with the
largest transmission loss discrepancies occuring at and around the lower-order panel
resonance frequencies.

The effects of panel thickness on structural tuning authority are discussed in Section
4.2. The initial studies of Section 4.2 show that the overall tuning capability of a

178
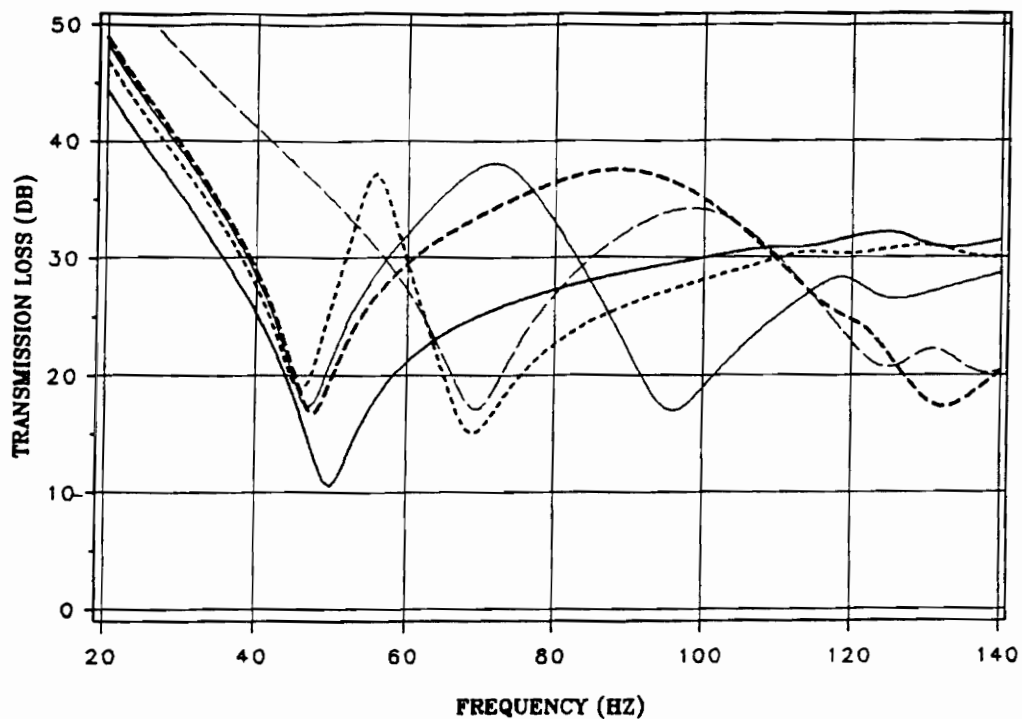
Panel Dimensions (meters)		
a	b	h
1.200	0.800	0.008

ACTIVATION SUMMARY:		
———	UNACTIVATED	
———	CASE A	
·········	CASE B	
– – –	CASE C	
— — —	CASE D	

Figure 4.32: Transmission Loss Versus Frequency for a Centrally Supported, ART-Activated Panel

given SMA hybrid composite material (in this case NiTi/GFRP) diminishes with increasing panel thickness. Decomposing the activation to compare ASET effects and APT effects shows that the influence of activation-induced strain-energy tuning due to large activation-induced membrane stresses tends to decrease, whereas the influence of activation-induced elastic properties transformation remains constant with panel thickness. This observation is theoretically supported by the fact that the activation-induced membrane stresses, which bear direct influence on active strain energy tuning, are linearly proportional to panel thickness. Flexural stiffnesses are cubically proportional to panel thickness; however, and directly proportional to elastic moduli. Structural stiffness increases more dramatically with panel thickness than in-plane loads. The influence of APT should remain constant for a given SMA hybrid composite material composition as panel thickness varies, and the influence of ASET should be considerably greater for thin panels.

The effects of structural damping on acoustic transmission loss are evaluated in Section 4.3 for a quasi-isotropic fiberglass panel. The analytical results presented in Section 4.3 suggest that low-frequency on-resonance and near-resonance transmission loss increases as damping increases. Off-resonance transmission loss was shown to decrease with increased damping at some frequencies. The effects of damping are shown to be less critical at higher modes.

In Section 4.4, dimensionless parameter study results are presented to evaluate the effects of panel length-to-width aspect ratio and ply stacking sequence. These results indicate that maximum structural tuning authority is achieved for SMA hybrid composite panels with plies oriented such that the fiber direction is parallel to the

180

shorter panel dimension. These non-dimensional studies are valid for panel width-to-thickness ratios of 100, and their results support the observation above, that the structural tuning authority of ASET is dominant over that of APT for thin panels; depending on the fiber activation, material characteristics, and fiber activation.

Structural acoustic and dynamic control by localized activation of SMA hybrid composite panels is demonstrated in Section 4.5. The results of Section 4.5 indicate that some low-frequency structural acoustic control and limited active mode shape modification are achievable by the localized activation scenarios considered, and that significant natural frequency modifications can be achieved by activating fibers where flexural deformation is greatest for a given mode shape.

Two concepts of low-frequency structural acoustic control by adaptive ART of SMA hybrid composite panels are presented and evaluated in Section 4.6. The first concept requires the generation of large, concentrated, activation-induced force resultants to produce a highly stiffened panel section, which functions as a support or pseudo-rib, causing the structure to respond to dynamic excitation like two elastically coupled sub-panels. The second concept considers a simple support at the center of the panel, which divides the structure into two coupled panels, which can be independently tuned to produce adaptive ART. Analytical results obtained considering both concepts suggest that adaptive ART is an effective technique for strategically controlling low-frequency sound transmission through SMA hybrid composite panel-like structures.

Chapter 5

Conclusions and Recommendations

5.1   Conclusions

Five major conclusions can be drawn from this research:

- Analytical models have been formulated and demonstrated for predicting the modal and structural acoustic response of symmetric, simply supported, SMA hybrid composite panels using finite panel acoustic radiation theory, the Rayleigh-Ritz method, and two plate theories (CLPT and FSDT). Another technique was developed for the evaluation of locally activated SMA hybrid composite panels with piece-wise 'homogeneous' elastic properties and strain-energy distributions.

- The analysis of Section 4.2 was conducted to study the influence of laminate thickness on the changes of resonant panel frequencies resulting from elastic properties transformation and activation-induced membrane stresses. By first evaluating the resonant panel frequency changes due to APT and then considering the effects of APT and ASET combined, it was shown in Section 4.2

182

(considering a quasi-isotropic, NiTi/GFRP laminate) that the control authority of APT is invariant with laminate thickness. The control authority due to ASET was found to vary significantly with panel thickness, such that thin SMA hybrid composite structures generally have more inherent control authority than thick structures. For example, the fundamental frequency of a thin (8mm) panel tuned by APT only was shown to increase by 10%, and the fundamental frequency of the same panel was shown to increase by 272% when tuned by APT with ASET. The fundamental frequency of a 64mm thick panel tuned by APT only was also shown to increase by 10%; however an increase of only 68% was noted with APT and ASET. The theoretical explanation for this trend is that the flexural panel stiffnesses (which can be modified by APT) are cubically proportional to panel thickness; whereas the in-plane force resultants of the activation-induced membrane stresses in a structure (by which ASET occurs) are linearly proportional to panel thickness.

- Results of normalized fudamental frequency analyses are presented in Section 4.4 for thin, eight-layer, angle-ply laminates. These results, which were produced to evaluate the effects of panel length-to-width aspect ratio and ply orientation on ASET and APT capabilities, show that the fundamental frequency of thin, NiTi/GFRP (20% NiTi by volume), square panels can be increased 6.25% to 11% by APT; and by 180% to 235%, when the combined effects APT and ASET (APT with ASET) are present. The greatest control authority is attainable for square panels when the plies are oriented at $\pm 90°$ or $\pm 0°$, and the least control authority is available for a ply orientation of $\pm 45°$. The fundamental frequencies of thin, rectangular panels with large length-to-width ratios ($\frac{a}{b} = 4$), can be increased 5% to 17% by APT, and by over 300% when APT

183

and ASET are applied. The greatest structural tuning authority can be realized for long, narrow members when the fiber orientation is biased parallel to the shortest structural dimension, and the minimum control authority is realized when the fibers are orientated in the longitudinal direction of the structure.

- Case study results are presented in Section 4.5 which show that adding the options of localized fiber activation to the globally activated options can increase the low-frequency structural acoustic control capability of an SMA hybrid composite panel by up to 7dB. At the fundamental unactivated panel resonance, analytical results predict that transmission loss can be increased by over 30dB by activating only the central half of the panel. The benefits of localized fiber activation over global activation are:

  1. More control versatility is available with localized activation, as many (rather than only two) fiber activation scenarios may be exploited.

  2. The net activation-induced force resultants throughout the structure and its supports are lower when fewer SMA fibers are activated.

  3. The total amount of electrical energy required to activate the structure is reduced when fewer SMA fibers are activated.

  4. Less internal heat energy is introduced within the structure when it is locally activated.

- A novel technique, adaptive ART, has been introduced for actively controlling low-frequency sound transmission through SMA hybrid composite panels. Two strategies are presented in Section 4.6 by which adaptive ART can be implemented. One method considers a single panel and a unidirectional layup. For

this concept to work most effectively, SMA fibers must be embedded in narrow bands such that large local concentrations of SMA fibers are placed strategically about the panel. When one of these bands is activated, the high concentration of localized activation-induced strain energy produces an activation-induced support or 'pseudo-rib'; which transforms the structure into two unactivated sub-panels, with a stiffened section between them. The dynamic behavior of the structure can then be modified in two ways:

1. The modal response of the structure can be altered such that the first structural resonance is dominated by the characteristic 2,1 mode shape.

2. The unactivated panel sections can be tuned to resonante above and below a particular frequency such that high transmission loss occurs due to the alternate resonance of theses panel sections when the structure is acoustically excited at or near that frequency.

The analytical results of Section 4.6.1 indicate that the transmission loss at and around around the first unactivated panel resonance can be increased by over 30dB when a 'pseudo-rib' is activated near the center of the panel, and that transmission loss at higher frequencies can be strategically increased by 5 to 10 dB by adaptive alternate resonance tuning.

Another adaptive ART concept has been introduced which considers placing a stiffener at the center of a simply supported SMA hybrid composite panel. SMA fibers on either or both sides of the stiffener can be activated to cause them to resonate at different frequencies, thereby producing alternate resonance tuning. Analytical results predict that broad-band structural acoustic control capabili-

ties for this concept can be realized such that from 0 to 90 Hz, transmission loss can be increased more than 10dB above the transmission loss for the unactivated structure.

5.2 Recommendations

The analyses of this thesis consider ideal activation scenarios, in which material behavior is assumed to be governed by the micromechanical model presented in Chapter 2. SMA fiber activation is assumed to occur at a given temperature, with uniform properties transformation and recovery stress. The thermal energy introduced in the SMA fibers during activation is assumed not to soften the composite matrix material into which these fibers embedded. Also, the SMA fibers are assumed to be perfectly bonded to the matrix material.

It can be anticipated that many departures from these assumptions may exist, including non-uniform heat energy distribution, thermal interraction between the SMA fibers and matrix materials, imperfect bonding between the SMA fibers and the matrix material, mechanical behavior that is inconsistent with the micromechanical model used, and temperature sensitive matrix material properties and behavior. To address these issues, fundamental experimental research is neccesary to evaluate activated and unactivated material response. Such activities may include system identification analyses to determine material properties and applied in-plane loads by measuring and evaluating modal response characteristics, durability tests and thermo-cycling evaluations.

Experimental work is recommended to verify the adaptive alternate resonance tuning

concepts demonstrated analytically in Chapter 4. Of the two concepts presented, the centrally supported concept is recommended for primary emphasis, as the actual capability of producing an activation-induced support or pseudo-rib may be very difficult to achieve. Furthermore, utilizing an actual support appears more effective as far as laminate construction versatility, SMA fiber volume fraction, and acoustic transmission control capabilities are concerned. To achieve reasonable agreement between experimental and analytical results, the models presented in Chapter 3 should be expanded to consider such effects as clamped boundary conditions and orthotropic stiffness-proportional damping.

Future activities may also consider multi-panel arrays (ie. 2 by 2 arrays) of independently supported SMA hybrid composite panels, which can be tuned by either localized or general activation. Another possibility may involve active structural acoustic control of SMA hybrid composite panel structures at higher frequencies by adaptively tuning higher modes, considering approaches similar to alternate resonance tuning.

The analytical approach of this research for evaluating the dynamic and structural acoustic response of locally activated panels is presented in the context of stiffness tuning. The energy prinicple considered is not limited to this consideration, and the model can easily be expanded to consider other effects such as point-force actuators or piezoelectric patch-type actuators. An interesting application in this regard is the simultaneous consideration of adaptive structural tuning of SMA hybrid composite structures with dynamically excited piezoelectric patch actuators.

References

Anders, W. S., and C. A. Rogers, 1990, "Vibration and Low-Frequency Acoustic Analysis of Piecewise-Activated Adaptive Composite Panels," submitted to the *Journal of Composite Materials.*

Anders, W. S., C. A. Rogers, and C. R. Fuller, 1990, "Control of Sound Radiation from Shape Memory Alloy Hybrid Composite Panels by Adaptive Alternate Resonance Tuning," Submitted for the AIAA/ASME/ASCE/AHS/ASC 32nd Structures, Structural Dynamics and Materials Conference, Baltimore, MD, April 8-10, 1991.

Anderson, E. H., 1989, **Piezoceramic Induced Strain Actuation of One- and Two-Dimensional Structures**, M.S. Thesis, MIT, Cambridge, MA.

Baily, T., and J. E. Hubbard, 1985, "Distributed Piezoelectric-Polymer Active Vibration Control of a Cantilever Beam," *J.Guidance*, Vol. 8, No. 5, pp. 605-611.

Barker, D. K., 1989, **Active Dynamic Response Tuning of Adaptive Composites, Utilizing Embedded Nitinol Actuators**, M.S. Thesis, VPI&SU, Blacksburg, VA.

Bliss, D. B., and J. A. Gottwald, 1989, "Reduction of Sound Transmitted through Fuselage Walls by Alternate Resonance Tuning (A.R.T.)," *AIAA Paper 89-1046*.

Buehler, W. J., and R. C. Wiley, 1965, "Nickel-Base Alloys," U.S. Patent 3,174,851, March 23.

Chaplin, G. B. B., Smith, R. A., and R. G. Bancroft, 1979, "Active Attenuation of Recurring Sounds," US Patent No. 4,153,815, May.

Conover, W., 1956, "Fighting Noise with Noise", *Noise Control*, Vol. 2, No. 2, pp. 78-82,92.

Craig, T. J., and D. J. Dawe, 1986, "Flexural Vibration of Symmetrically Laminated Composite Rectangular Plates Including Transverse Shear Effects",*Int. J. Solids Structures*, Vol. 22, No. 2, pp. 155-169.

Crawley, E. F. and J. de Luis, 1986, "The use of Piezoelectric Actuators as Elements of Intelligent Structures," *AIAA Journal*, Vol. 25, No. 10, AIAA Paper 86-0878.

Cudney, H. H., 1989, **Distributed Stuctural Control Using Multilayered Piezoelectric Actuators**, PhD. Dissertation, State University of New York at Buffalo.

Elmer-Dewitt, P., 1989, "Fighting Noise with Antinoise", *Time Magazine*, December 4, p. 94.

Fahy, F., 1989, **Sound And Structural Vibration; Transmission and Response**, Academic Press, London, UK.

Fuller, C. R., and J. D. Jones, 1987, "Experiments on Reduction of Propeller Induced Noise by Active Control of Cylinder Vibration," *J. Sound Vibration*, Vol. 12, No. 2, pp. 389-395.

Fuller, C. R., C. A. Rogers, and H. H. Robertshaw, 1989, "Active Structural Acoustic Control, *Proceedings of SPIE Conference 1170 on Fiber Optic Smart Structures and Skins II.*

Guicking, D. K., K. Karcher, and M. Rollwage, 1985, "Coherent Active Methods for Applications in Room Acoustics," *J. Acoust. Soc. Am.*, Vol. 78, No. 4, pp. 1426-1434.

Hawley, M. E., and E. D. Simshauser, 1961, "Noise Reduction System," U.S. Patent No. 2,792,018, February 14.

Heitman, K. E., and J. S. Mixson, 1986, "Laboratory Study of Cabin Acoustic Treatments Installed in an Aircraft Fuselage," *J. Aircraft*, Vol. 23, No. 1, pp. 32-38.

Hesselmann, N., 1978, "Investigation of Noise Reduction on a 100kVA Transformer Tank by Means of Active Methods" *Applied Acoustics*, Vol. 11, pp. 27-34.

Hodgson, D. E., 1988, "Using Shape Memory Alloys," Shape Memory Alloy Applications, Inc., Cupertino, CA.

Holmer, C. I., 1969, **Sound Transmission through Structures: a Review**, M.S. Thesis, John Carrol University, Cleveland, OH.

Hunt, F. V., 1976, **Origins in Acoustics; The Science of Sound from Antiquity to the Age of Newton**, Yale University Press, New Haven, CT.

Jia, J., and C. A. Rogers, 1989, "Formulation of a Mechanical Model for Composites with Embedded SMA Actuators," *Proceedings of the 8th Biennial ASM Conference on Failure Prevention and Reliability*, Montreal, Canada, Sept. 18-20.

Jones, J. D., 1987, **Study of Active Control Techniques for Noise Reduction in an Aircraft Fuselage Model**, PhD. dissertation, Virginia Polytechnic Institute and State University, Blacksburg, VA.

Jones, J. D., and Fuller, C. R., 1987, "Active Control of Sound Fields in Elastic Cylinders by Multi-Control Forces," *AIAA Paper 87-2707*.

Jones, R. M., 1975, **Mechanics of Composite Materials**, Hemisphere Publishing Corp., New York, NY.

Kandebo, S. W., 1988, "Propfan Flight Tests will Examine Design, Noise Issues," *Aviation Week & Space Technology*, January 25, pp. 36-37.

Kinsler, L. E., A. R. Frey. A. B. Coppens, and J. V. Sanders, 1982, **Fundamentals of Acoustics**, 3rd edition, John Wiley and Sons, NY.

Liang, C., 1990, **The Constitutive Modeling of Shape Memory Alloys**, PhD. Dissertation, Department of Mechanical Engineering, Virginia Polytechnic Institute and State University, Blacksburg, VA.

Liang, C., J. Jia, and C. A. Rogers, 1989, "Behavior of Shape Memory Alloy reinforced Composite Plates - Part II Results," Proceedings of the *AIAA/ASME/ASCE/AHS/ASC 30th Structures, Structural Dynamics and Materials Conference*, Mobile, AL.

Liang, C., and C. A. Rogers, 1990, "One-Dimensional Relations for Shape Memory Materials," *Journal of Intelligent Materials Systems and Structures*, Vol. 1, No. 2, pp. 201-233.

Lindsay, R. B., 1972, **Acoustics; Historical and Philosophical Development**, Dowden, Hutchinson and Ross, Inc., Stroudsburg, PA.

Lindsay, R. B., 1967, "The Story of Acoustics," *Journal of the Acoustical Society of America*, Vol. 39, No. 4, pp. 629-644.

Lueg, P., 1937, "Ver Fahren zur Dampfung von Schellschwingungen," German Patent DPR no. 655,508, December 30.

Mandic, D. S., and Jones, J. D., 1989, "Active Noise Control in Damped Elastic Cylinders using Vibrational Force Inputs," *Proceedings of the 1989 Conference on Noise Control Engineering*, Long Beach, CA.

Mandic, D. S., and Jones, J. D., 1989, "Adaptive Control of Enclosed Sound Fields in Elastic Cylinders Via Vibrational Inputs," *AIAA Paper 89-1075*.

Mixson, J. S., and C. A. Powell, 1985, "Review of Recent Research of Interior Noise of Propeller Aircraft," *J. Aircraft*, Vol. 22, No. 11, pp. 931-939.

Morris, W. H. (ed.), 1978, **The American Heritage Dictionary of the English Language**, Houghton Miflin Co., Boston, MA.

Olson, H. F., and E. G. May, 1953, "Electronic Sound Absorber," *J. Acoustical Soc. Am.*, Vol. 25, No. 6, pp. 1130-1136.

Revell, J. D., and F. J. Balena, 1972, "Interior Noise Control by Fuselage Design for High-Speed Propeller-Driven Aircraft," *J. Aircraft*, Vol. 19, No. 1, pp. 39-45.

Rogers, C. A., 1990a, "Active Structural Acoustic Control with Shape Memory Alloy Hybrid Composites," *119th Meeting of the Acoustical Society of America*, May 21-25, State College, Pa.

Rogers, C. A., 1990b, "Active Vibration and Structural Acoustic Control of Shape

Memory Alloy Hybrid Composites: Experimental Results," *Proceedings of the International Congress on Recent Developments in Air and Structural Borne Sound and Vibrations*, Auburn University, 6-8 March, pp. 695-708.

Rogers, C. A., and D. K. Barker, 1990, "Experimental Studies of Active Strain Energy Tuning of Adaptive Composites," *Proceedings of the AIAA/ASME/ACSE/AHS/ASC 31st Structures, Structural Dynamics and Materials Conference*, Long Beach, CA.

Rogers, C. A., C. Liang, and D. K. Barker, 1989, " Dynamic Control Concepts Using Shape Memory Alloy Reinforced Plates," *Smart Materials, Structures and Mathematical Issues*, Technomic Publishing Co. Lancaster, PA.

Rogers, C. A., C. R. Fuller, and C. Liang, 1990, "Active Control of Sound Radiation from Panels Using Embedded Shape Memory Alloy Fibers," *J. Sound Vibration*, Vol. 136, No. 1, pp. 164-170.

Rogers, C. A., C. Liang, and J. Jia, 1989, "Behavior of Shape Memory Alloy Reinfoced Composites - Part I: Model Formulations and Control Concepts," *Proceedings of the AIAA/ASME/ASCE/AHS/ACS 30th Structures, Structural Dynamics and Materials Conference*, Mobile, AL.

Rogers, C. A., and H. H. Robertshaw, 1988a, "Development of a Novel Smart Material," *ASME Paper 88-WA/DE-9*.

Rogers, C. A., and H. H. Robertshaw, 1988a, "Shape Memory Alloy Reinforced Com-

posites," *Engineering Science Preprints 25, ESP 25.88027, Society of Engineering Sciences.*

Roussos, L. A., 1985, "Noise Transmission Loss of a Rectangular Plate in an Infinite Baffle," *NASA Technical Paper 2328.*

Saunders, W. R., H. H. Robertshaw, and C. A. Rogers, 1990, "Experimental Studies of Structural Acoustic Control for a Shape Memory Alloy Composite Beam," *Proceedings of the AIAA/ASME/ASCE/AHS/ACS 31st Structures, Structural Dynamics and Materials Conference*, Long Beach, CA.

SenGupta, G., 1978, "Reduction of Cabin Noise and Vibration by Intrinsic Structural Tuning," *AIAA Journal*, Vol. 16, No. 6, pp. 545-546.

SenGupta, G., 1979, "Reduction of Cabin Noise During Cruise Conditions by Stringer and Frame Damping," *AIAA Journal*, Vol. 113, No. 3, pp. 229-236.

Silcox, R. J., C. R. Fuller, and H. C. Lester, 1987, "Mechanisms of Active Control in Cylindrical Fuselage Structures," *AIAA Paper 87-2703.*

Simpson, M. A., T. M. Luong, M. A. Swinbanks, M. A. Russell, and H. G. Leventhall, 1989, "Full Scale Demonstration Tests of cabin Noise Reduction Using Active Structural Acoustic Control," *Proceedings of the 1989 Conference on Noise Control Engineering*, Longbeach, CA.

Swanson, D. C., 1989, "Active Attenuation of Acoustic Noise: Past, Present, and Future," *ASHRAE Journal*, pp. 63-76.

Swinbanks, M. A., 1973, "The Active Control of Sound Propagation in Large Ducts," *J. Sound Vibration*, Vol. 27, No. 3, pp. 411-436.

Vaicaitis, R., and J. S. Mixson, 1985, "Theoretical Design of Acoustic Treatment for Noise Control in a Turboprop Aircraft," *J. Aircraft*, Vol. 22, No. 4, pp. 318-324.

Ver, I. L., and Holmer C. I., 1971, in "Noise and Vibration Control," (L.L. Beranek, ed.), McGraw Hill Publishing Co., pp. 270-357.

Wallace, C. E., 1972, "Radiaion Resistance of a Rectangular Panel," *Journ. Acoustical Soc. Am.*, Vol. 51, No. 3, pp. 946-952.

Wang, B. T., E. K. Dimitriadis, and C. R. Fuller, 1990, "Active Control of Structurally Radiated Noise Using Multiple Piezoelectric Actuators," *Proceedings of the 31st SSDM Conference*, Long Beach, CA.

Whitney, J. M., 1987, **Structural Analysis of Laminated Anisotropic Plates**, Technomic Publishing Co., Lancaster, PA.

Yang, J. C. S., and Tsui, C. Y., 1987, "Optimum Design of Structures of Composite Materials in Response to Aerodynamic Noise and Noise Transmission," NASA-CR-155332.

Appendix A

Rayleigh-Ritz Formulation Using FSDT

The Section 3.3 presents a technique for analyzing the transmission of plane-wave acoustic incidence through a thin, simply supported, symmetrically laminated composite panel. For thick plates, the effects of rotary inertia and transverse shear deformation significantly affect the vibratory and modal response of the structure. Although these effects will not be studied in much detail in this thesis, it is useful to understand how transverse shear deformation and rotary inertia influence structural acoustic and modal behavior, and under what conditions these effects are critical to the accuracy of the CLPT model formulated in the previous section.

For this purpose, and to assist future researchers in the area of active structural acoustic control using SMA hybrid composite materials, a finite panel acoustic radiation analysis model is formulated in this section using first order shear deformation theory (FSDT).

The primary differences between FSDT and CLPT pertain to assumptions 1,6, and 11 of Section 3.3. FSDT considers the the effects of transverse shear deformation and

197

rotary inertia, whereas CLPT assumes these effects to be negligible. Where CLPT is accurate only for thin structures, FSDT can be used to more accurately analyze thicker members with relatively low width-to-thickness ratios.

The FSDT finite panel acoustic radiation analysis model initiates with the micromechanical analyses of the material transverse shear modulii. The other elastic lamina properties are already available from Section 2.3.1. Only G_{13} and G_{23} remain to be determined.

Obtaining G_{13} is quite simple, as per Whitney (1987);

$$G_{13} = G_{12}. \tag{A.1}$$

The other transverse shear modulus, G_{23} requires a bit more effort;

$$G_{23} = \frac{G_{23m}G_a}{v_m G_a + v_a G_{23m}} \tag{A.2}$$

where

$$G_{23m} = \frac{E_{22m}}{2(1 + \nu_{23m})}. \tag{A.3}$$

The next step of this formulation is to define the stiffness and compliance coefficients associated with transverse shear deformation. The compliance terms are simply:

$$\begin{aligned} S_{44} &= \frac{1}{G_{23}} \\ S_{55} &= \frac{1}{G_{13}} \end{aligned} \tag{A.4}$$

and the stiffness coefficients are

$$Q_{44} = G_{23}$$

$$Q_{55} = G_{13}. \tag{A.5}$$

Incorporating these with the constitutive relations of Section 2.3.1, the material stiffness matrix can be written as

$$[Q] = \begin{bmatrix} Q_{11} & Q_{12} & 0 & 0 & 0 \\ Q_{12} & Q_{22} & 0 & 0 & 0 \\ 0 & 0 & Q_{44} & 0 & 0 \\ 0 & 0 & 0 & Q_{55} & 0 \\ 0 & 0 & 0 & 0 & Q_{66} \end{bmatrix} \tag{A.6}$$

For a rotated layer, in which the material axes are rotated relative to the global coordinate axes, the following stress-strain relations apply:

$$\begin{Bmatrix} \sigma_x \\ \sigma_y \\ \tau_{yz} \\ \tau_{xz} \\ \tau_{xy} \end{Bmatrix} = \begin{bmatrix} \overline{Q}_{11} & \overline{Q}_{12} & 0 & 0 & \overline{Q}_{16} \\ \overline{Q}_{12} & \overline{Q}_{22} & 0 & 0 & \overline{Q}_{26} \\ 0 & 0 & \overline{Q}_{44} & \overline{Q}_{45} & 0 \\ 0 & 0 & \overline{Q}_{45} & \overline{Q}_{55} & 0 \\ \overline{Q}_{16} & \overline{Q}_{26} & 0 & 0 & \overline{Q}_{66} \end{bmatrix} \begin{Bmatrix} \varepsilon_x \\ \varepsilon_y \\ \gamma_{yz} \\ \gamma_{xz} \\ \gamma_{xy} \end{Bmatrix} + \begin{Bmatrix} \sigma_x \\ \sigma_y \\ 0 \\ 0 \\ \tau_{xy} \end{Bmatrix} \tag{A.7}$$

where

$$\overline{Q}_{44} = Q_{44} \cos^2 \theta + Q_{55} \sin^2 \theta$$

$$\overline{Q}_{45} = (Q_{44} - Q_{55}) \cos \theta \sin \theta$$

$$\overline{Q}_{55} = Q_{44} \sin^2 \theta + Q_{55} \cos^2 \theta \tag{A.8}$$

The activation-induced stresses, σ_x, σ_y and τ_{xy} are already presented in Eq. (2.20).

For FSDT, the displacements are defined by Whitney (1987) as

$$u = u^\circ(x, y, t) + z\psi_x(x, y, t)$$

$$v = v^{\circ}(x, y, t) + z\psi_y(x, y, t)$$

$$w = w(x, y, t) \tag{A.9}$$

where t is the time dimension, and ψ_x and ψ_y are the total rotations along the respective x- and y- directions as shown in Fig. A.1.

By definition,

$$\psi_x = u_{,z}$$

$$\psi_y = v_{,z} \tag{A.10}$$

Based on the displacement relationships above, the FSDT strain displacement equations are

$$\varepsilon_x = \varepsilon_x^{\circ} + z\psi_{x,x}$$

$$\varepsilon_y = \varepsilon_y^{\circ} + z\psi_{y,y}$$

$$\gamma_{yz} = v_{,z}^{\circ} + w_{,y} = \psi_y + w_{,y}$$

$$\gamma_{xz} = u_{,z}^{\circ} + w_{,x} = \psi_x + w_{,x}$$

$$\gamma_{xz} = u_{,y}^{\circ} + v_{,x}^{\circ} = \gamma_{xy}^{\circ} + z(\psi_{x,y} + \psi_{y,x}) \tag{A.11}$$

The constitutive relations are

$$
\begin{Bmatrix} N_x \\ N_y \\ N_{xy} \\ M_x \\ M_y \\ M_{xy} \end{Bmatrix} =
\begin{bmatrix}
A_{11} & A_{12} & A_{16} & B_{11} & B_{12} & B_{16} \\
A_{12} & A_{22} & A_{26} & B_{12} & B_{22} & B_{26} \\
A_{16} & A_{26} & A_{66} & B_{16} & B_{26} & B_{66} \\
B_{11} & B_{12} & B_{16} & D_{11} & D_{12} & D_{16} \\
B_{12} & B_{22} & B_{26} & D_{12} & D_{22} & D_{26} \\
B_{16} & B_{26} & B_{66} & D_{16} & D_{26} & D_{66}
\end{bmatrix}
\begin{Bmatrix} \varepsilon_x^{\circ} \\ \varepsilon_y^{\circ} \\ \gamma_{xy}^{\circ} \\ \psi_{x,x} \\ \psi_{y,y} \\ \psi_{x,y} + \psi_{y,x} \end{Bmatrix} +
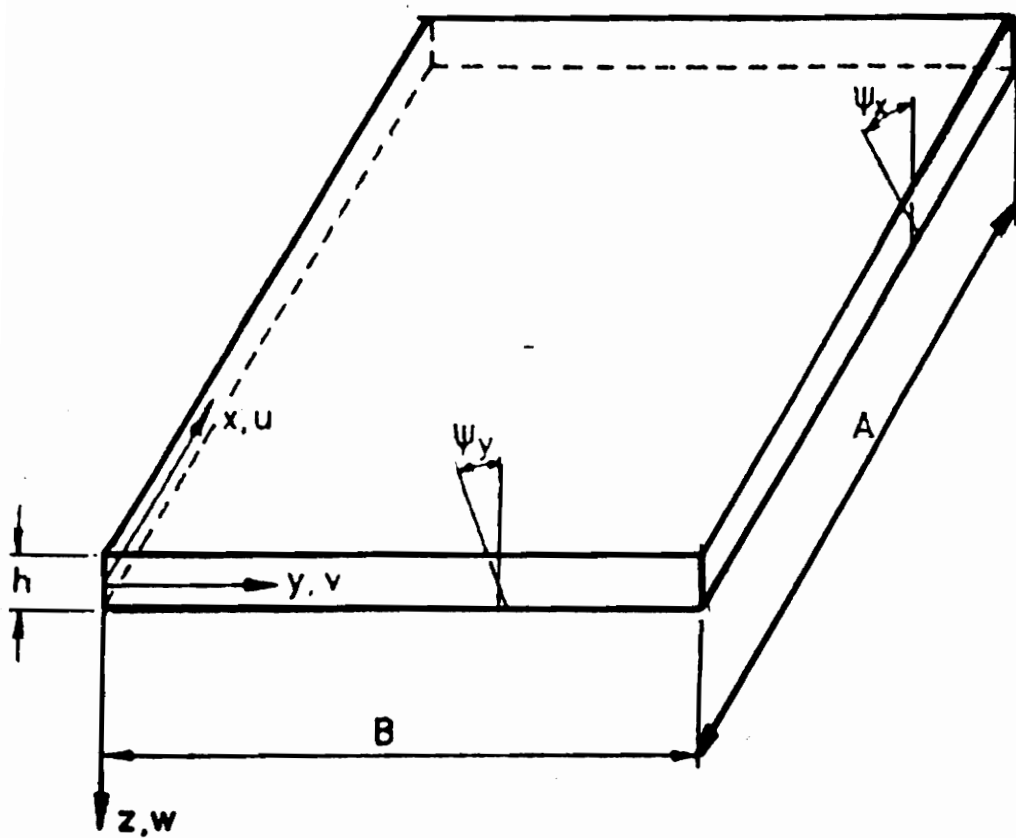\begin{Bmatrix} N_x \\ N_y \\ N_{xy} \\ M_x \\ M_y \\ M_{xy} \end{Bmatrix}
$$

$$\tag{A.12}$$

200

Figure A.1: ψ_x and ψ_y; after Craig and Dawe, 1986

and

$$\left\{ \begin{array}{c} Q_x \\ Q_y \end{array} \right\} = k \left[\begin{array}{cc} A_{44} & A_{45} \\ A_{45} & A_{55} \end{array} \right] \{w_{,x} + \psi_x w_{,y} + \psi_y\} \qquad (A.13)$$

where A_{ij}, B_{ij}, D_{ij}, N_x, N_y, N_{xy}, M_x, M_y, and M_{xy} are defined in Section 2.3.1.

The variable, k, known as the shear correction factor, is determined by comparing FSDT and elasticity solutions.

Because this analysis only considers symmetric laminates, the B_{ij} terms equal zero, and the constitutive relations can be rewritten as:

$$\left\{ \begin{array}{c} N_x \\ N_y \\ N_{xy} \\ M_x \\ M_y \\ M_{xy} \end{array} \right\} = \left[\begin{array}{cccccc} A_{11} & A_{12} & A_{16} & 0 & 0 & 0 \\ A_{12} & A_{22} & A_{26} & 0 & 0 & 0 \\ A_{16} & A_{26} & A_{66} & 0 & 0 & 0 \\ 0 & 0 & 0 & D_{11} & D_{12} & D_{16} \\ 0 & 0 & 0 & D_{12} & D_{22} & D_{26} \\ 0 & 0 & 0 & D_{16} & D_{26} & D_{66} \end{array} \right] \left\{ \begin{array}{c} \varepsilon_x \\ \varepsilon_y \\ \gamma^o_{xy} \\ \psi_{x,x} \\ \psi_{y,y} \\ \psi_{x,y} + \psi_{y,x} \end{array} \right\} + \left\{ \begin{array}{c} N^*_x \\ N^*_y \\ N^*_{xy} \\ M^*_x \\ M^*_y \\ M^*_{xy} \end{array} \right\}$$

$$(A.14)$$

$$\left\{ \begin{array}{c} Q_x \\ Q_y \end{array} \right\} = \left[\begin{array}{cc} kA_{44} & kA_{45} \\ kA_{45} & kA_{55} \end{array} \right] \left\{ \begin{array}{c} w_{,x} + \psi_x \\ w_{,y} + \psi_y \end{array} \right\} \qquad (A.15)$$

The expression above consists of eight linear equations. Because the B_{ij} terms are all zero, the in-plane and transverse deflections decouple. Since only transverse responses are sought, only the bottom five equations need to be considered for this analysis. The constitutive relations can therefore be reduced to:

$$\left\{ \begin{array}{c} M_x \\ M_y \\ M_{xy} \\ Q_x \\ Q_y \end{array} \right\} = \left[\begin{array}{ccccc} D_{11} & D_{12} & D_{16} & 0 & 0 \\ D_{12} & D_{22} & D_{26} & 0 & 0 \\ D_{16} & D_{26} & D_{66} & 0 & 0 \\ 0 & 0 & 0 & kA_{44} & kA_{45} \\ 0 & 0 & 0 & kA_{45} & kA_{55} \end{array} \right] \left\{ \begin{array}{c} \psi_{x,x} \\ \psi_{y,y} \\ \psi_{x,y} + \psi_{y,x} \\ w_{,x} + \psi_x \\ w_{,y} + \psi_y \end{array} \right\} + \left\{ \begin{array}{c} M_x \\ M_y \\ M_{xy} \\ 0 \\ 0 \end{array} \right\} \quad (A.16)$$

202

To determine dynamic and modal response, the Rayleigh-Ritz method is used. This method initiates with the application of Hamilton's principle. The governing equations of motion are obtained by considering the total energy functional:

$$\Pi = U + V + W - T \tag{A.17}$$

where Π is the total energy, U is the strain energy, V is the potential energy due to applied in-plane forces, w is the potential energy of the transverse forcing function, and T is the kinetic energy.

The above expression can be rewritten in the context of FSDT as:

$$
\begin{aligned}
\Pi = {} & \frac{1}{2}\{D_{11}\psi_{x,x}^2 + 2D_{12}\psi_{x,x}\psi_{y,y} + D_{66}(\psi_{x,y} + \psi_{y,x})^2 + D_{22}\psi_{y,y}^2 \\
& + 2D_{16}\psi_{x,x}(\psi_{x,y} + \psi_{y,x}) + 2D_{26}\psi_{y,y}(\psi_{x,y} + \psi_{y,x}) \\
& + kA_{44}(\psi_y^2 + 2\psi_y w_{,y} + w_{,y}^2) + kA_{55}(\psi_x^2 + 2\psi_x w_{,x} + w_{,x}^2) \\
& + 2kA_{45}(\psi_x\psi_y + \psi_x w_{,y} + \psi_y w_{,x} + w_{,x}w_{,y}) + N_x w_{,x}^2 \\
& + N_y w_{,y}^2 + 2N_{xy}w_{,x}w_{,y} - 2qw - m_p\omega^2 w^2 + C_{D_p}i\omega w \\
& - m_r\omega^2\psi_x^2 + C_{D_r}i\omega\psi_x - m_r\omega^2\psi_y^2 + C_{D_r}i\omega\psi_y\}dxdy
\end{aligned}
\tag{A.18}
$$

where q is the transverse forcing function, m_p is the mass per unit area, and m_r is the mass moment of inertia per unit area, determined by

$$m_r = \int_{-\frac{h}{2}}^{\frac{h}{2}} \rho z^2 dz = \frac{1}{3}\sum_{k=1}^{N}\rho^k(z_k^3 - z_{k-1}^3), \tag{A.19}$$

and C_{D_p} is the mass proportional damping coefficient. The rotary damping coefficient, C_{D_r} is:

$$2m_r\xi \tag{A.20}$$

203

Before solving the total energy equation to obtain the governing equations of motion, boundary conditions must be evaluated to provide assumed forms of solution for $\psi_x(x, y, t)$, $\psi_y(x, y, t)$, and $w(x, y, t)$. These boundary conditions are

At $x = 0$ and $x = a$;

$$w = \psi_x = 0 = M_x = 0, \tag{A.21}$$

and at $y = 0$ and $y = a$;

$$w = \psi_y = M_y = 0. \tag{A.22}$$

These conditions are satisfied by

$$
\begin{aligned}
\psi_x(x, y, t) &= \sum_{i=1}^{M} \sum_{j=1}^{N} A_{mn} \cos \frac{m\pi x}{a} \sin \frac{n\pi y}{b} e^{i\omega t} \\
\psi_y(x, y, t) &= \sum_{i=1}^{M} \sum_{j=1}^{N} B_{mn} \sin \frac{m\pi x}{a} \cos \frac{n\pi y}{b} e^{i\omega t} \\
W(x, y, t) &= \sum_{i=1}^{M} \sum_{j=1}^{N} C_{mn} \sin \frac{m\pi x}{a} \sin \frac{n\pi y}{b} e^{i\omega t}
\end{aligned}
\tag{A.23}
$$

Substituting Eq.(A.21) into Eq.(A.16) and minimizing the total energy expression with respect to the displacement amplitude coefficients, A_{mn}, B_{mn} and C_{mn} yields three governing equations of motion:

$$
\begin{aligned}
\Pi_{A,mn} &= \sum_{i=1}^{m} \sum_{j=1}^{N} \zeta_{11} A_{mn} + \zeta_{12} B_{mn} + \zeta_{13} C_{mn} = 0 \\
\Pi_{B,mn} &= \sum_{i=1}^{m} \sum_{j=1}^{N} \zeta_{21} A_{mn} + \zeta_{22} B_{mn} + \zeta_{23} C_{mn} = 0
\end{aligned}
\tag{A.24}
$$

204

$$\Pi_{C,mn} = \sum_{i=1}^{m}\sum_{j=1}^{N} \zeta_{31}A_{mn} + \zeta_{32}B_{mn} + \zeta_{33}C_{mn} - q_{mn}\int_0^a\int_0^b \sin\frac{\pi m x}{a}\sin\frac{\pi n y}{b}dxdy = 0$$

where the ζ_{ij} coefficients are

$$
\zeta_{11} = \quad \frac{\pi^2 im}{a^2}D_{11}[SSSS] + \frac{\pi^2 jn}{b^2}D_{66}[CCCC] - \frac{\pi^2 mj}{ab}D_{16}[CSCS]
$$
$$
+A_{55}[CCSS] - \frac{\pi^2 mj}{ab}D_{16}[CSCS] + (C_{D_r}i\omega - m_r\omega^2)[CCSS] \quad (A.25)
$$

$$
\zeta_{12} = \quad \frac{\pi^2 in}{ab}D_{12}[SSSS] - \frac{\pi^2 im}{a^2}D_{16}[SCSC] + \frac{\pi^2 mj}{ab}D_{66}[CCCC]
$$
$$
-\frac{\pi^2 jn}{b^2}D_{26}[CSCS] + A_{45}[CSSC] \quad (A.26)
$$

$$
\zeta_{13} = \quad \frac{\pi m}{a}A_{55}[CCSS] + \frac{\pi n}{b}A_{45}[CSSC] \quad (A.27)
$$

$$
\zeta_{21} = \quad \frac{\pi^2 mj}{ab}D_{12}[SSSS] - \frac{\pi^2 im}{a^2}D_{16}[SCSC] + \frac{\pi^2 in}{ab}D_{66}[CCCC]
$$
$$
-\frac{\pi^2 jn}{b^2}D_{26}[SCSC] + A_{45}[SCCS] \quad (A.28)
$$

$$
\zeta_{22} = \quad \frac{\pi^2 jn}{b^2}D_{22}[SSSS] + \frac{\pi^2 im}{a^2}D_{66}[CCCC] - \frac{\pi^2 in}{ab}D_{26}[SCSC]
$$
$$
+(A_{44}[SSCC] - \frac{\pi^2 mj}{ab}D_{16})[CSCS] + (C_{D_r}i\omega - m_r\omega^2)[CCSS] \quad (A.29)
$$

$$
\zeta_{23} = \quad \frac{\pi n}{b}A_{44}[SSCC] + \frac{\pi m}{a}A_{45}[SCCS] \quad (A.30)
$$

$$
\zeta_{31} = \quad \frac{\pi i}{a}A_{55}[CCSS] + \frac{\pi j}{b}A_{45}[CSSC] \quad (A.31)
$$

$$
\zeta_{32} = \quad \frac{\pi j}{b}A_{44}[SSCC] + \frac{\pi i}{a}A_{45}[CSSC] \quad (A.32)
$$

$$\zeta_{33} = \frac{\pi^2 im}{a^2}(A_{55} + N_x^*)[CCSS] + \frac{\pi^2 jn}{b^2}(A_{44} + N_y^*)[SSCC]$$

$$+\frac{\pi^2 mj}{ab}(A_{45} + N_{xy}^*)[SCCS] + \frac{\pi^2 in}{ab}(A_{45} + N_{xy}^*)[CSSC]$$

$$+(C_{D_r} i\omega - m_p \omega^2)[SSSS] \qquad (A.33)$$

$$(A.34)$$

and

$$[CCCC] = \cos\frac{\pi ix}{a} \cos\frac{\pi mx}{a} \cos\frac{\pi jy}{b} \cos\frac{\pi ny}{b} \qquad (A.35)$$

$$[CCSS] = \cos\frac{\pi ix}{a} \cos\frac{\pi mx}{a} \sin\frac{\pi jy}{b} \sin\frac{\pi ny}{b} \qquad (A.36)$$

$$[CSCS] = \cos\frac{\pi ix}{a} \sin\frac{\pi mx}{a} \cos\frac{\pi jy}{b} \sin\frac{\pi ny}{b} \qquad (A.37)$$

$$[CSSC] = \cos\frac{\pi ix}{a} \sin\frac{\pi mx}{a} \sin\frac{\pi jy}{b} \cos\frac{\pi ny}{b} \qquad (A.38)$$

$$[SCCS] = \sin\frac{\pi ix}{a} \cos\frac{\pi mx}{a} \cos\frac{\pi jy}{b} \sin\frac{\pi ny}{b} \qquad (A.39)$$

$$[SCSC] = \sin\frac{\pi ix}{a} \cos\frac{\pi mx}{a} \sin\frac{\pi jy}{b} \cos\frac{\pi ny}{b} \qquad (A.40)$$

$$[SSCC] = \sin\frac{\pi ix}{a} \sin\frac{\pi mx}{a} \cos\frac{\pi jy}{b} \cos\frac{\pi ny}{b} \qquad (A.41)$$

$$[SSCC] = \sin\frac{\pi ix}{a} \sin\frac{\pi mx}{a} \cos\frac{\pi jy}{b} \cos\frac{\pi ny}{b} \qquad (A.42)$$

$$[SSSS] = \sin\frac{\pi ix}{a} \sin\frac{\pi mx}{a} \sin\frac{\pi jy}{b} \sin\frac{\pi ny}{b}. \qquad (A.43)$$

These equations can be rewritten in matrix form to evaluate forced dynamic and static response as

$$\begin{bmatrix} \zeta_{11} & \zeta_{12} & \zeta_{13} \\ \zeta_{21} & \zeta_{22} & \zeta_{23} \\ \zeta_{31} & \zeta_{32} & \zeta_{33} \end{bmatrix}_{st} \begin{Bmatrix} A \\ B \\ C \end{Bmatrix}_t = \begin{Bmatrix} 0 \\ 0 \\ q \end{Bmatrix}_s \tag{A.44}$$

where

$$s = (m-1)N + n$$
$$t = (i-1)N + j$$

or to determine modal response as

$$\left(\begin{bmatrix} \overline{\zeta}_{11} & \zeta_{12} & \zeta_{13} \\ \zeta_{21} & \overline{\zeta}_{22} & \zeta_{23} \\ \zeta_{31} & \zeta_{32} & \overline{\zeta}_{33} \end{bmatrix}_{st} - \begin{bmatrix} \eta_{11} & 0 & 0 \\ 0 & \eta_{22} & 0 \\ 0 & 0 & \eta_{33} \end{bmatrix}_{st} \omega^2 \right) \begin{Bmatrix} A_t \\ B_t \\ C_t \end{Bmatrix} = \begin{Bmatrix} 0 \\ 0 \\ 0 \end{Bmatrix}. \tag{A.45}$$

The $\overline{\zeta}_{ii}$ and η_{ii} terms are

$$\overline{\zeta}_{11} = \zeta_{11} - (C_{D_r} i\omega - m_r \omega^2)[CCSS] \tag{A.46}$$

$$\overline{\zeta}_{22} = \zeta_{22} - (C_{D_r} i\omega - m_r \omega^2)[SSCC] \tag{A.47}$$

$$\overline{\zeta}_{33} = \zeta_{33} - (C_{D_p} i\omega - m_p \omega^2)[SSSS] \tag{A.48}$$

$$\eta_{11} = m_r \omega^2 [CCSS] \tag{A.49}$$

$$\eta_{22} = m_r \omega^2 [SSCC] \tag{A.50}$$

$$\eta_{33} = m_p \omega^2 [SSSS] \tag{A.51}$$

Next, the acoustic forcing function must be determined. Only transverse pressure

207

components are considered, and therefore, as in the other two previous formulations, the following forcing function is considered:

$$q(x, y, t) = \sum_{m=1}^{M} \sum_{n=1}^{N} q_{mn} \sin \frac{\pi m x}{a} \sin \frac{\pi n y}{b} e^{i\omega t}. \tag{A.52}$$

To analyze sound transmission through the panel, the technique of Roussos (1985) is again utilized, and the forcing function function $q(x, y, t)$ can be expressed as the blocked pressure:

$$q(x, y) = 2P_i exp[-(\omega/c)i(x \sin\theta_i \cos\phi_i + y \sin\theta_i \cos\phi_i)], \tag{A.53}$$

The distributed forcing function can be rewritten in the form

$$q_s = 2P_i \overline{I}_m \overline{I}_n, \tag{A.54}$$

where $\overline{I}_m$ and $\overline{I}_n$ are defined in Eqs.(3.14) and (3.15).

By solving the simultaneous equations produced by Eq.(A.23), the displacement coefficients (C_t) can be determined. Knowing these values for a given pressure incidence, θ_i and ϕ_i, the transmitted pressure can again be found using the Rayleigh integral approach as

$$P_t(r, \theta, \phi) = -\frac{\omega^2 \rho a b}{2\pi r} \exp\{i\omega[t - \frac{r}{c} - \frac{\sin\theta}{2c}(a \cos\phi + b \sin\phi)]\} \sum_{m=1}^{m} \sum_{n=1}^{N} C_{mn} I_m I_n, \tag{A.55}$$

where

$$U_r = \frac{P_t}{\rho c}. \tag{A.56}$$

Considering U_r^* to be the complex conjugate of U_r, the transmitted acoustic intensity

is defined as

$$I_t(r, \theta, \phi) = \frac{1}{2} Re[P_t U_r^*]. \qquad (A.57)$$

The transmitted acoustic power, Π_t, can be determined as

$$\Pi_t = \int_{\phi=0}^{2\pi} \int_{\theta=0}^{\frac{\pi}{2}} I_t r^2 \sin \theta d\theta d\phi. \qquad (A.58)$$

Where Π_i, is defined as

$$\Pi_i = \frac{(P_i^2 ab \cos \theta_i)}{2\rho c}. \qquad (A.59)$$

The transmission loss can be found as

$$TL = 10 log(\frac{\Pi_i}{\Pi_t}). \qquad (A.60)$$

Vita

William S. Anders was born in Hampton, Virginia on January 17, 1961. He grew up in Springfield, Virginia where he graduated from Thomas Jefferson High School in 1979. His Engineering experience began at Atlantic Research Corporation in 1980, where worked as a co-op student until receiving his bachelor's degree in Mechanical Engineering in 1984 from Virginia Polytechnic Institute and State University. He then accepted full-time employment at Saginaw Division, G.M., where he worked in the Advanced Engineering and Front Wheel Drive Halfshaft groups until 1988, when he returned to Virginia Tech to pursue a master's degree in Mechanical Engineering. Shortly before returning to school for graduate studies, he wed Lori Lynn Alexander. During their stay in Blacksburg, the Anders family was blessed with the birth of a lovely daughter, Sarah Grace; named for her beloved paternal grandmother, Sarah S. Howard, and recently deceased great grandmother, Grace S. Strader. Upon completing his master's degree, William will return to Saginaw, Michigan to resume his career with General Motors, with possible aspirations to someday continue his studies in pursuing a Ph. D. in Mechanical Engineering.

William S. Anders